

**UNCLASSIFIED**

**AD 435973**

**DEFENSE DOCUMENTATION CENTER**

**FOR**

**SCIENTIFIC AND TECHNICAL INFORMATION**

**CAMERON STATION, ALEXANDRIA, VIRGINIA**



**UNCLASSIFIED**

**NOTICE:** When government or other drawings, specifications or other data are used for any purpose other than in connection with a definitely related government procurement operation, the U. S. Government thereby incurs no responsibility, nor any obligation whatsoever; and the fact that the Government may have formulated, furnished, or in any way supplied the said drawings, specifications, or other data is not to be regarded by implication or otherwise as in any manner licensing the holder or any other person or corporation, or conveying any rights or permission to manufacture, use or sell any patented invention that may in any way be related thereto.

ESD-TDR-64-103

Volume I

**PROCEEDINGS OF THE SECOND TROPOSPHERIC  
REFRACTION EFFECTS TECHNICAL REVIEW MEETING**

(In Three Volumes)

TECHNICAL DOCUMENTARY REPORT NO. ESD-TDR-64-103

MARCH 1964

Prepared for

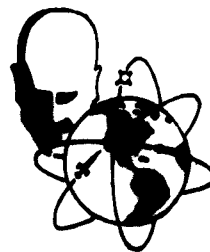
**DIRECTORATE OF AEROSPACE INSTRUMENTATION**

**ELECTRONIC SYSTEMS DIVISION**

**AIR FORCE SYSTEMS COMMAND**

**UNITED STATES AIR FORCE**

**L. G. Hanscom Field, Bedford, Massachusetts**



Project 705.1

Prepared by

**THE MITRE CORPORATION**

**Bedford, Massachusetts**

**Contract AF19(628)-2390**

NO. OTS

435973  
DDC  
1964 NO.

DDC release to OTS is not authorized.

Qualified requesters may obtain copies from DDC. Orders will be expedited if placed through the librarian or other person designated to request documents from DDC.

When US Government drawings, specifications, or other data are used for any purpose other than a definitely related government procurement operation, the government thereby incurs no responsibility nor any obligation whatsoever; and the fact that the government may have formulated, furnished, or in any way supplied the said drawings, specifications, or other data is not to be regarded by implication or otherwise, as in any manner licensing the holder or any other person or corporation, or conveying any rights or permission to manufacture, use, or sell any patented invention that may in any way be related thereto.

Do not return this copy. Retain or destroy.

**PROCEEDINGS OF THE SECOND TROPOSPHERIC  
REFRACTION EFFECTS TECHNICAL REVIEW MEETING**

**(In Three Volumes)**

**TECHNICAL DOCUMENTARY REPORT NO. ESD-TDR-64-103**

**MARCH 1964**

**Prepared for**

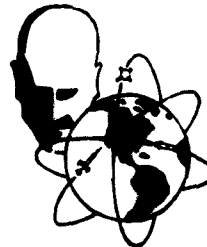
**DIRECTORATE OF AEROSPACE INSTRUMENTATION**

**ELECTRONIC SYSTEMS DIVISION**

**AIR FORCE SYSTEMS COMMAND**

**UNITED STATES AIR FORCE**

**L. G. Hanscom Field, Bedford, Massachusetts**



**Project 705.1**

**Prepared by**

**THE MITRE CORPORATION**

**Bedford, Massachusetts**

**Contract AF19(628)-2390**

## FOREWORD

The collection of papers in this publication covers the presentations made at the Second Tropospheric Refraction Effects Technical Review Meeting, sponsored by the Electronic Systems Division of the Air Force. The first meeting in this series was held at the National Bureau of Standards Laboratory in Boulder, Colorado in July 1963. The date and location for the third meeting has not been set at this time, but will be held in 1964. Consideration is being given to increasing the scope of the next meeting and also including industry participation.

These meetings have been very useful for the exchange of information between the cognizant individuals at the various ranges and government agencies concerned with refraction research activities. It has also helped to pinpoint the phases of this problem which are currently receiving the greatest attention and equally important, it has provided a means of determining the areas which are being neglected.

The publication of these proceedings does not constitute official Air Force or MITRE endorsement, acceptance, or approval of the techniques proposed and used in the work, or of the results reported. Rather, it is a record of what has been reported and provides a useful collection of ideas, basic data, and measurement results to stimulate further advancement as well as a ready reference on the current state-of-the-art. These papers are grouped into five sections, each section corresponding to the agency or type of organization sponsoring the work.

I wish to express my appreciation to the representatives of the various agencies for their excellent cooperation, to all the participants of the meeting, and to the Range Measurements Division of the Directorate of Aerospace Instrumentation for suggestions and assistance. The enthusiastic response has made all of us feel that the time and energy spent in preparing for the meeting was well worthwhile.

Louis J. Galbiati,  
Chairman

## ABSTRACT

This publication covers the papers presented at the Second Tropospheric Refraction Effects Technical Review Meeting, sponsored by the Electronic Systems Division of the Air Force. The meeting was held at The MITRE Corporation on November 13 and 14, 1963. The papers are grouped into five sections, each section corresponding to the agency or type of organization sponsoring the work. The first section covers work on tropospheric refraction sponsored by the Electronic Systems Division in support of metric instrumentation on the national missile ranges. This work is under the technical direction of The MITRE Corporation. Other sections cover the activities of the National Aeronautics and Space Administration, the national missile ranges, the other prime agencies and the government laboratories. Results of the most up-to-date measurement data available at the time of the meeting are included.

## REVIEW AND APPROVAL

This technical documentary report has been reviewed and is approved.

*Roy D. Ragdale*

ROY D. RAGSDALE  
Colonel, USAF  
Director, Aerospace Instrumentation



## TABLE OF CONTENTS

### VOLUME I

	<u>Page</u>
AGENDA	vii
OPENING REMARKS	xiii
INTRODUCTION	xv
SECTION I      ELECTRONIC SYSTEMS DIVISION	
ESD Tropospheric Refraction Effects Task	1-3
Meteorological Aspects of Range and Range- Rate Error	1-15
The MITRE Line Integral Refractometer	1-77
Testing of the Line Integral Refractometer	1-91
Comments by Kenneth Norton	1-107
A Summary of Tropospheric Phase Stability Measurements	1-113
Boulder, Colorado, Measurement Results	1-119
Optical Scintillation - Review of the Literature	1-131
Residual Range and Range-Rate Errors Due to the Troposphere	1-143
Effects of Tropospheric Refraction in Earth- Space Links	1-155

TABLE OF CONTENTS (Continued)

VOLUME II

	<u>Page</u>
SECTION II    NATIONAL AERONAUTICS AND SPACE ADMINISTRATION	
The Troposphere and Its Influence on Spacecraft Tracking	2-197
The Real-Time Compensation for Tropospheric Effects on the Measurement of Range and Range Rate	2-211
SECTION III    NATIONAL MISSILE RANGES	
<u>Atlantic Missile Range</u>	
Accuracy of Tropospheric Refraction Correction Procedures	3-233
Tracking Data Accuracy	3-239
<u>Pacific Missile Range</u>	
Correction of Radar Elevation Angles Less Than One Degree	3-241
Tracking Errors at Low-Elevation Angles Due to Tropospheric Refractive Effects	3-259
<u>White Sands Missile Range</u>	
Measurements of Radar Pointing Errors at Low-Elevation Angles and Comments on N-Bar Approach to Refraction Error Corrections	3-309
SECTION IV    OTHER PRINCIPAL AGENCIES	
Multipath Propagation	4-317
Canadian Reflection-Interferometer Elevation Angle Error Measurements	4-325

**TABLE OF CONTENTS (Continued)**

**VOLUME III**

	<u><b>Page</b></u>
<b>SECTION V</b>	
<b>GOVERNMENT LABORATORIES AND CENTERS</b>	
RADC Exploratory Research Program in Propagation as It Relates to Range Instrumentation	5-347
Tropospheric Phase Path Fluctuations at S-Band	5-357
Target Accuracy -- Radio Seeing Through the Troposphere	5-369
Optical-Microwave Refraction Comparisons	5-383
The Dual-Cavity Refractometer	5-387
New Values of the Optical Air Mass and the Refraction and Comparison with Previous Tables	5-391
Refractometer Activity	5-401
<b>BIBLIOGRAPHY</b>	I-407
<b>LIST OF PARTICIPANTS</b>	II-441

**TROPOSPHERIC REFRACTION EFFECTS MEETING**

**November 13 and 14, 1964**

**Gaither Building Room 1A-401**

**MITRE CORPORATION**

<u><b>TIME</b></u>	<u><b>SUBJECT</b></u>
November 13, 1963	
8:45-8:50	Opening Remarks Col. G. Lundquist
8:50-9:05	ESD Tropospheric Refraction Effects Task Dr. L. J. Galbiati
9:05-10:35	Cambridge Research Laboratory Dr. R. M. Cunningham <ul style="list-style-type: none"><li>a. General Description</li><li>b. AMR Measurement Results</li><li>c. Noise Error Analysis Results</li></ul>
10:35-10:45	Coffee Break
10:45-12:15	MITRE Corporation J. F. Sullivan and H. M. Richardson <ul style="list-style-type: none"><li>a. General Description Line-Integral Refractometer Task</li><li>b. Measurement Techniques</li><li>c. Measurement Results</li></ul>
12:15-1:15	Lunch Period
1:15-2:45	National Bureau of Standards Dr. M. C. Thompson <ul style="list-style-type: none"><li>a. General Description</li><li>b. Boulder Measurement Results</li><li>c. Optical Study Results</li></ul>
2:45-2:55	Coffee Break
2:55-4:05	National Aeronautics & Space Administration Dr. F. O. Vonbun <ul style="list-style-type: none"><li>a. General Description</li><li>b. Real Time Compensation on Range Measurements (Dr. J. J. Freeman)</li></ul>
4:05-4:50	Open Discussion

<u>TIME</u>	<u>SUBJECT</u>
November 14, 1963	
8:30-8:45	Atlantic Missile Range Dr. C. L. Carroll <ul style="list-style-type: none"> <li>a. Accuracy of Tropospheric Refraction Correction Procedures - Dr. C. F. Martin</li> <li>b. Tracking Data Accuracy - Dr. W. A. Dryden</li> </ul>
8:45-9:00	Pacific Missile Range L. T. Bankston <ul style="list-style-type: none"> <li>a. Low Elevation Angle Measurements</li> <li>b. Corrections Using Measured vs. Exponential Profile (C. Gardner)</li> </ul>
9:00-9:15	White Sands Missile Range C. W. Querfeld Radar Pointing Errors at Low Elevation Angles
9:15-9:30	Space Systems Division - Aerospace R. E. Ringe Techniques for Measuring Multipath Effects - E. W. Heinzerline
9:30-9:55	Discussion
9:55-10:05	Coffee Break
10:05-10:25	ESD Deputy for Engineering and Technology R. K. Crane Canadian Reflection-Interferometer Elevation Angle Error Measurements
10:25-10:40	U.S. Army Engineers J. F. Hannigan Refraction Effects Activity
10:40-11:20	Rome Air Development Center L. Colin <ul style="list-style-type: none"> <li>a. Air Craft Beacon - 100 M &amp; 1KM Interferometer Measurements H. A. Von Biel</li> <li>b. Target Accuracy and Multipath Dr. J. B. Smyth</li> </ul>

<u>TIME</u>	<u>SUBJECT</u>
11:20-12:05	Cambridge Research Laboratory R. B. Toolin a. Optical-Microwave Refraction Comparison - A. R. Boileau b. Dual Cavity Balloon Borne Refractometer - Lt. L. Fisher c. Recalculation of BEMPORAD Values of Optical Air Mass - Y. M. Treve
12:05-12:30	Discussion
12:30-1:30	Lunch Period
1:30-2:10	Refractometer Activities Dr. M. C. Thompson
2:10-4:30	Open Discussion; Tour of Instrumented Aircraft and Vans

OPENING REMARKS: TROPOSPHERIC REFRACTION MEETING

Colonel G. E. Lundquist

Deputy for Engineering and Technology  
Electronic Systems Division (ESD)  
Hanscom Field, Bedford, Massachusetts

It is a pleasure to welcome you to our Tropospheric Refraction Technical Review Meeting. This meeting will occupy two full days; during this period, presentations will be given by representatives from the organizations currently conducting significant activities regarding the effects of tropospheric refraction on metric measurement signals. Today's presentations include those of the Cambridge Research Laboratories, The MITRE Corporation, the National Bureau of Standards, and the National Aeronautics and Space Administration. Tomorrow, representatives of the three national missile ranges, the Space Systems Division, the U.S. Army Corps of Engineers, the Rome Air Development Center and the Cambridge Research Laboratories will provide brief presentations of their activities.

This two-day meeting was planned as part of Electronic Systems Division's Tropospheric Refraction Effects Task. The sessions should enable all of us to familiarize ourselves with the latest work in this field being carried on by the different agencies throughout the country and insure that each one of us is not duplicating work being done elsewhere. Dr. Louis Galbiati of The MITRE Corporation, who is responsible for the technical direction of the ESD task, will cover the purpose of this meeting in detail and the technical aspects of the ESD Tropospheric Refraction Effects Task.

May I again say that it is a pleasure to welcome you to our Tropospheric Refraction Technical Review Meeting. Now, I would like to introduce Dr. Louis Galbiati.

## INTRODUCTION

Louis J. Galbiati

The MITRE Corporation  
Bedford, Massachusetts

Many phases of tropospheric refraction effects will be covered by the various speakers during the next two days. The speakers, from organizations throughout the country which are conducting the most significant activities in the area, will mention both their problems and results of the work they are funding. Thus, this meeting will assure that our work is not a duplication of what someone else is doing, and will give us an opportunity to assess the current state-of-the-art. The specific purpose of this meeting is threefold:

First — To provide us with the opportunity to cover the organization, objectives and status of the different phases of the Electronic Systems Division's tropospheric refraction effects work currently being conducted in support of range trajectory measurement instrumentation. The work agents carrying on the effort are: the Cloud Physics Branch of the Air Force Cambridge Research Laboratories, the Radar Systems and Techniques Department of MITRE, and the Central Radio Propagation Laboratory of the National Bureau of Standards at Boulder, Colorado.

Second — To ensure the widest possible dissemination of information regarding the results of our activity and that conducted by other government agencies. This meeting should result in a large decrease in the time period between the acquisition of the measurement data and the publication of the results. It should be mentioned that



the results to be presented at this meeting are based on very recent measurements and that all the data may not have been completely analyzed at this time. For example, the report by one of the first three organizations on the program today is based on data taken during late October and early November, 1963.

Third - To stimulate the exchange of ideas between people doing actual work in the field -- people who have the best technical grasp of the subject. We will hear about the types of problems others have encountered in performing measurements relating to refraction, and will be able to advance our individual progress by utilizing their solutions, when applicable.

The work sponsored by the Electronic Systems Division, and under the technical direction of MITRE, is covered in Section I. While this effort is in support of metric measurement instrumentation on the national missile ranges, it has not necessarily been constrained to specific system configurations. The results will be organized and presented in a general form, and thus be applicable to systems as they evolve. The elevated baseline work, sponsored by the Avionic Lab at Wright-Patterson Air Force Base, is also included in Section I, since this effort utilizes the same equipment used by the Electronic System Division's Maui, Hawaii, program.

Section II will be devoted to the activities of the National Aeronautics and Space Administration. The discussion will focus on the influence of the troposphere on the tracking systems utilized by the Administration, both from the calibration and the orbit determination points of view. The interest and future plans in the field of tropospheric studies necessary for tracking and orbit determination, along with tropospheric models and methods for predicting their effects on range and range-rate measurements, will be covered.

The presentation by the representatives of the three national missile ranges in Section III will include a review and assessment of

tropospheric refraction correction methods, comments on tracking data accuracy, methods of processing data, and the results of measurements performed with the FPS-16 radars.

Section IV contains presentations by other principal agencies. Techniques used for the multipath propagation tests, currently being conducted on Eleuthera Island, B.W.I., will be described, and a discussion included on the results of the measurements to date. Results of some precise measurement tests, conducted jointly by the U.S. and Canadian Air Forces, on the average effects of refractive index structure on elevation-angle measurement will also be covered, and refractive effects activities of the U.S. Army Corps of Engineers will be described.

The projects sponsored by the Rome Air Development Center and the Cambridge Research Laboratories will be presented in Section V. The Rome presentation includes both the data and results of measurements on tropospheric phase path fluctuations at S-band frequencies and results of a target accuracy study performed with the sea interferometer on the West Coast. The Cambridge Research Laboratories presentation includes a discussion of both optical and microwave refraction activities, and details on the status of the new airborne refractometer development. The last discussion at the meeting concerns airborne refractometer measurement considerations.

**SECTION I**

**ELECTRONIC SYSTEMS DIVISION**

## ESD TROPOSPHERIC REFRACTION EFFECTS TASK

L. J. Galbiati

The MITRE Corporation  
Bedford, Massachusetts

The net result of the tropospheric refraction effects on tracking systems is to introduce uncertainty as to the actual location of the object (Figure 1-1). For our application, we can say that, generally,

- (a) the object appears higher in elevation and at a greater distance than it actually is;
- (b) the clear-atmospheric refractive effect is smaller in the optical region of the spectrum than in the microwave region, but can still be appreciable at low-elevation angles;
- (c) the clouds and other special meteorological conditions can introduce noise or uncertainties in metric measurement systems, and
- (d) the characteristic of the noise is dependent on the size and type of the "cloud" structure.

There is a pressing need to:

Minimize tropospheric refractive effects at radio frequencies. (The effects will probably always be present, but we should design systems and develop correction techniques in such a way as to minimize the impact.)

## REFRACTION EFFECTS

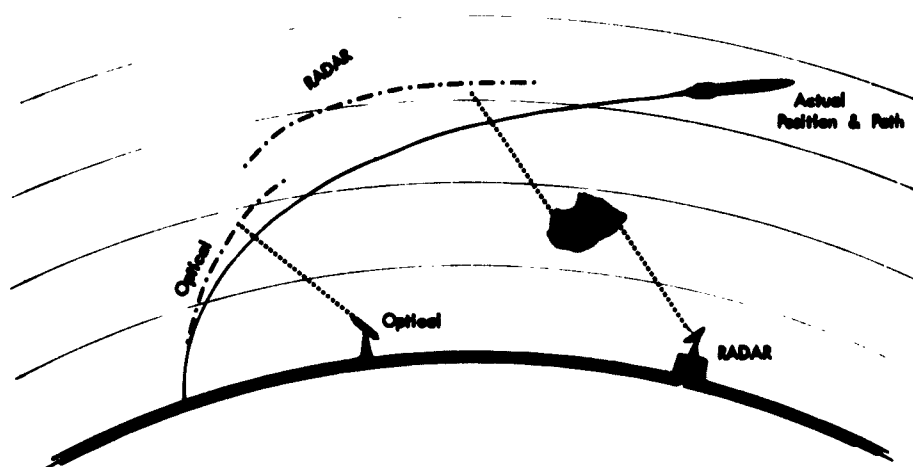


Figure 1-1

Determine the extent of tropospheric effects on optical systems. (Even if the effects are small we still need data applicable to our environment; in addition, the requirements on this type of system are so high that the effect also limits the precision of this type of measurement.)

Obtain real-time correction for refractive effects. (Ideally, one would desire simultaneous measurements of the refractive effects and metric data; on the other hand, if we cannot have simultaneous measurement, then we should have some idea as to how close in time these two inputs of data can be.)

In May 1962, the National Academy of Science Ad Hoc Panel on Electromagnetic Propagation was convened in Washington at the request of Headquarters, Air Force Systems Command. The panel, consisting of individuals from the various organizations indicated in Figure 1-2 met to determine the state-of-the-art regarding tropospheric refraction effects. The panel's applicable conclusions regarding errors set forth in ACAFSC 103 were:

Tropospheric bias errors are highly predictable using radiosonde or refractometer profiles; residual errors from 1 to 3 per cent of the initial bias levels are commonly attained.

Tropospheric fluctuation errors are not correctable using any known procedure, and will amount to a few tenths of a foot in range, and 10 to 50  $\mu$ radians in angle (depending on the baseline or aperture used for measurement), under normal weather conditions.

In range instrumentation applications, where the beam is not fixed, the residual "bias" and long-term error components will change as the beam moves, and additional

**PARTICIPANTS OF THE NATIONAL ACADEMY OF SCIENCE**  
**AD HOC PANEL ON ELECTROMAGNETIC PROPAGATION**

NBS	NASA
NRL	IRIG
DIAMOND FUSE LABS	
WHITE SANDS MISSILE RANGE	
LINCOLN LABORATORY	
PATRICK AIR FORCE BASE	
INDUSTRY AND UNIVERSITIES	

**FIGURE 1-2**

**BACKGROUND**

atmospheric rate errors will be generated. These errors will be proportional to the tangential velocity of the missile, and will typically be 5 to 50 times the errors measured for a fixed beam.

The uncertainty in tropospheric path leads to errors equivalent to motion of the instrument on the ground.

The errors due to atmospheric conditions may be increased or decreased by a factor of two or three for different weather conditions.

There was very little in the way of available data that one could use to make a positive estimate of the situation for an operational system located somewhere on the Atlantic Missile Range.

The applicable panel recommendations to achieve a future increase in accuracy were (Figure 1-3):

Future tracking systems should be designed to tolerate the unpredictable fluctuations of the measurement ray paths in the atmosphere. When targets of high velocity must be tracked with accurate three-coordinate velocity measurements, the measurement systems baselines should be as long as possible and consistent with target altitude.

Work on a specific procedure for measuring and correcting tropospheric errors on a real-time basis should receive full support from the Air Force. Theoretically, this technique appears very promising, and it is a question of determining whether experimental verification can be obtained.

The over-all technical approach adopted by MITRE was to determine the types of data or results needed to best satisfy the requirements set forth by the panel; to outline the measurement activities needed to obtain the data, and to identify the organization best qualified to perform the measurements.



<u>RECOMMENDATION</u>	<u>TECHNICAL APPROACH</u>
7.1 DESIGN AROUND UNPREDICABLE FLUCTUATIONS	DYNAMIC WEATHER EFFECTS
7.2 REAL TIME CORRECTION	LINE INTEGRAL REFRACTOMETER
7.3 SPATIAL AND TEMPORAL CORRELA- TION OF TROPOSPHERIC RANGE ERRORS	FIXED-END-POINTS PHASE MEASUREMENTS

FIGURE 1-3  
APPLICABLE PANEL RECOMMENDATIONS

It can be seen that the over-all task approach (Figure 1-4) is designed to meet the panel's recommendations. The next step was to identify each item of the technical approach with an agency best qualified to do the work. The Central Radio Propagation Laboratory of the National Bureau of Standards at Boulder had existing facilities for performing the required fixed end-point measurements. The use of the Bureau for this phase of the task meant that the results would be more readily available to everyone and, in addition, the type of measurements needed were in line with the long-range goals of the unit. The Air Force was able to obtain specific information in a short time period by supporting the National Bureau of Standards effort, and, at the same time, the Bureau obtained the basic data needed for its work.

Arrangements were made for the Air Force to support the feasibility field test of The MITRE Line Integral Differential Phase Refractometer technique. The Line Integral Differential Phase Refractometer, referred to simply as the Line Integral Refractometer in the balance of these Proceedings, was developed on MITRE in-house funds. This technique utilizes the relative tropospheric-induced phase shift, at 15.6 and 31.2 gc, as a measure of water vapor refractive effect, and offers the best possible potential solution to the real-time correction problem. In fact, this is the only practical method proposed up to this time. Preliminary results were very encouraging, and will be reported on in the second session of this meeting (see Section I).

The Cloud Physics Branch of the Air Force Cambridge Research Laboratories was engaged to perform dynamic meteorological measurements at the Atlantic Missile Range and to investigate the relationship of the data to metric measurement errors. Data on the effect of meteorological conditions at the Atlantic Missile Range location are needed in order to design a system which could tolerate the fluctuation; that is, we require applicable data on the cause and effect relationship

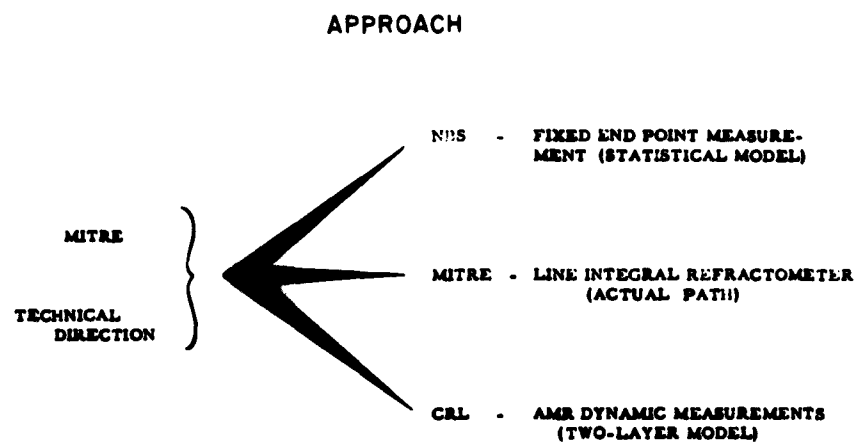


Figure 1-4

between the weather and metric systems errors. In this way, costs would be minimized since advantage was taken of CRL's vast amount of experience in this type of work; and related projects under CRL direction in this area could be utilized to supply essential information. We are also keeping abreast of certain work utilizing IR techniques for determining refractive effects; however, these efforts are still in the preliminary stages.

While the description of the work will be covered in detail by each organization during its presentation, it probably would be of value to cover all the different phases briefly at this time in order to provide the proper background for the detailed discussion of the other speakers. The National Bureau of Standards will utilize a fixed-point test facility (Figure 1-5) to determine the applicability of the correction techniques and to determine the effect of baseline length, orientation, and antenna aperture variation. This effect should provide data necessary to determine the validity of the correction techniques and to provide parameter data for the improvement of existing and future metric measurement systems. Studies are also being performed by Dr. Burroughs on the effect of beam movement through the atmosphere; a condensed version of his results will be included in Section I of these Proceedings. A state-of-the-art study in optics is being performed by Dr. Meyer-Arendt to indicate what areas in optics need further work. A National Bureau of Standards technical memo will be issued early in 1964 on the subject, but the conclusions will be presented at this meeting (see Section I).

The Radar Systems and Techniques Department of The MITRE Corporation is concerned with the application and testing of the Line Integral Refractometer technique which provides a measure of the refractive effects of water vapor along the actual transmission path. The system (Figure 1-6) is capable of modification at a later date to include the determination of the effect of the dry constituents. The technique provides the possibility of achieving real-time correction

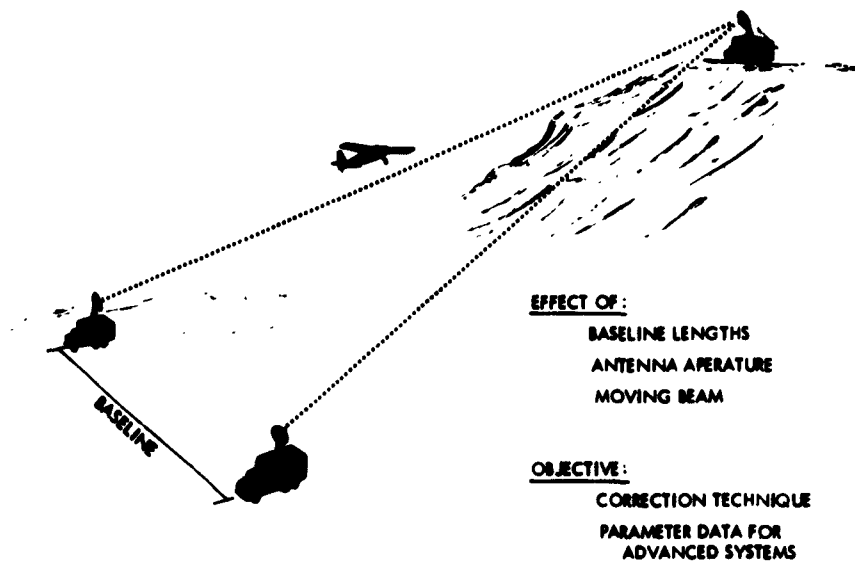


Figure 1-5

MITRE — LINE INTEGRAL REFRACTOMETER

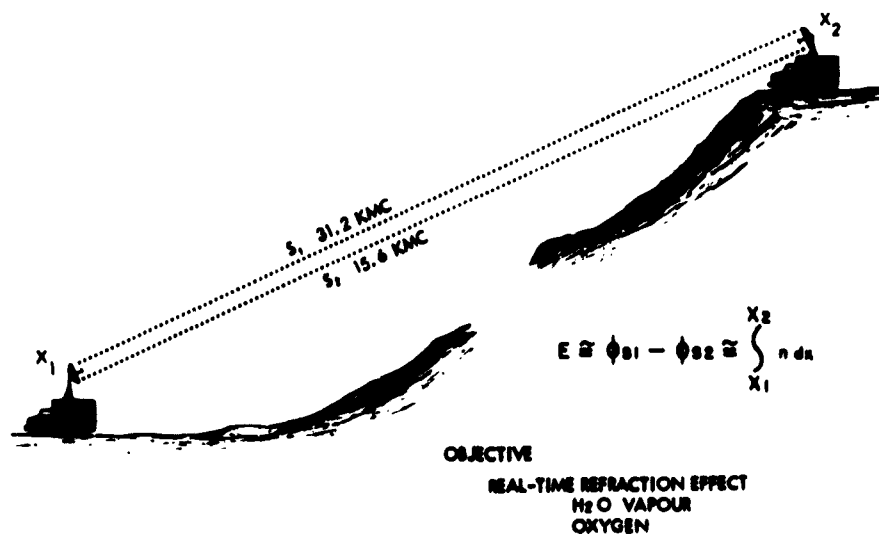


Figure 1-6

for the refractive effects and a reduction in the non-predictable fluctuation error which was mentioned earlier. The original test was performed using two elevated fixed location sites. Plans are being formulated to perform tests on a slanted path to minimize multipath effects due to stratification. For an operational system, the transmitter would be mounted in the moving vehicle.

The airborne and ground meteorological measurements at the Atlantic Missile Range are being performed under the auspices of the Cambridge Research Laboratories. This effort should provide data on the noise effects of meteorological conditions and indicate the possibility of scheduling critical missile flights during periods of projected low-residual noise in the metric measurement system. Aircraft will be flown through different cloud formations and metric data will simultaneously be taken from the ground (Figure 1-7). In addition, a little later in the program we hope to investigate certain meteorological conditions with a ground radar station. The ground radar station we had planned to use for this work is being modified at this time, so no measurements have been made to date. The refractive index profile data will be converted to digital form and a computer will be used to investigate the moving beam effect, et cetera, on tracking system noise.

This gives, in brief, the range instrumentation requirements which make it necessary for the Air Force to be involved with the measurements on tropospheric refraction, indicates how the task is organized to insure that the goals we have set for ourselves are achieved, and outlines the phase of the activity carried on by different work agents. In general, I can say that we have been very satisfied with the level of activity maintained by the three organizations doing this work for us and with the progress to date. The validity of the criteria we used in the selection of the work agents has been proved, and I see no obstacle to our achievement of the long-range goals set at the start of the task.

## CRL — DYNAMIC MEASUREMENTS

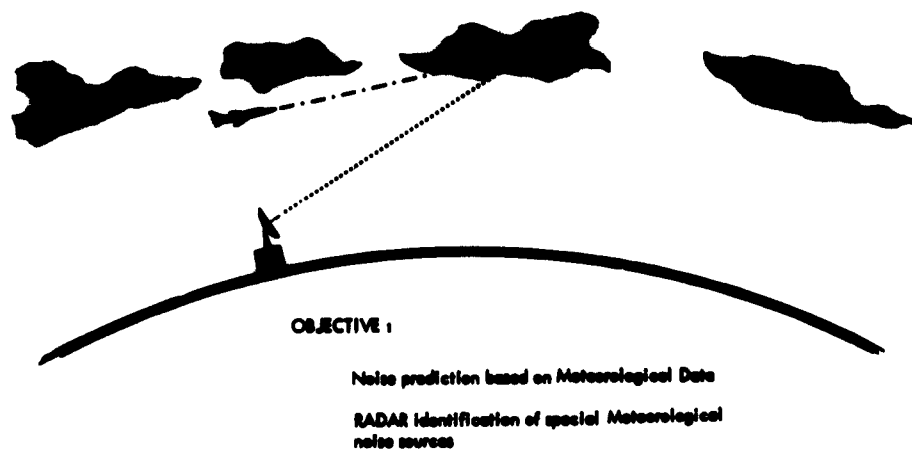


Figure 1-7

## METEOROLOGICAL ASPECTS OF RANGE AND RANGE RATE ERROR

Robert M. Cunningham

Air Force Cambridge Research Laboratories

### INTRODUCTION

A semi-popular weekly has just recently said we are "Zeroing in on Tracking System Noise." As you will see from what follows, this headline writer was, as is usually the case with headline writers, overstating the case. I hope we all are zeroing in on the problem, but at present I believe it is down a long somewhat refracted line of sight.

As is usually the case in the early stages of an investigation, the first report is largely descriptive in nature. Our plan of attack is described, some samples of this summer's data are shown, and a few numerical results, range and range rate errors are given. Our part of the program might be outlined as

Task 5930.07 AFCRL Portion.

### Approach

- (a) Compare meteorological conditions with measured errors, (both the fixed and random components).
- (b) Determine the refractive index climatology in the locale of a metric measurement system.
- (c) Explore indirect means of measuring meteorological effects, and cross-compare with direct measurements.



### Objectives

- (a) Knowledge of the types and scales of atmospheric structure responsible for system noise.
- (b) Forecast of bias errors and degree of noise.
- (c) Suggestions regarding improved systems to minimize meteorological effects.

We are accomplishing the above by utilizing the experience and facilities of our "in-house" organizations plus those contractors who have been associated with various phases of similar problems or who have previously dealt with instrumentation similar to that required. The organizations associated with the AFCRL portion of Task 5930.07 since last spring are listed below.

### Task Divisions (AFCRL)

- (1) AFCRL - Cloud Physics Branch (CRHC)  
"In-house" research,  
direct observation with the Branch's C-130, Aircraft,  
analysis of data-collected during special periods,  
coordination of program.
- (2) AFCRL - Ionospheric Propagation Branch (CRUQ)  
Ray-tracing (includes contract with Electronic Associates).
- (3) Technical Operations, Inc.  
Analysis of CRL data taken for MA shot series,  
study of cloud effects at several scales on the noise  
output of radio interferometer.
- (4) Electromagnetic Research Corp.  
Collection of refractive index and other related data in  
the vicinity of radio interferometer systems at the  
Atlantic Missile Range (AMR),  
analysis and interpretation of data-collected.

(5) Singco Inc.

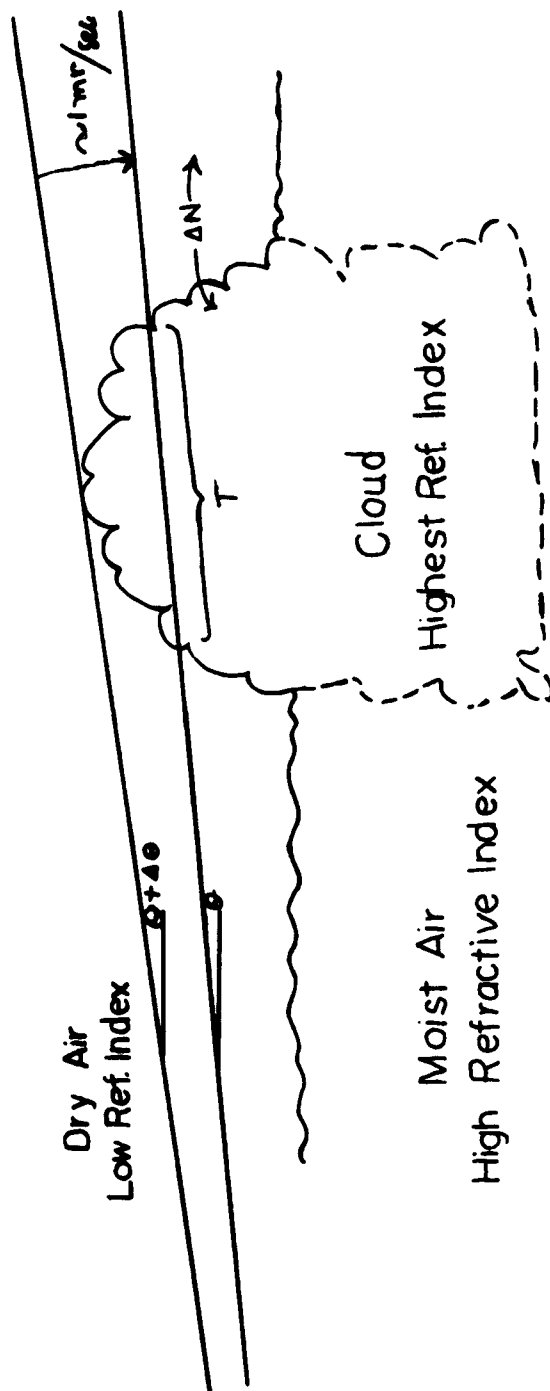
Equipment development and fabrication for the above data-collection program at AMR.

We are, at present, concentrating on data collection and analysis pertinent to the first item of work under Approach. Previous studies<sup>[1,2]</sup> have suggested that a model consisting of a two-layered atmosphere with a rough interface is a helpful guide in placing much of our data into a useable framework. Realistic atmospheric models have been constructed, based on the data taken. Ray-tracing and refractivity integration along rays sweeping through these models then give estimates of the range and range rate errors that certain atmospheric conditions may produce.

The roughest interface in the two-layered model is caused by growing cumulus clouds. Cloud photography is a very valuable tool because this cloud-caused roughness is visible. Figure 1-1 is a sketch showing the relation between the two-layer model, with cloud, sweeping the line-of-sight, and the resulting error quantity. In the case of a single cloud, the quantities contributing to a momentary error in an interferometer system are the value of the difference of refractivity between the clear and cloudy air ( $\Delta N$ ), the sweep rate, and the shape of the cloud top, i.e., the rapidity of the increase of "T" with angular change ( $\Delta \theta$ ).

Figure 1-2, illustrates some of the geometrical and atmospheric considerations. An attempt is made to demonstrate the source and magnitude of range rate errors created by cloud towers. To simplify the picture, the problem of cloud shape is ignored at this point. The interface in the two-layered model is assumed to have a step change so that a line-of-sight intersects the upper corner of this step. A line-of-sight is swept through this step at the rate of one milliradian per second. The resulting values of range rate errors and their sources are given for various altitudes and distances from the surface station. Values of the horizontal speed at a point along

# SINGLE CLOUD EFFECTS



1-18

$$\text{ERROR (R)} = \frac{10^{-6}}{R^2} \int_0^{\infty} \Delta N ds \approx 10^{-6} \Delta N T$$

Figure 1-1

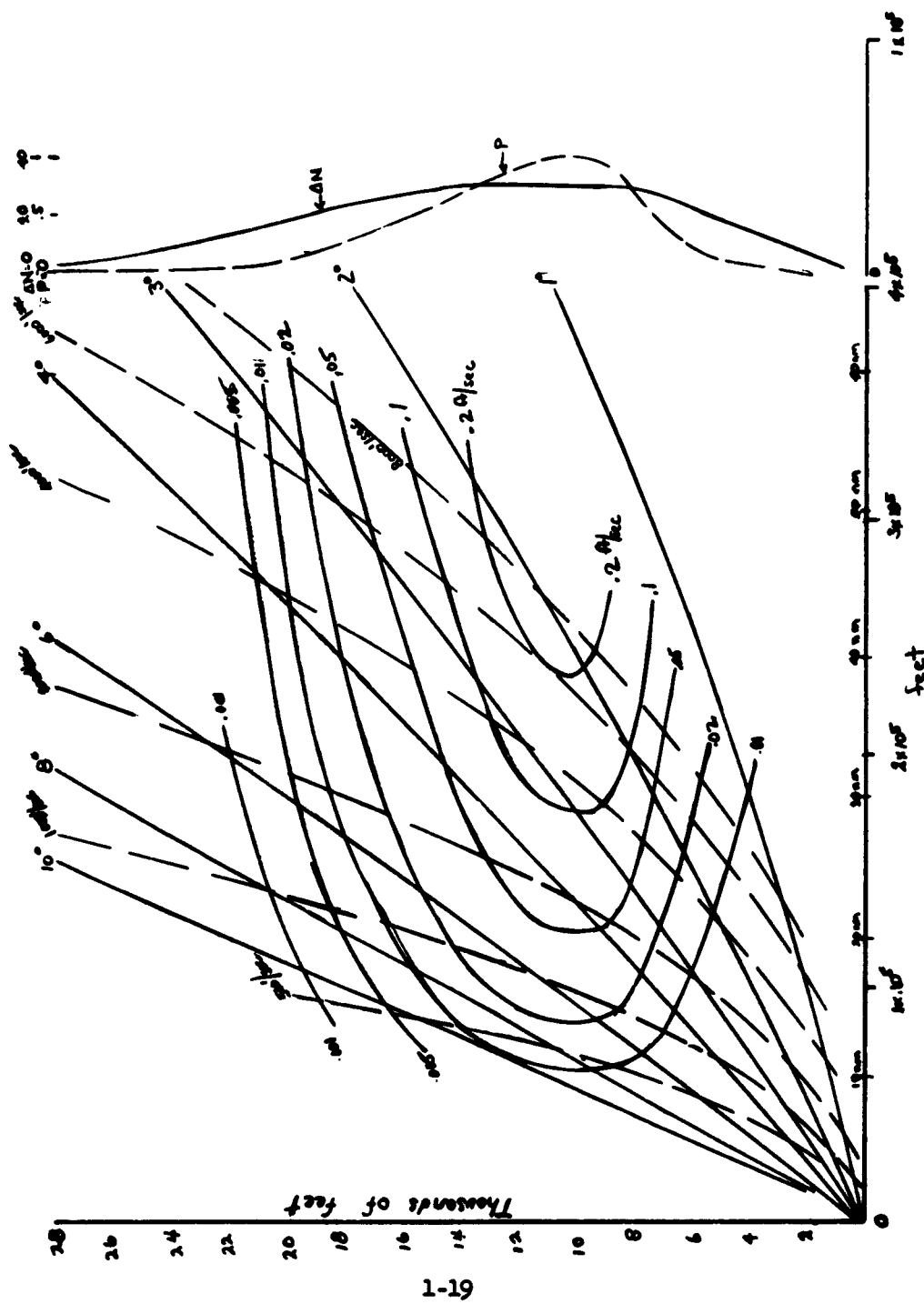


Figure 1-2

the ray are also given. It is further assumed that the number of such steps encountered per sweep is given by the quantity  $P$ , which is a function of height. (This is to simulate the fact that cumulus cloud tops are more frequently found at mid-altitudes.)

The value of  $\Delta N$  is also a function of height, and is greatest where the more vigorous clouds tower into the dry air. The value of  $\Delta N$  decreases at greater height because of the colder temperatures and resulting lower saturation, vapor pressure and lower total value of the moisture contribution to refractivity.

A combination of all these factors gives the range rate errors (feet per second), shown by the isolines with this particular model. This chart (Figure 1-2) indicates that an appreciable range rate error is frequently produced at 6 degrees by the sweeping of a ray through disturbances in the middle atmosphere (10,000 feet), 15 to 20 horizontal miles from the ground receiver.

Analysis, until this fall, has been concentrated on the computation of range and range rate errors from the two-layer model with roughened interface, roughened by wind sheer, gravity waves or by strato cumulus cloud development. The results of this work have been published.<sup>[1]</sup>

The atmosphere has a great variety of structures. One discussed in the publication showed the effect of the undulating interface between a moist layer near the sea surface and dry air above on an interferometer tracking system. The extensive measurement program of this past August near the MISTRAM Valkaria system was designed to produce data on quite a different structure, one dominated by towering columns and bubbles of very moist air made visible by condensation as they rise into the middle drier atmosphere. This particular structure is very prevalent during the summer months over the Florida Peninsula — in fact, a daily occurrence. One aspect of this structure of great importance to the Florida MISTRAM is the difference in the daily cycle of cumulus growth over land and over the water to the east.

It is normal in summer to have the line-of-sight from the inland MISTRAM station sweep through many clouds, while the two coastal stations sweep through a fairly smooth (in terms of a refractive index) cloudless atmosphere.

An extensive effort was initiated in August (1963) to gather three-dimensional meteorological data over the Florida MISTRAM site for a detailed look at the effect of summertime atmospheric structures on MISTRAM errors.

This investigation was greatly assisted by cooperating groups interested in cloud physics, mesometeorology and atmospheric electricity.

A cross section (Figure 1-3), between MISTRAM's 100K west station, through the central MISTRAM station, to a point offshore shows types and some of the locations of the equipment used in the August period. The Tiros Satellite was not in the schedule but fortunately it passed by quite often, producing some interesting pictures of cloud patterns over the state of Florida to compare with the detailed cloud pictures obtained by the U-2 used on this project. The U-2 which flew for this project on almost every mission day is the aircraft used and instrumented by our laboratory. Its flight pattern was generally a racetrack, with one leg in the plane of the cross section and the other five miles south. Three refractometer-equipped aircraft were used - AFCRL's Cloud Physics C-130, and two AMR C-131's. One was under the technical control of RCA with AF project operators, the other newly equipped and project-operated by Electromagnetic Research Corp. for this project. Except for the two days of pertinent missile shots, one or more of these latter aircraft flew at various altitudes in the plane of this cross section. AMR, under OD No. 069, supplied many radiosondes and wiresondes, and operated the cloud cameras and surface weather instruments at the five MISTRAM stations.

A double-theodolite Pibal station was operated by the AFCRL Cloud Physics Branch midway between the 100K and MISTRAM central stations.

TIROS

← U-2

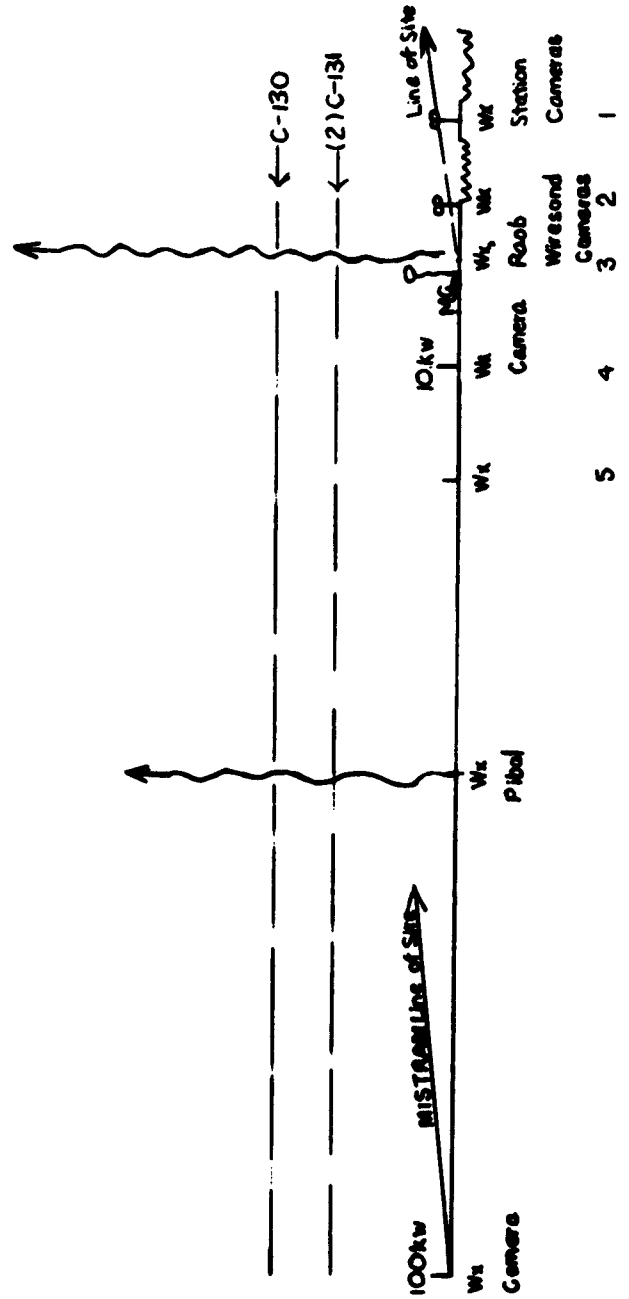


Figure 1-3

The list of various units and organizations involved in the August project are given in Table 1-1. A glance at this chart will show that, except for weekends, most of the observational tools were operating for sixteen days. On two days, we operated along with a missile shot tracked by MISTRAM. On August 2, the missile was tracked only for a short time, and on August 21, the shot was delayed until the whole MISTRAM area was closed-in with heavy rain and thunderstorms. Some meteorological data on this latter day may be comparable with MISTRAM results. Because of the complexity of the weather during the afternoon of August 21, these data have not been analyzed as yet. An idea as to the difficulty of obtaining data for a comparison between radio and meteorological parameters can be obtained from the record of this August period. Electromagnetic Research Corporation's continuous operations from Patrick Air Force Base increase the probability of obtaining a significant number of cases with both meteorological and MISTRAM data.

Three sets of data for the early missions in August were recently assembled. They illustrate the typical summer morning-to-midday weather development and refractive index structure change in the Florida MISTRAM area.

The first case analyzed was for August 9. The refractive index profiles computed from the four radiosonde soundings on the ninth are shown in Figure 1-4. The ability to obtain more than the usual one radiosonde during a short period is a great asset, as is evident on inspection of these profiles; trends can be found, it can be determined whether excursions from a smooth change with altitude are momentary moist regions, such as cloud, or features that may last several hours. Compare, for instance, the anomaly at 17,000 feet, which slowly fades out from 08:07 to 10:50 EST, and the momentary pulses at 9500 feet at 10:50 EST. Analysis of a series of this type of radiosonde data will indicate how representative the bias corrections are when based on one radiosonde and used to correct MISTRAM data.



Table 1-1  
MISTRAM AREA, FLORIDA  
Log of Cloud Physics Refractive Index - Atmospheric Electricity Research

	1	2	3	4	5	6	7	8	9	10	11	12
SATELLITE	V						V	V	V			V
AIRCRAFT	Tiros (NASA WxB CRL)											
	{ U-2 (CRL-AFFTC)											
	{ C-130 (CRL-ESD)											
	{ C-131 (CRL-ERC-AFFTC)											
GROUND RADAR	{ C-131 (AFFTC-RCA)											
	{ Super V (ADL)											
	{ Weather CPS-9 (AWS-4th WX)											
	{ Tracking FPS-8 (AMR)											
SPERICS	{ APN 59 XX (ADL-ONR)											
	{ Sparsa K (Gen M.-CRL-ONR)											
	{ Sparsa (Gen M.-CRL-4th Wx)											
	{ T-11's (CRL)											
GROUND PHOTOGRAPHY	{ 35 mm (Max 12) (CRL-UC-AMR-ADL)											
	{ Whole Sky Site 3 (AMR)											
	{ Whole Sky Site 6 (CRL)											
	{ Radiosonde (AMR)											
BALLOON	{ Wiresonde (AMR)											
	{ Pibal(s) Site 6 (CRL)											
	{ MISTRAM Stas Mx 5 (AMR)											
	{ C.P. Proj. Stas Mx 10 (CRL-UC-WxB)											
WEATHER STATION	{ C.P. Proj. Extra Pres.Sta (CRL-UC)											
	{ C.P. Proj. Extra Rain Sta (CRL-UC)											
	58	71	71	71	64	58	64	63	71	57	57	68
GROUND ELECTRIC FIELD	{ ADL Site (ADL)											
	{ MISTRAM 10K + Mobile (CRL)											
	{ MISTRAM Radio Data											
	V	V	V	V	V	V	V	V	V	V	V	V
		X										

Table 1-1 (Continued)

	13	14	15	16	17	18	19	20	21	22	23
SATELLITE	V		V	V	V	V		V	V		V
	Tiros (NASA Wx B CRL)										
AIRCRAFT	V	V	V	V			V	V	V	V	V
	U-2 (CRL-AFFTC)										
	C-130 (CRL-ESD)										
	C-131 (CRL-ERC-AFMTIC)										
	C-131 (AFMTC-RCA)										
	Super V (ADL)										
GROUND RADAR	V	V	V	V	V	V	V	V	V	V	V
	Weather CPS-9 (AMS-4th Wx)										
	Tracking FPS-8 (AMR)										
	APN 59 XX (ADL-ONR)										
SFERICS	V	V	V	V							
	Sparsa K (Gen M.-CRL-ONR)										
	Sparsa (Gen M.-CRL 4th Wx)										
GROUND PHOTOGRAPHY	V	V	V	V	V	V	V	V	V	V	V
	T-11's (CRL)										
	35 mm (Max 12) (CRL-UC AMR-ADL)										
	Whole Sky Site 3 (AMR)										
	Whole Sky Site 6 (CRL)										
BALLOON	V	V	V	V	V			V	V	V	V
	Radiosonde (AMR)										
	Wiresonde (AMR)										
	Pibal(s) Site 6 (CRL)										
WEATHER STATION	V	V	V	V	V	V	V	V	V	V	V
	MISTRAM Stas Mx 5 (AMR)										
	C.P. Proj. Stas Mx 10 (CRL-UC-Wx B)										
	C.P. Proj. Extra Pres. Sta (CRL-UC)										
	C.P. Proj. Extra Rain Sta (CRL-UC)										
GROUND ELECTRIC FIELD	V	V	V	V	V	V	V	V	V	V	V
	ADL Site (ADL)										
	MISTRAM 10K + Mobile (CRL)										
	MISTRAM Radio Data										

Table 1-1 (Continued)

Footnotes

NASA	-	National Aeronautics and Space Administration
WxB	-	U.S. Weather Bureau
CRL	-	Air Force Cambridge Research Laboratory
AFFTC	-	Air Force Flight Test Center
ESD	-	Electronic Systems Division
ERC	-	Electromagnetic Research Corp.
AFMTC	-	Air Force Missile Test Center
RCA	-	Radio Corporation of America
ADL	-	Arthur D. Little Company
AWS	-	Air Weather Service
AMR	-	Atlantic Missile Range
ONR	-	Office of Naval Research
Gen M.	-	General Mills Electronics Group (now called Litton Systems, Inc.)
U.C.	-	University of Chicago

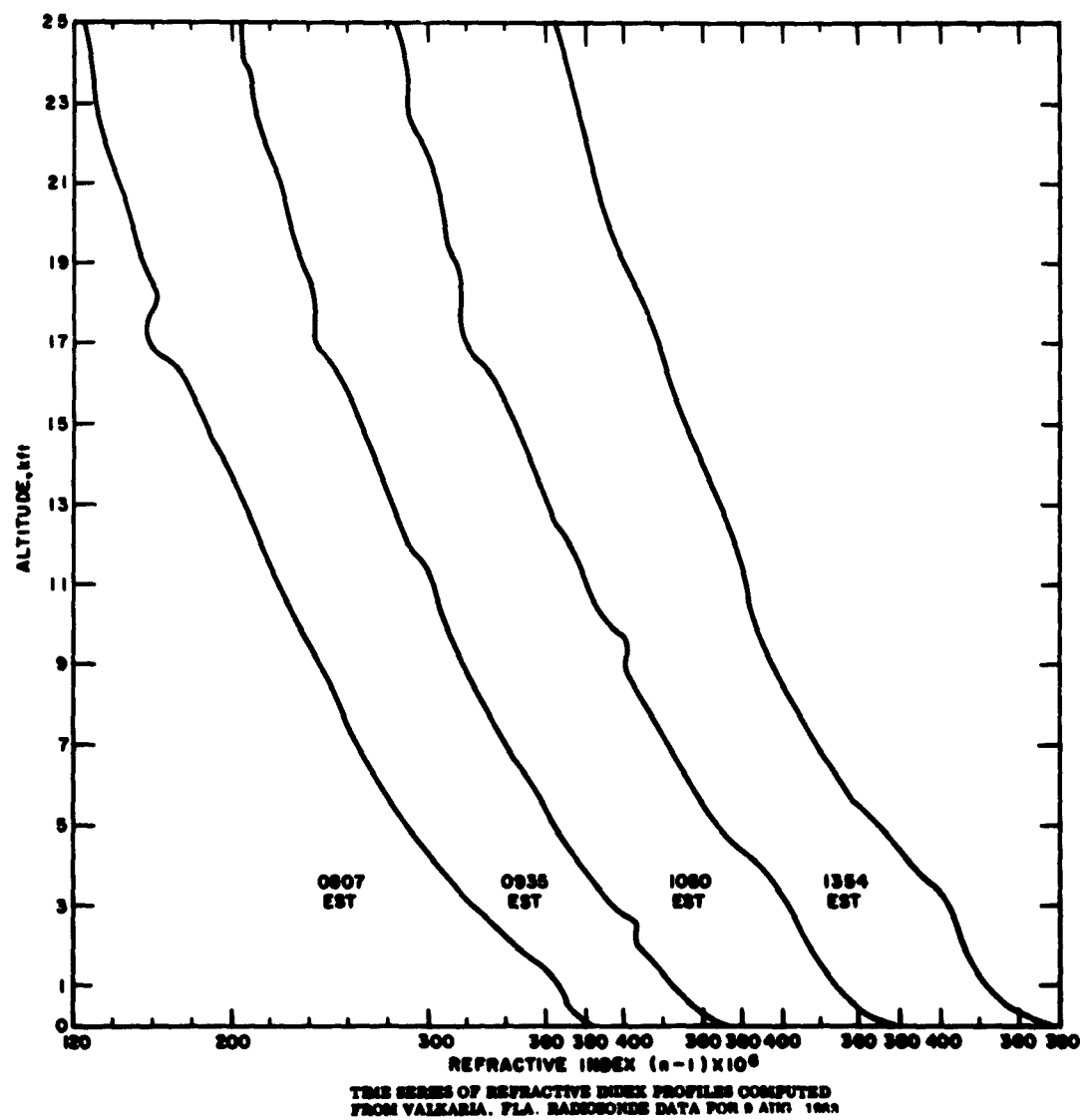


Figure 1-4

These four radiosonde refractive index profiles show no major structural change during the morning of the ninth. Heating of the first 2000 feet of air between 08:07 and 09:35 caused the lowest layer index values to drop by some 15N units.

Radiosonde data can be used to obtain an estimate of the cloud-to-clear air difference in refractivity. This use is illustrated in Figure 1-5. A complete explanation of the method used is given in Reference 1. The difference between the value of refractivity at saturation and that computed from radiosonde data, is a close estimate of the difference in refractivity ( $\Delta N$ ) between cloud and ambient air. This difference drops from about 25N units in the lower levels to 10N through the 24,000 foot level. This is true because the temperature inside clouds rarely differs by more than one degree from the ambient and because the radiosonde does not usually go through clouds since the clouds in the situations for which this method is used cover less than half the sky.

The next four figures show the pattern of cloud development and related surface mesometeorology for the period probed with the aircraft. While examining these figures, one should keep in mind that essentially each cloud coincides with a sharp-edge hemisphere-capped cylindrical "blob" in the atmosphere which produces a large refractivity excess.

Figure 1-6 is a mosaic made of pictures taken with a special camera from the U-2. The match between strip pictures is only perfect along the center line (cloud bases were matched, not ground features). Parts of the same cloud will appear twice at the individual picture edges at the top and bottom of this mosaic. The outer coastline is visible at the extreme right of this figure - Melbourne beach is in the upper right, Sebastian inlet at the lower right. A cross on the right side of the picture marks MISTRAM central - MISTRAM's two short legs are dimly visible. The 100K west MISTRAM station is marked by the cross at the left side of Figure 1-6.

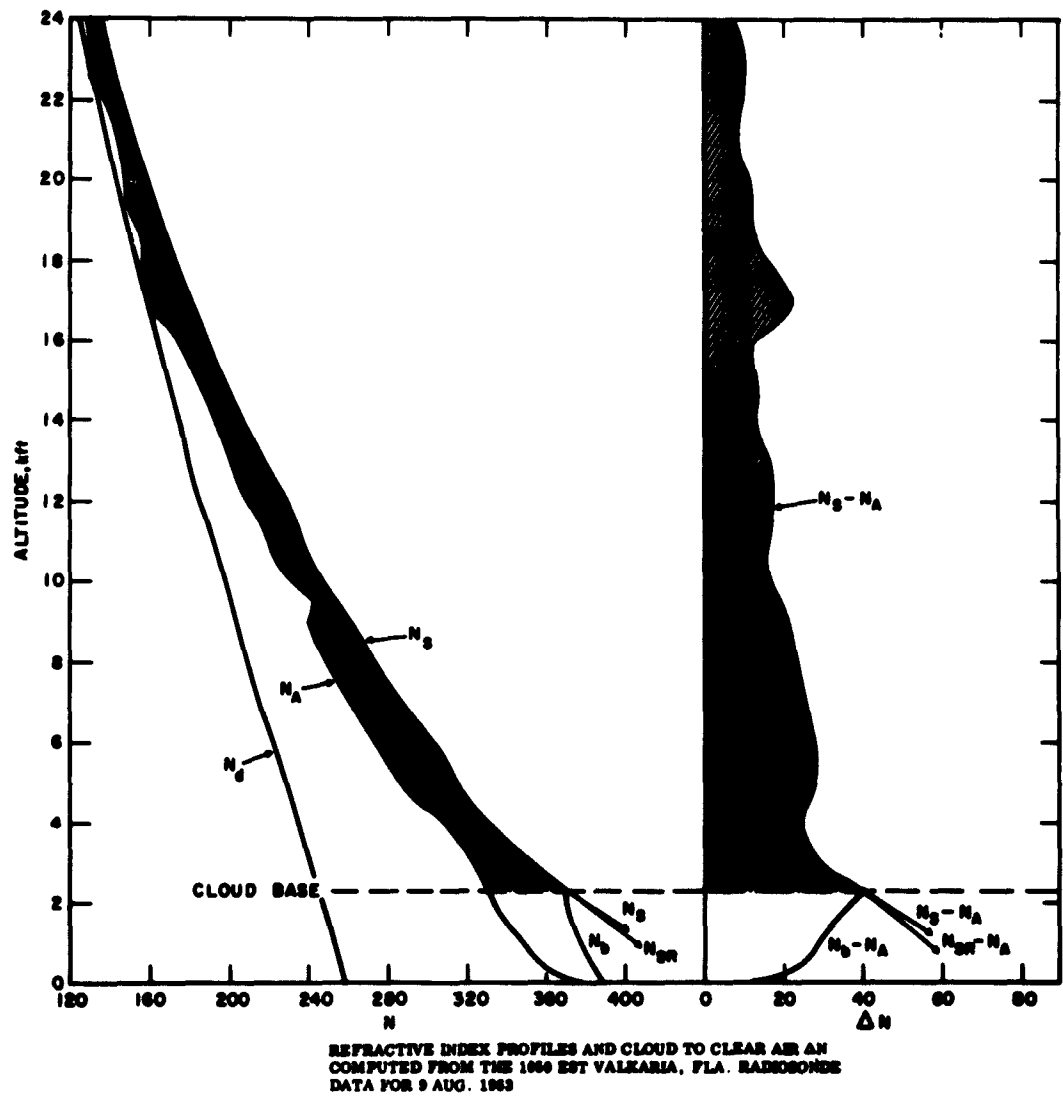


Figure 1-5



9 AUGUST 1963 1021 EST

Figure 1-6

One may visualize a line-of-sight sweeping down across the many clouds in any direction from 100K west. In the downrange direction, the 100K west station radio line-of-sight would intersect four or five clouds. At angles below 8 degrees, the top portion of only a few smaller clouds are intersected as the clouds disappear eastward beyond the coastline. A line eastward from central MISTRAM (and also presumably from 100K) would, at the lower angles of interest, sweep down underneath the nearby clouds and through the clear, smooth atmosphere over the Atlantic.

A surface map (Figure 1-7) shows the approximate stream lines of surface air flow, temperature and mixing ratio 4 feet above the ground. The dark, shaded areas are the cloud outlines as traced, approximately corrected for prospective distortion, from the U-2 mosaic. This is a typical day with a gentle wind flow from the W NW. The beginning of a sea "turn" is in evidence at the Sea Dunes motel station along the outer coast.\* Note the temperature maximum for the time of day (10:20 EST) at the outer beach station. At this time, it is under clear skies with very light winds. Moisture isolines are drawn for values of the mixing ratio, computed from hairpropygraph\*\* and thermograph recordings at each of the 15 surface stations. The 2g/kg difference between the coastal stations and stations a few miles inland should be noted with reference to bias error calculations. A value of 2g/kg at the temperatures shown corresponds to a difference of 13N units. This map also shows the location of all but three of the special surface stations. The triangle in the lower right portion of the map indicates the location of the principal Arthur D. Little (ADL) station.

---

\* Wind velocity "Feathers" are double the standard scale. One full feather indicates a 4-to-6-knot wind.

\*\* The readings were adjusted so that the maximum nighttime indication, a flat-topped record, would read 100 per cent humidity, a humidity in agreement with the frequent radiation fog observed.



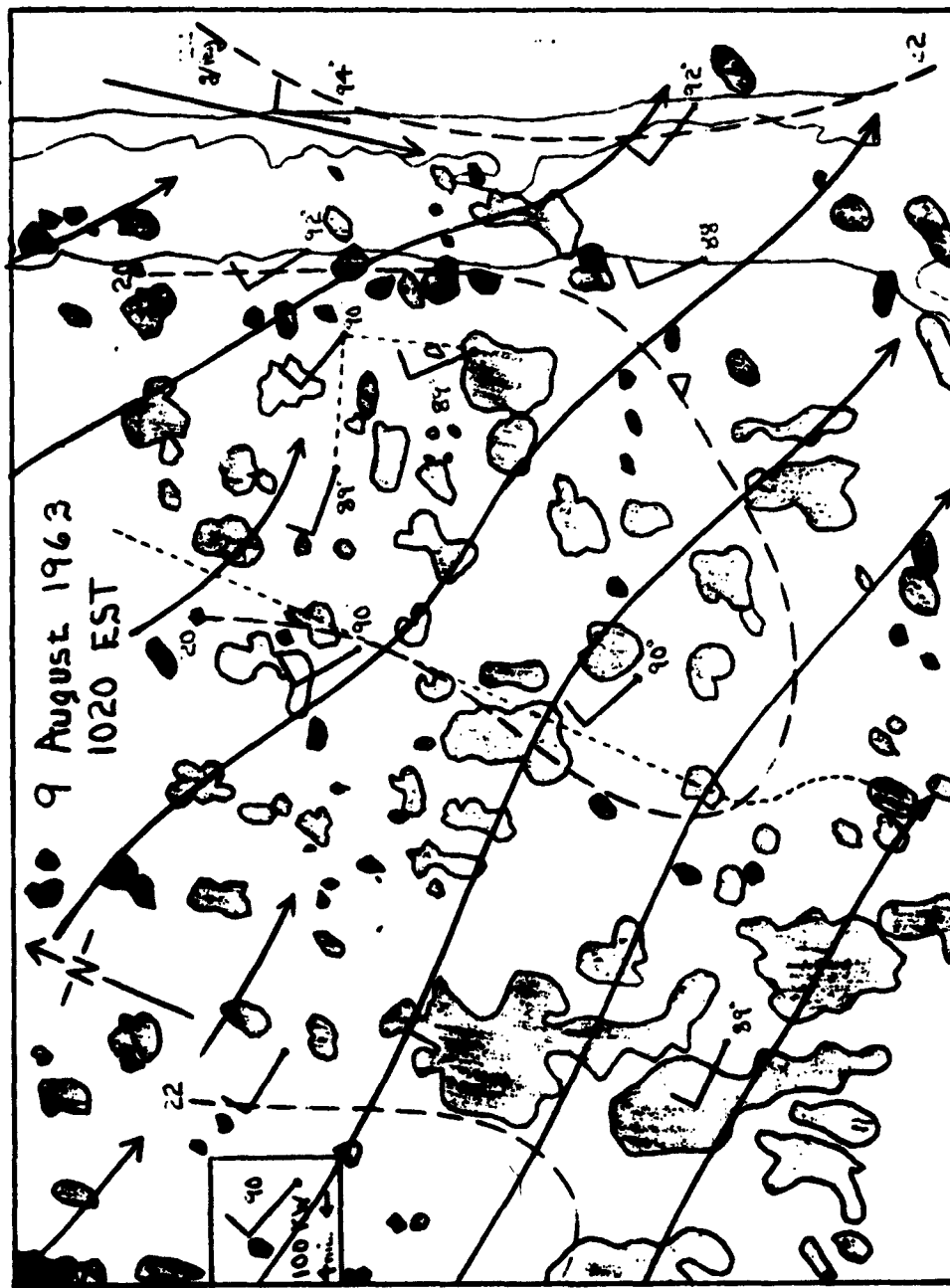
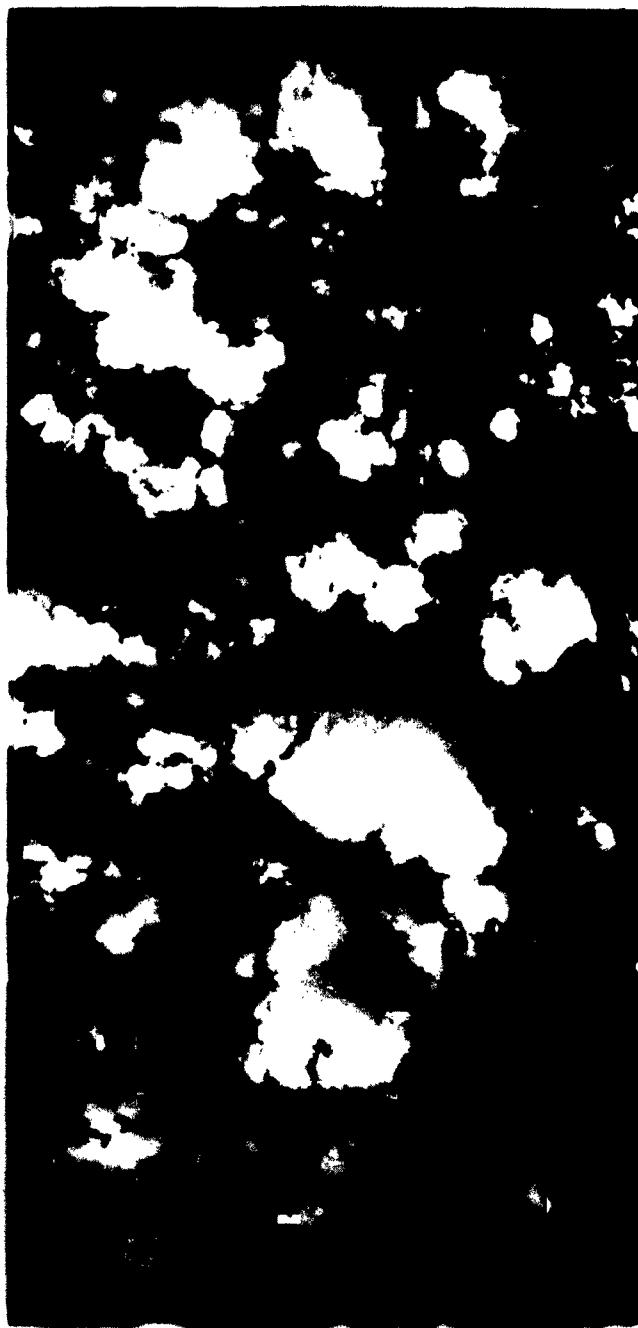


Figure 1-7

In but 50 minutes the clouds grew considerably in both horizontal and vertical dimensions (Figure 1-8). Several clouds are, at their bases, 10,000 feet in diameter. Clouds are rapidly bunched along the coastal strip. Just east of 100K, where they had a head start, they grew to 30,000 feet in height and produced showers. The tallest and largest clouds are exaggerated in size, as their tops reach half-way to the U-2 aircraft. The mesoscale map, Figure 1-9 indicates light winds along the main coast, with a steady 5-knot sea breeze crossing the strand. Clouds are concentrated along this region.

Flight data for five passes and a cloud cross section have been plotted Figure 1-10. The refractive index recordings in N units are plotted in the upper portion of the figure. To a true scale, the clouds, roughly corresponding to conditions on Run 5, are plotted from a synthesis of the flight data and both U-2 and C-130 photographic coverage. The flight refractive index data are traced directly from the original "100-pen" record; the time scale is, therefore, the same for each pass, but the distance scale changes. Identification points are marked, i.e., the ocean beach (BEACH); Route 1 along the main shore (RT 1); MISTRAM central; a north-south main road, Babcock extension (BAB); AFCRL's Pibal Site (SITE 6) and the 100K west MISTRAM station. Time is indicated as total time in seconds, since the clocks were started on the runway. Passage time in EST over MISTRAM central is indicated on the right. The most striking general characteristic of these traces, a characteristic of most of the days sampled, is the change from small-amplitude fluctuations at the lowest level to large fluctuations at cloud base and at mid-cloud level, to a smooth trace of the highest levels except for the spikes and "square" waves caused by the clouds. Just below cloud base, the major changes in refractivity appear to be downward from a vague, high average, while at 1000 to 2000 feet above cloud base level, excursions are upward from a vague low average. The downward excursions below base are probably associated with relatively dry air from descending currents around the cloud edges, currents that



9 AUGUST 1963 1112 EST

Figure 1-8



Figure 1-9

0406.1001



**Figure 1-10**

originate from evaporating cloud edge material.

While this figure gives the impression of a randomly turbulent atmosphere, note should be made of the nonlinear arrangement of heights chosen for the passes (roughly, each pass height is twice the height of the previous pass). One may be justified in applying statistical analysis procedures to the data of passes 1, 2, and 3, but should not for the data of passes 4 and 5. Power spectra are shown at the end of this paper for passes 1 and 3. A different statistical analysis method is being considered for the upper passes. This method will use the U-2 cloud mosaics, and the cloud refractive index "square" wave concept to generate sufficient data for significant statistical processing.

A glance at the data from run 5 suggests that not all of the pass data shown fit the category of good "square" waves. The next six figures compare in detail the refractive index trace with the condition of the cloud probed.

Figures 1-11 and 1-12 are companion figures. The refractive index trace shown in Figure 1-11 exemplifies what we have called a "square" wave cloud trace. The very sharp rise in the refractive index at entrance and exit to the cloud is obvious. The slight rounding of the exit trace reflects the slight lag and mixing associated with the refractometer ducting system and a cavity flushing time. The sharp change occurs in less than one-tenth of a second or less than 35 feet (probably in about 10 feet). The sharp dip just after entrance and before cloud exit corresponds to a common eddy size, or size of the main cauliflower-like roughness on the cloud surface, of the order of 500 feet.

The variations in the cloud interior are due partly to temperature changes but primarily to cloud evaporation; partly dry, unsaturated air is being mixed in from the top or side. The two photographs shown in Figure 1-12 were taken by the nose time-lapse camera 36 seconds before

Refractive Index Trace  
through a  
Growing Cumulus Cloud

August 9, 1963  
Flight No. 244  
Run No. 5

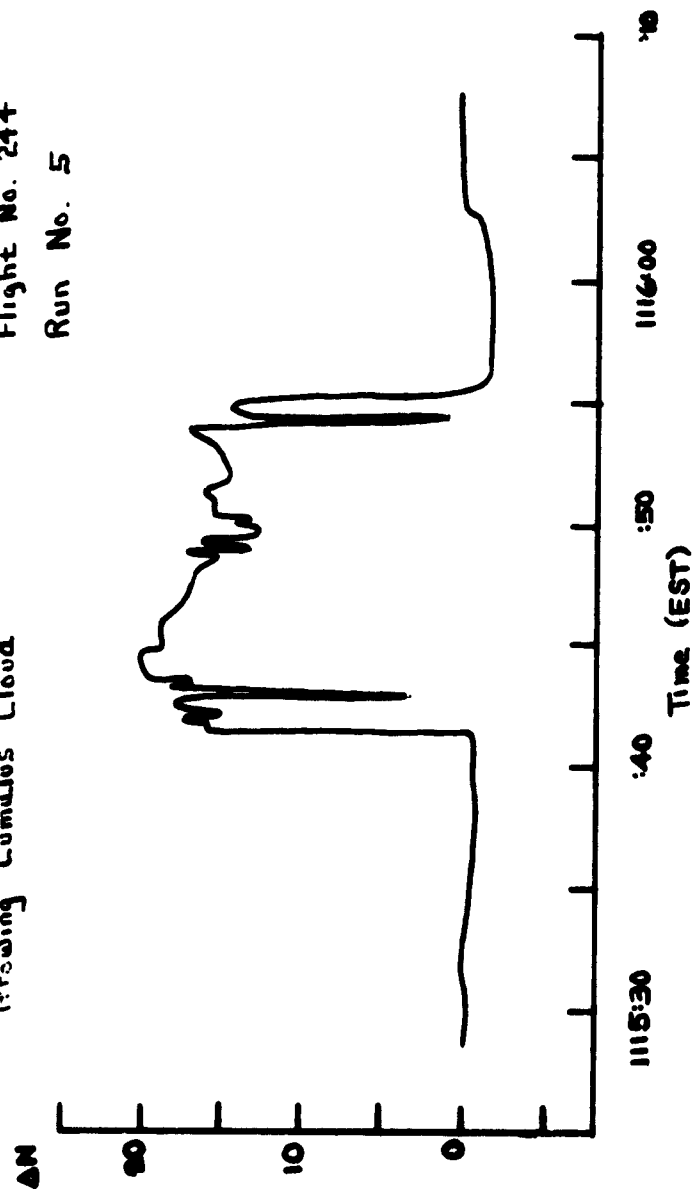


Figure 1-11



**36 sec BEFORE PENETRATION**



**15 sec BEFORE PENETRATION**

**C-130 16 mm NOSE TIME-LAPSE PHOTOGRAPHS OF CLOUD PENETRATION AT 9042 sec (1116 EST.) DURING RUN NUMBER 5 (ALT. 14.5 kft) OF FLIGHT 244 9 AUG. 1963**

**Figure 1-12**



penetration and 15 seconds before penetration, respectively. The sharp edges of the cloud are evident.

The refractive index record from the cloud probed near the coast on pass 5 is shown in Figure 1-13. Nose camera photos of this cloud are printed in Figure 1-14. Much old evaporating cloud material is concentrated around the center cloud core. The photographs, in particular the close-up shot, show the diffused nature of the cloud edge. The hard, small, top pinnacle, visible in the left picture, is the top of the next cloud to be discussed.

The cloud penetrated at mid-course has an older, large chimney cumulus with a top of 32,000 feet, (Figures 1-15 and 1-16). One large section of the cloud at mid-altitude was composed of rain. The upper portion, well above flight altitude, was still growing upward. The aircraft passed along the edge of the rainshaft, as shown in the right picture of Figure 1-16. Two short sections of saturated cloud were intersected. The most interesting feature is the section of record showing (Figure 1-15) values of refractive index lower than the ambient by 10 to 15N units. Presumably, the cooling of the atmosphere by evaporating rain drives the air downward far enough so that the absolute moisture value of this air, originally at a much greater height level, is, at this new level, even less in absolute terms than the moisture value outside the cloud. From this pass it is obvious that the refractive index structure of a mixed rain and cloud tower can be very complex.

Two further examples of cloud development and associated refractive index structure were analyzed, for the seventh and eighth of August. The series of refractive index profiles from the AMR radiosonde data are given for the eighth in Figure 1-17. The persistence of the dip at 7000 to 8000 feet and the change in shape at 15,000 feet is evident throughout the morning and early afternoon. The inflection at 15,000 feet corresponds to the level where the humidity drops to a negligible amount. The change from a probably

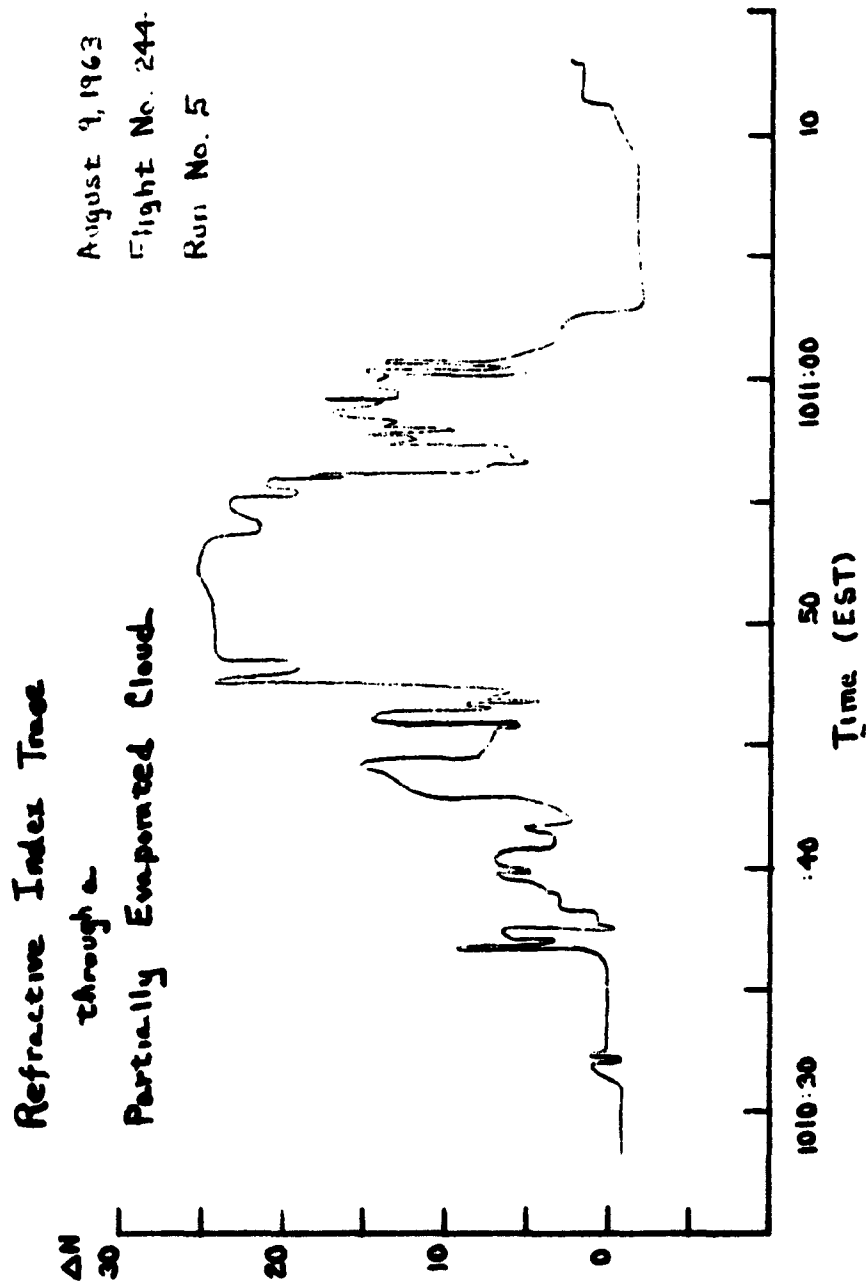
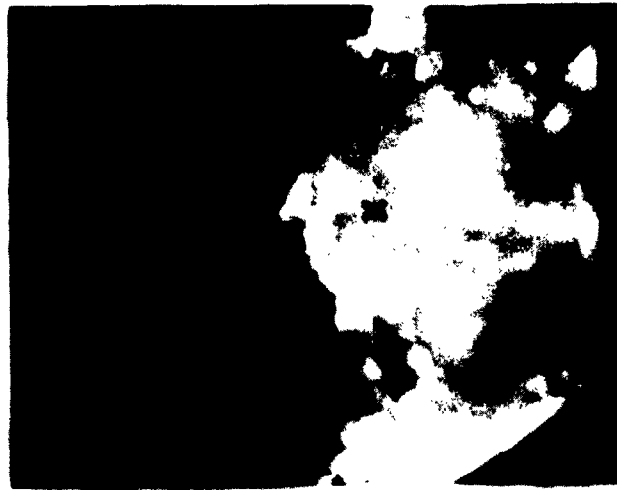


Figure 1-13



**61 sec BEFORE PENETRATION**



**22 sec BEFORE PENETRATION**

**C-130 16 mm NOSE TIME-LAPSE PHOTOGRAPHS OF CLOUD  
PENETRATION AT 8743 sec (1110 EST) DURING RUN NUMBER  
5 (ALT. 14.5 kft) OF FLIGHT 244 9 AUG. 1963**

**Figure 1-14**

# Refractive Index Trace through an Evaporating Cloud

August 9, 1963  
Flight No. 294  
Run No. 5

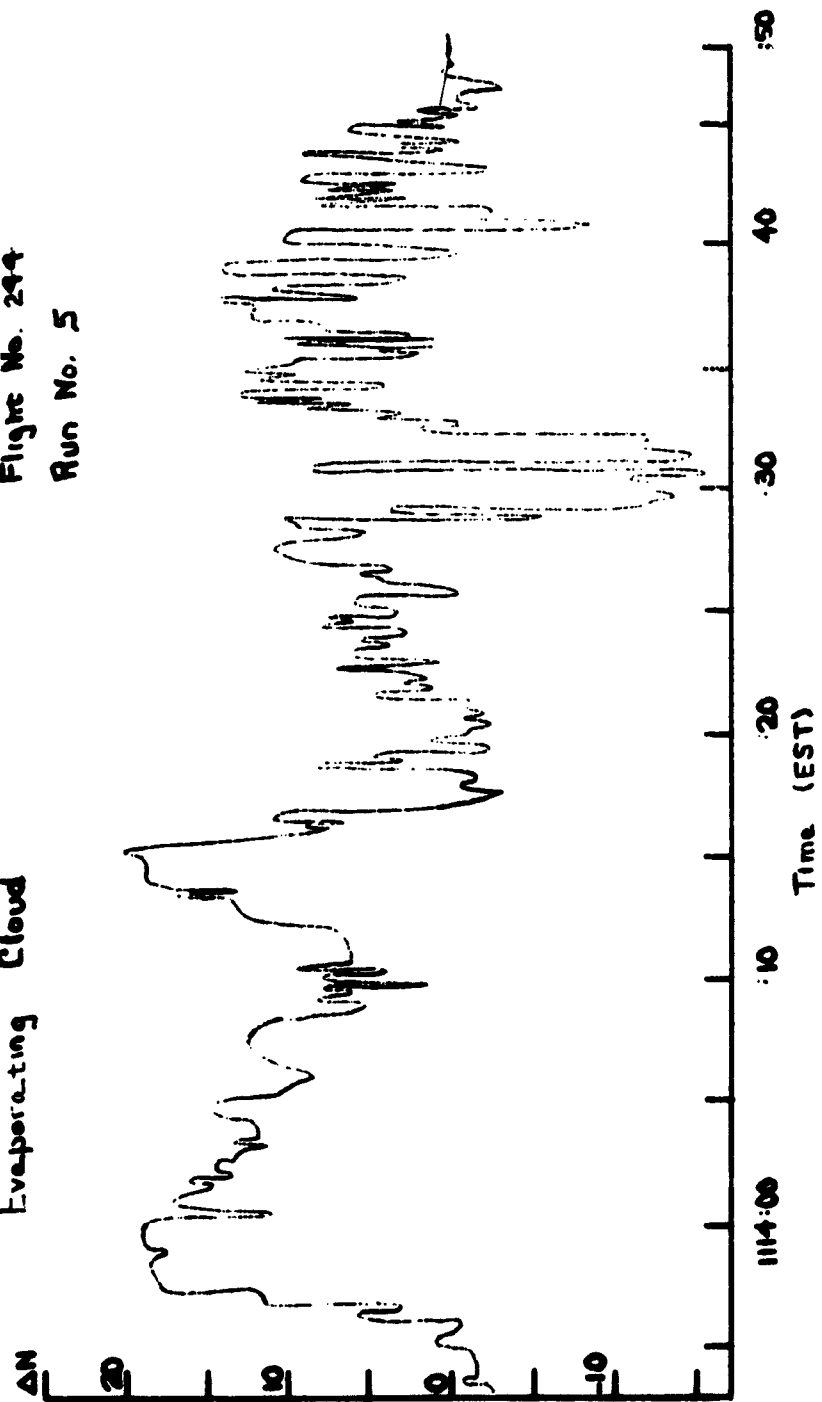


Figure 1-15



101 sec BEFORE PENETRATION    62 sec BEFORE PENETRATION  
C-130 16 mm NOSE TIME-LAPSE PHOTOGRAPHS OF CLOUD  
PENETRATION AT 8936 sec (1114 EST.) DURING RUN NUMBER  
5 (ALT. 14.5 kft) OF FLIGHT 244 9 AUG. 1963

Figure 1-16

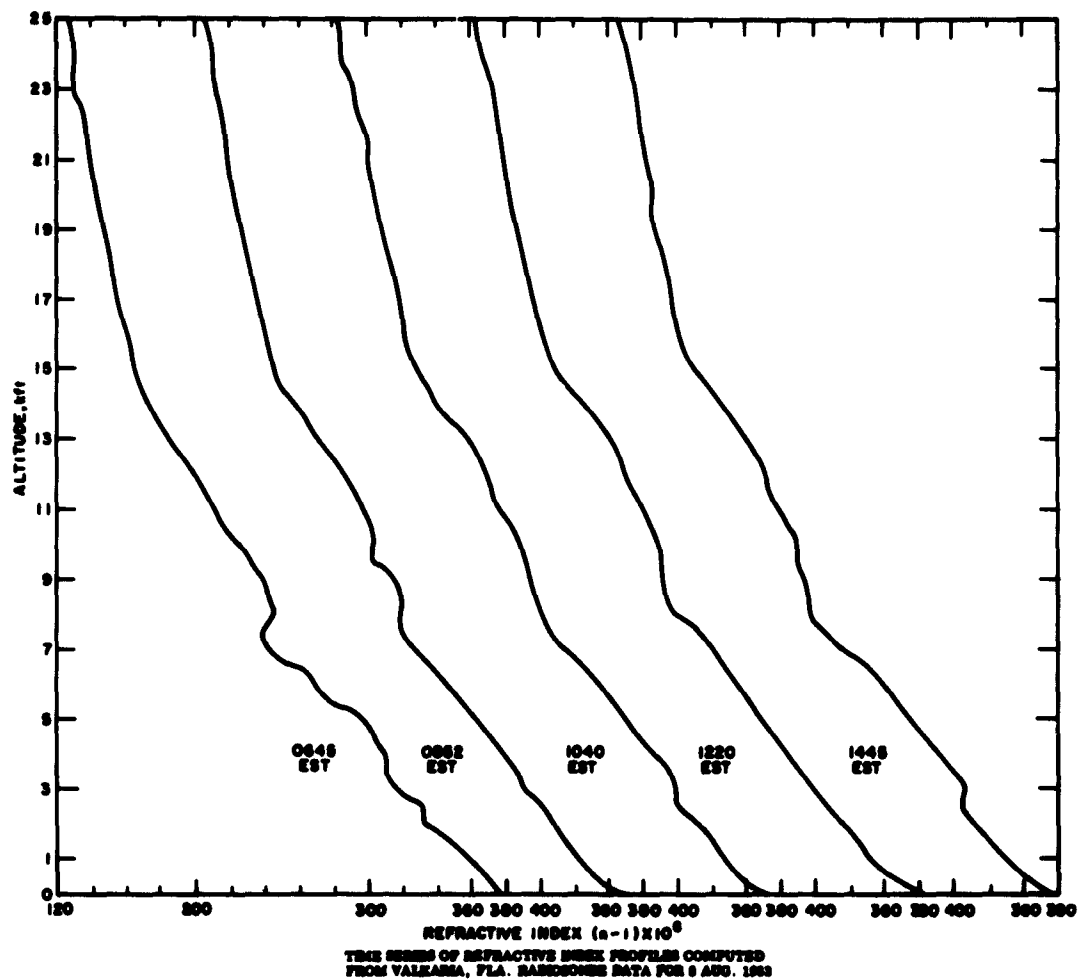


Figure 1-17

complex multi-layered atmosphere between 2000 and 7000 feet at 06:45 EST to a smooth atmosphere by 08:52 is probably the result of mixing by convection, eliminating the stratification that frequently occurs in the subsiding air mass at night.

Figure 1-18 shows the cloud  $\Delta N$  analysis of the 1040 radio-sonde data. Cloud-to-clear air  $\Delta N$  values remained high: 25 to 30N to 19,000 feet on this date. The clouds were smaller and started later on this day (Figure 1-19) than in the previous example. Some of the largest clouds are forming right at the main coastline, with the strand largely clear. A sea breeze on the strand is blowing inland at 5 knots (Figure 1-20). A large moisture gradient is associated with the sea breeze at 4g/kg, or about 26N units. Figure 1-21 shows the cloud distribution at 12:02. The low values of 18g/kg over the three short-base MISTRAM stations are probably caused by an instrumentation problem. Within 75 minutes, the clouds grew considerably and consolidated; many are quite sharp-edged. Again, the marked effect of the sea breeze is evident. MISTRAM central has a clear view from north through east to southeast. Lines-of-sight from the 100-K west station will intersect several solid clouds. The wind flow pattern shown in Figure 1-22 checks very nicely with the cloud pattern.

The results of flight runs made by the AFCRL C-130 are shown in Figure 1-23. This set illustrates the change from minor fluctuations at 900 feet to maximum fluctuation at 6000 feet in an even more dramatic way than the case of August 9. Again, the excursions appear to drop from a high average value at the cloud base. They appear to rise from a long wave length undulation of a short average at mid-cloud level (6000 feet). At 10,000 feet, the  $N$  changes are largely associated with cloud passes; the ambient air, however, appears quite disturbed, probably from the effects of previous cloud turrets. Above 10,000 feet, the clouds are the only disturbing feature to a remarkably smooth atmosphere. Another feature of interest is the

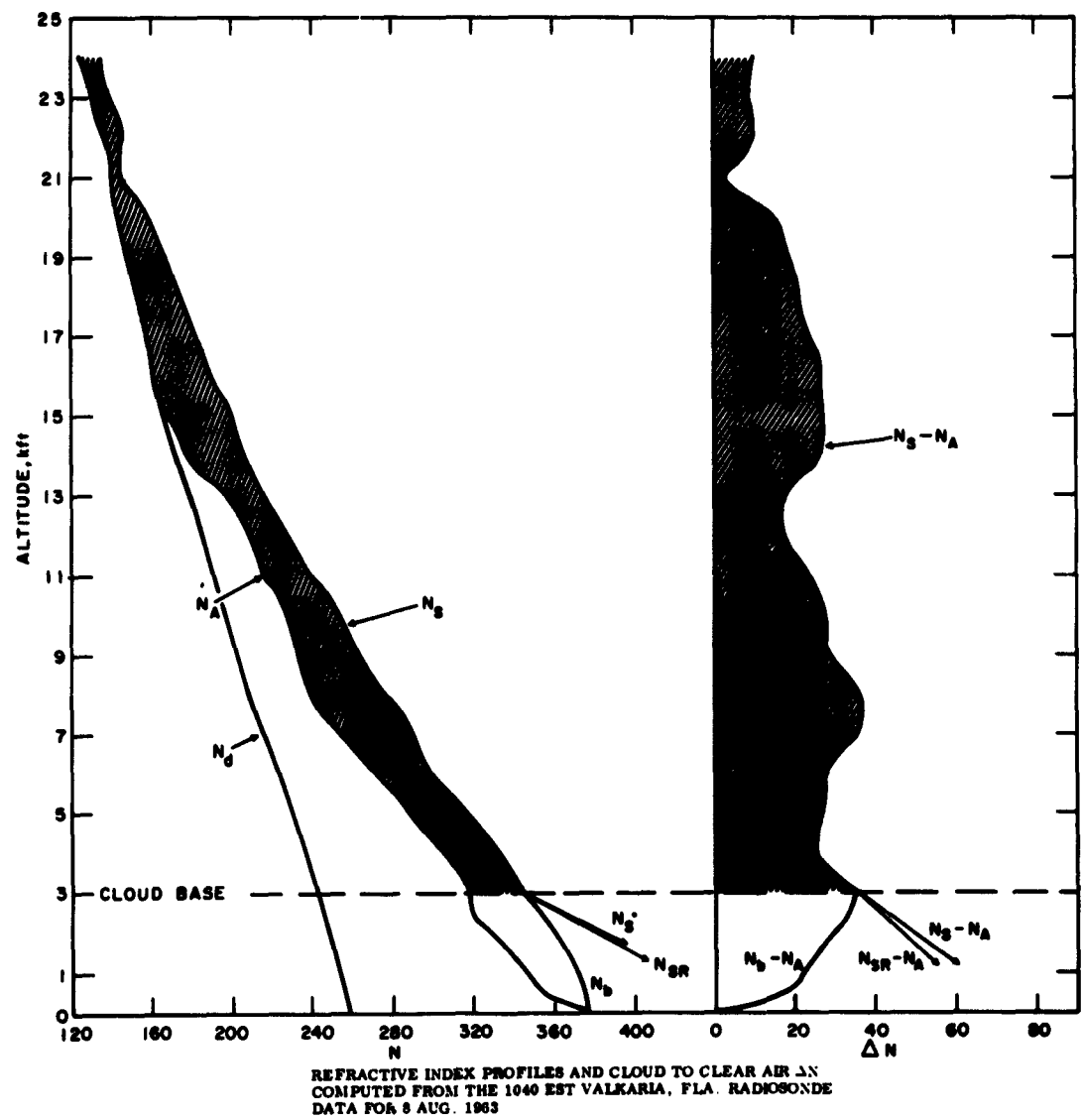


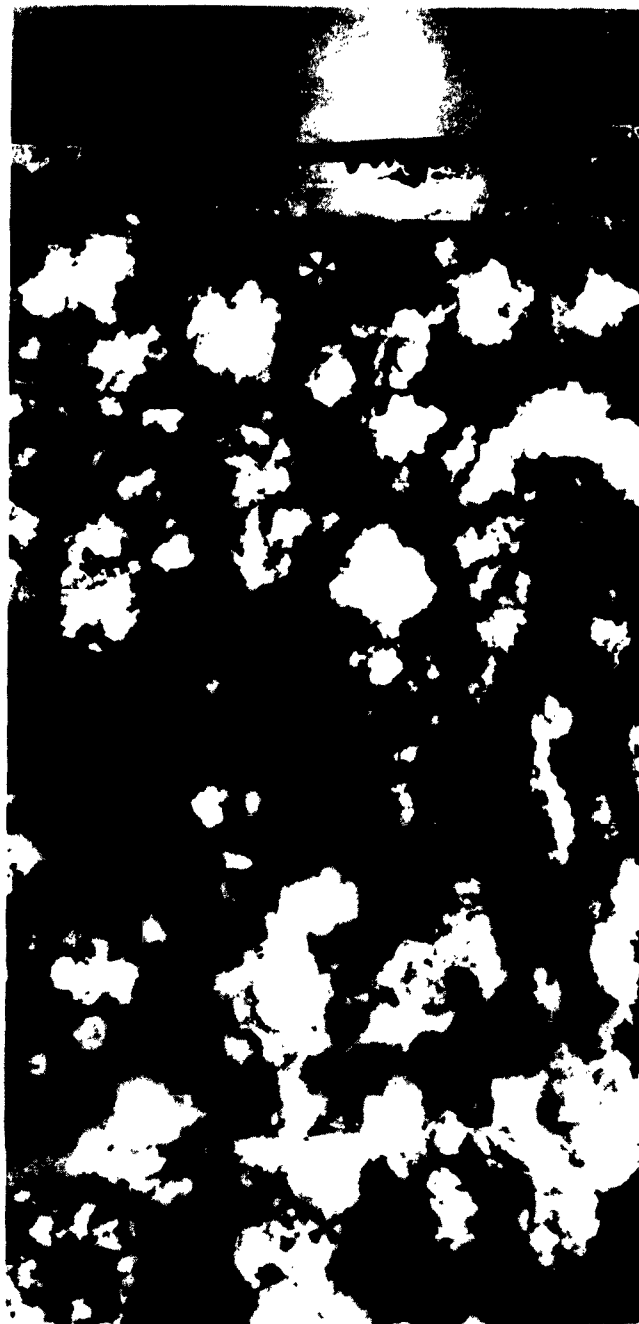
Figure 1-18





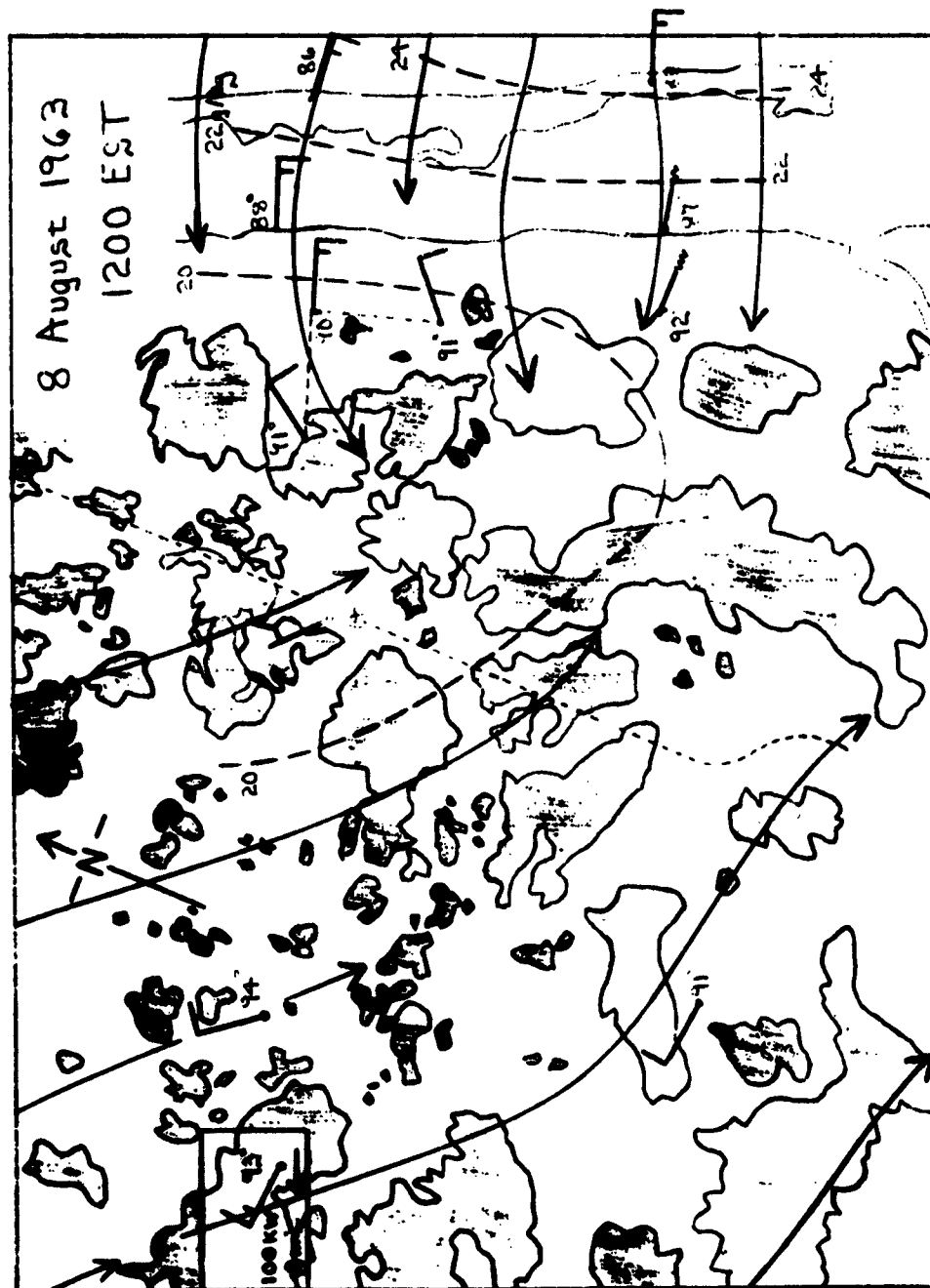
8 AUGUST 1963 1047 EST  
Figure 1-19





8 AUGUST 1963 1202 EST

Figure 1-21



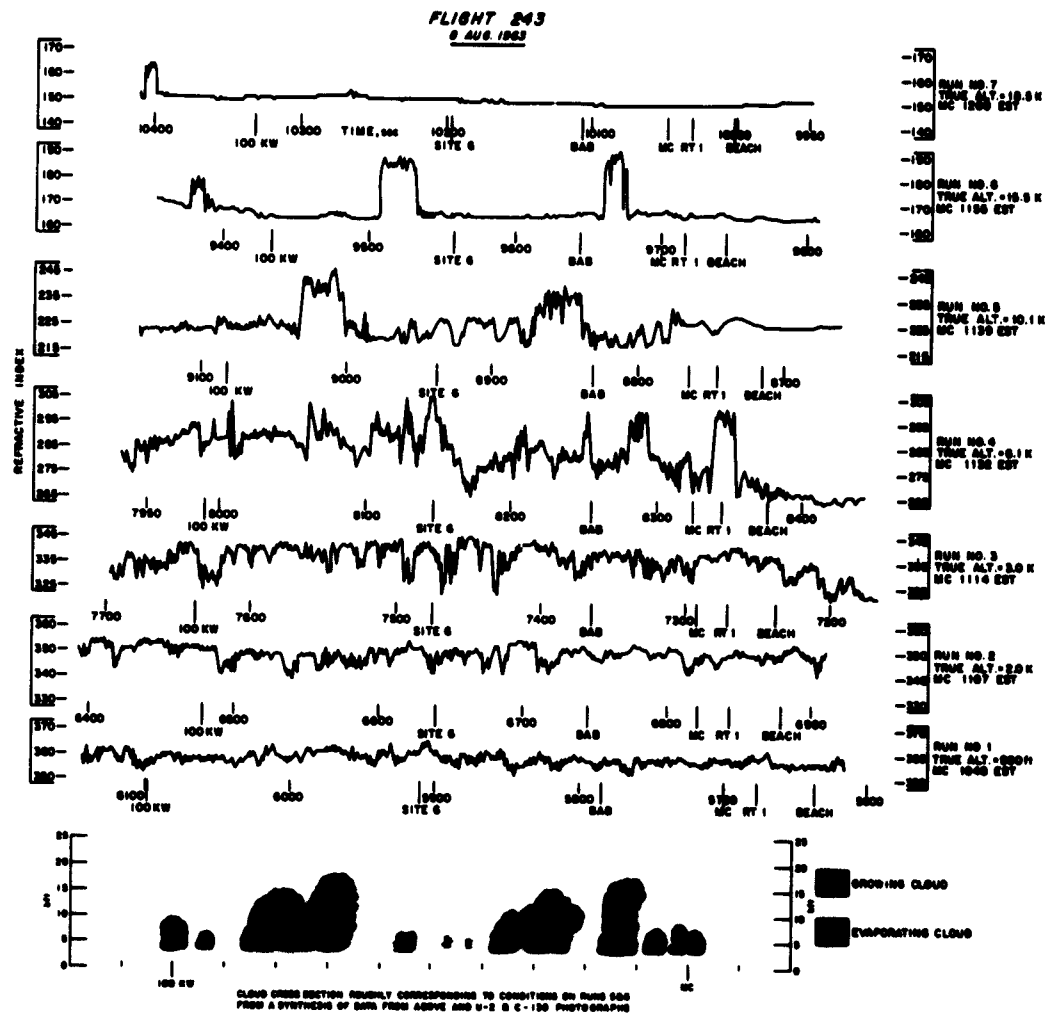


Figure 1-23

decrease of the index east of the beach at 3000 and 6000 feet and the smooth trace from the beach eastward at 10,000 feet. At the MISTRAM central, the sea breeze is 1500 feet thick at 1220 (1220 radiosonde wind data). Above this level, the air is blowing off shore (NW 7-knots). The refractive index fluctuations at 3000 feet were produced inland by convection and carried southeast by the 7-knot wind. At 6000 feet and above, the wind was weaker and parallel to the beach. The moist products of convection were not evident east of the beach above 6000 feet.

The profiles for the last complete case to be discussed, August 7, are shown in Figure 1-24. Here again the early morning change in the slope of the profile in the first 2000 feet is evident. An inflection of the profile at 11,000 to 13,000 feet, where the humidity drops to very low values, is present. Otherwise, the various undulations on the profile appear to be of a momentary nature. In particular, note the excursion at 2000 feet at 13:42 EST. Presumably, the balloon rose through a cloud. The cloud  $\Delta N$  plot, (Figure 1-25) exhibits a rather extreme plot of  $\Delta N$ . This was a day of very low humidity above 8000 feet, winds from the east were moderate through 25,000 feet. This was probably caused by dry air advection from the subsiding air mass of a ridge aloft to the north.

This case shows one of the best developed coastal cloud bands of the August period. By 09:35 (Figures 1-26 and 1-27) an almost solid line of clouds existed west of 10K west. Only scattered small clouds were developing in the calm surface air to the west, and no clouds were present in the gentle east wind over the strand and main coast line. By 10:31 (Figures 1-28 and 1-29) the line of clouds along the "sea" breeze front dominated the picture. Probably because of the extreme dryness of the air above 8000 feet, however, clouds did not grow above 15,000 feet. The cloud line and sea breeze front had reached the Babcock extension by 10:30 EST. For this case, a Tyros photograph was available for comparison. Figure 1-30 is an

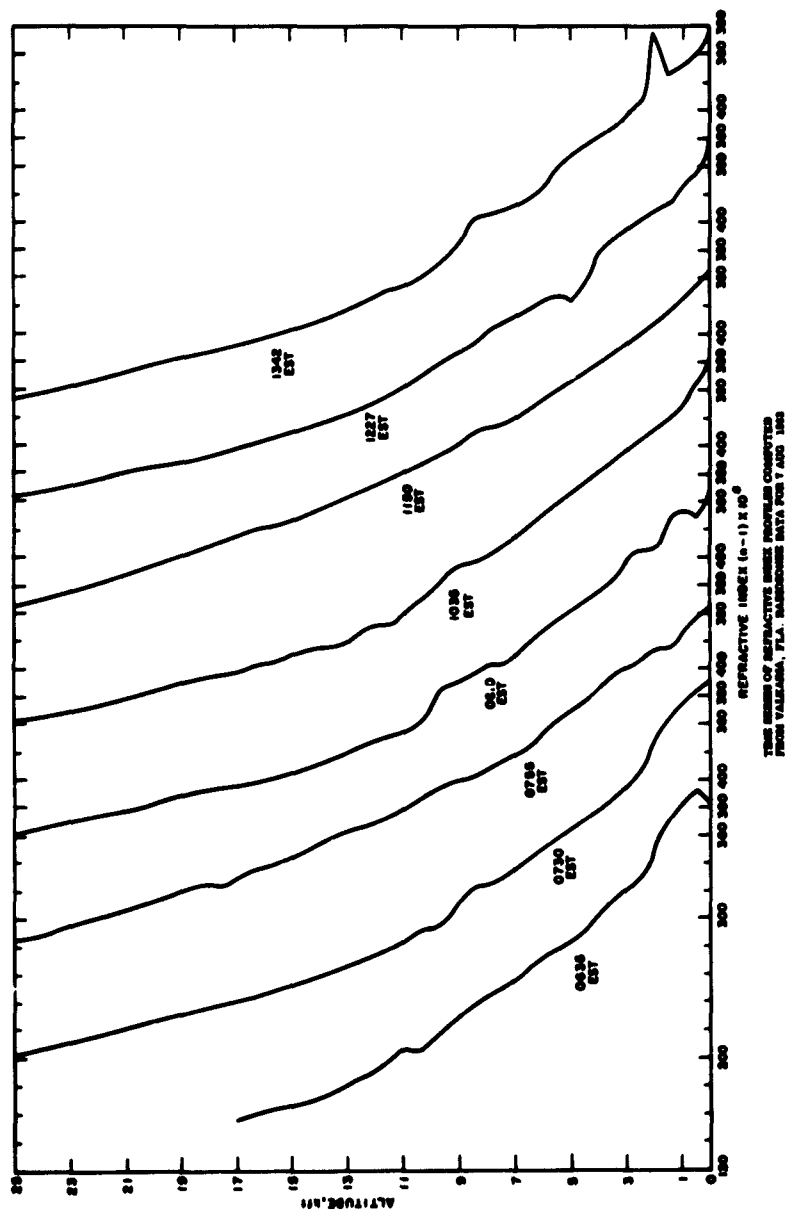


Figure 1-24

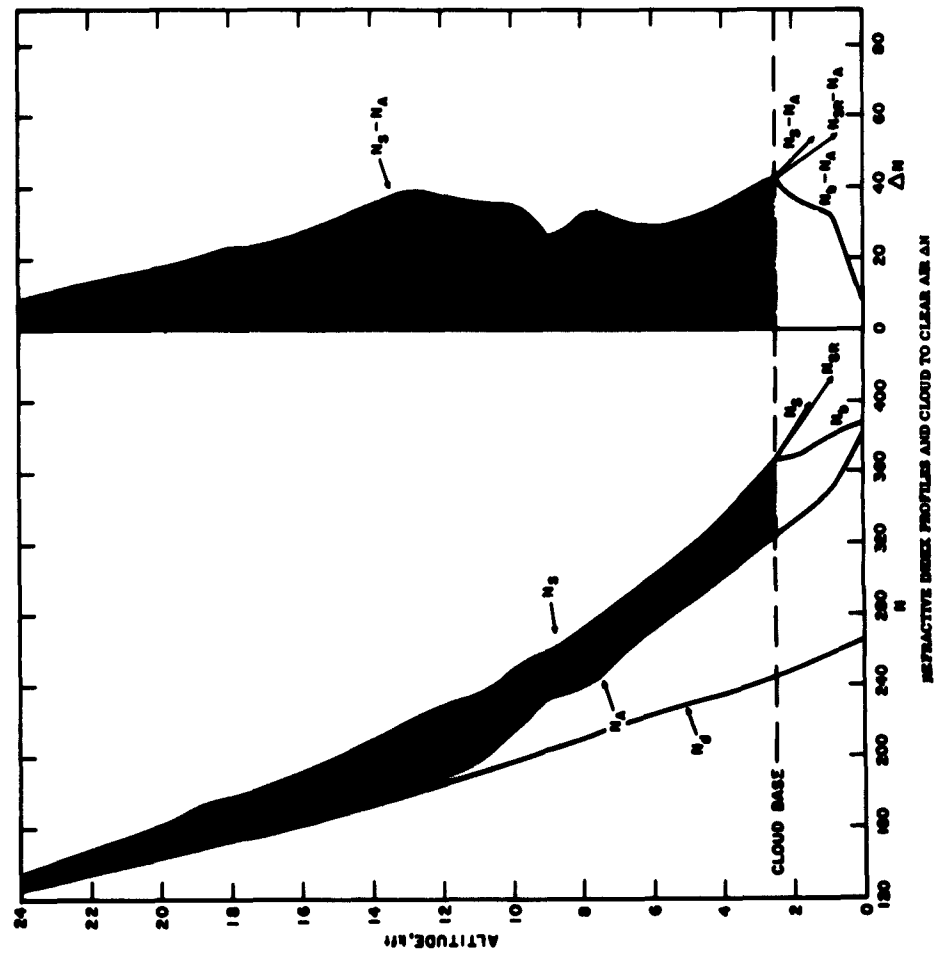
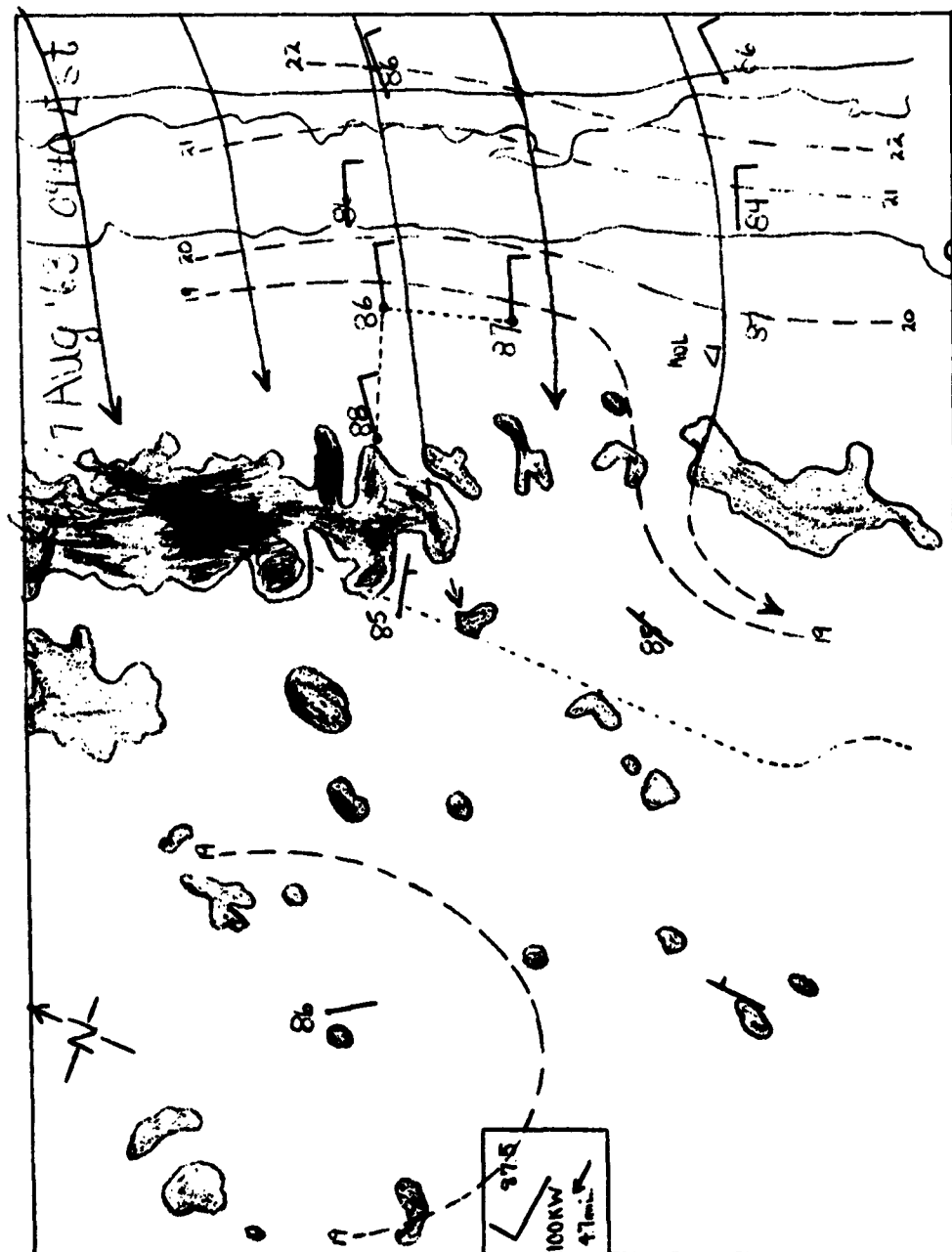


Figure 1-25





7 AUGUST 1963 0935 EST  
Figure 1-26





7 AUGUST 1963 1031 EST

Figure 1-28



Figure 1-29



Figure 1-30

enlargement of an original 35 mm negative. The coastal band over the MISTRAM area is clearly visible. Scattered clouds over the rest of Florida are apparent. Lake Okeechobee can be identified. Note that many of the cloud streaks from offshore (Atlantic side) dissipate 30 or so miles east of the mid-eastern Florida coast. This seems to be a common occurrence, in part associated with the edge of the Gulf Stream, in part associated with the sea-land circulation of the whole peninsula.

The flight cross section refractive index data for this case are given in Figure 1-31. Before discussing these data, it should be remembered that the cloud line moved inland during the time span of this cross section, so that for run 1, it is about 2000 feet west of MISTRAM central and at 10:31, it is just west of Babcock. With this time change in mind, one can see moisture and refractive index changes (of a scale of several miles) associated with the sea breeze front. At the lowest level probed (900 feet), moderate moisture fluctuations appear downwind from the outer beach. A pronounced moisture refractive index excess appears west of the inner beach line over MISTRAM central at 1400 feet. For this case, the higher frequency fluctuations of  $N$  appear to be of about the same magnitude from near the surface to 5000 feet. Near the cloud base altitude, above 2000 feet, a pronounced excess of moisture (and refractive index) is apparent with a dip under and to the left of the cloud line. At mid-cloud level (5000 feet), the transition from cloudless air moving west in the general air mass flow to the cloud wall is abrupt. The low value observed just before aircraft passage through the cloud wall is probably associated with some downward motion, perhaps of cloud origin. The 10,000-foot run was in a fairly uniform air mass, except for the point over the sea breeze front where a sharp-edge cloud was probed. The atmosphere at 15,000 feet was unaffected by all the turbulence occurring below.

**Figure 1-31**

This set of data illustrates the rather large refractive index changes of a semi-stationary nature that can exist along a wind shift line such as a slow moving sea breeze convergence line (front).

The detailed record of the pass in the sharp-edged cloud with the large N unit change probed on run 5 is shown in Figure 1-32. The extremely sharp edge of the cloud is obvious. The interesting low refractive index (dry) values just outside the cloud need further investigation. The 40N unit change found in this pass agrees well with the 37N change predicted from the radiosonde data. Figure 1-33 pictures the cloud before entry. The cloud is sharp-edged, but some scud is noticeable in the flight path six seconds before penetration.

Figures 1-34(a), 1-34(b) and 1-35 are samples of flight data for two other days. The change at mid-morning (Figure 1-34(a)) from excursions of 20N units at 1000 feet, to rapid oscillations of 25N units or more near cloud base, to 36N units above cloud base, to  $\pm$  a few N units above clouds is even more dramatic than the previous, more completely analyzed data. Note the undisturbed records east of the beach at 2000 feet.

Figure 1-34(b) depicts a set of runs on the same day, two hours later. The sea breeze with its high moisture content in the lower levels ends apparently at MISTRAM central. In two hours the character of the traces changed from semi-random oscillations to large-scale, semi-permanent oscillations associated with the sea breeze clouds. By the end of the period, the clouds penetrated the 5000-foot level.

Figure 1-35 is an example of a set of runs accompanying a missile shot. The flight path was designed to give a cross section along the line-of-sight of the MISTRAM system as a missile was followed down range. This set started at the 100K west station with the flight path heading of 107 degrees. The length of the legs was designed to cover angles, from the 100K west station, for elevations



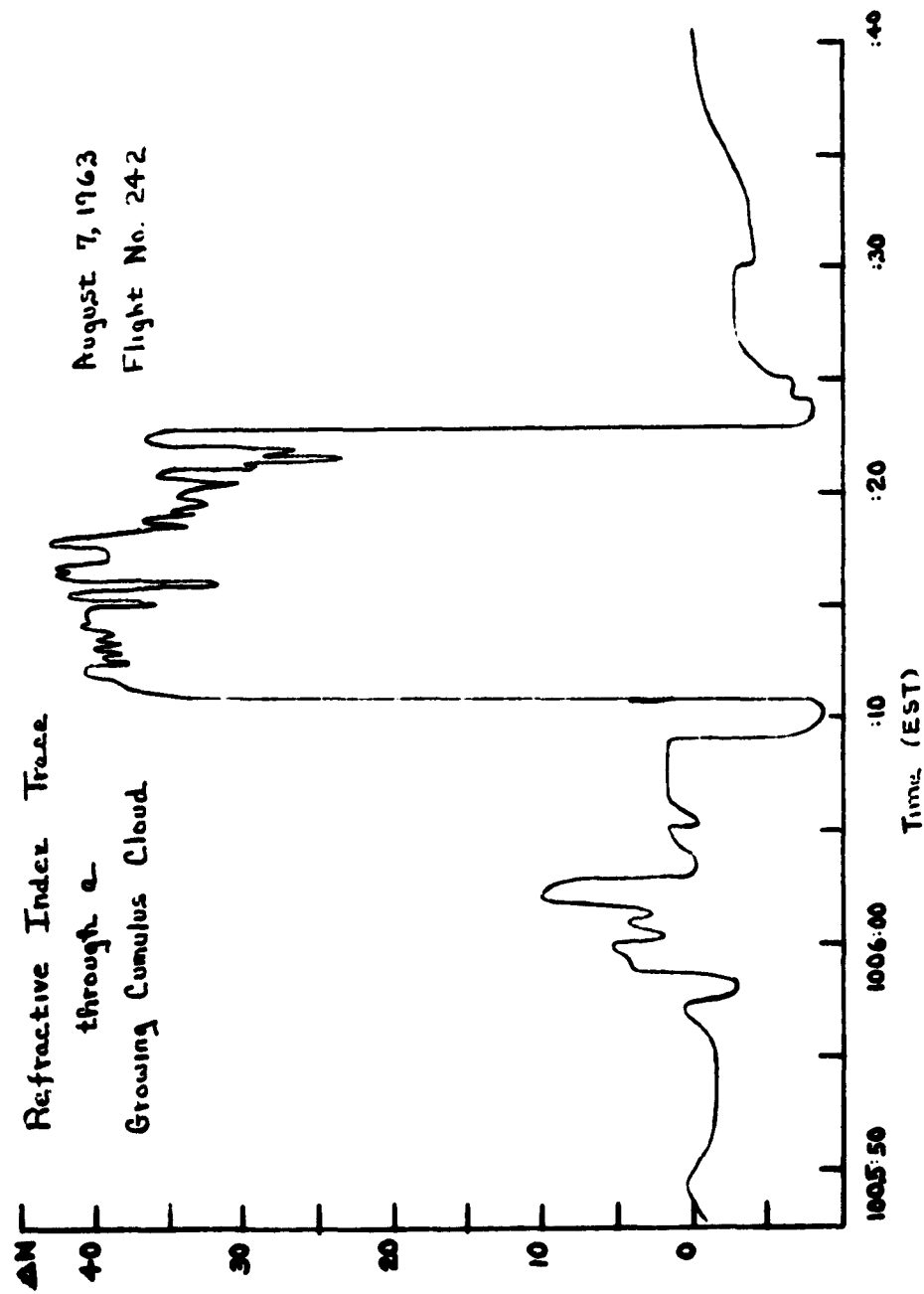
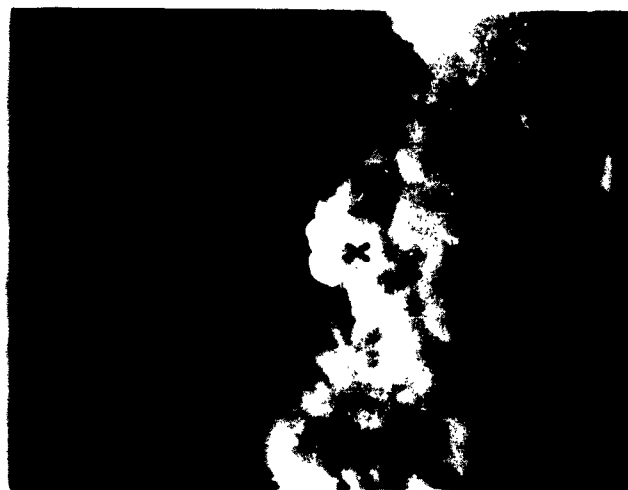
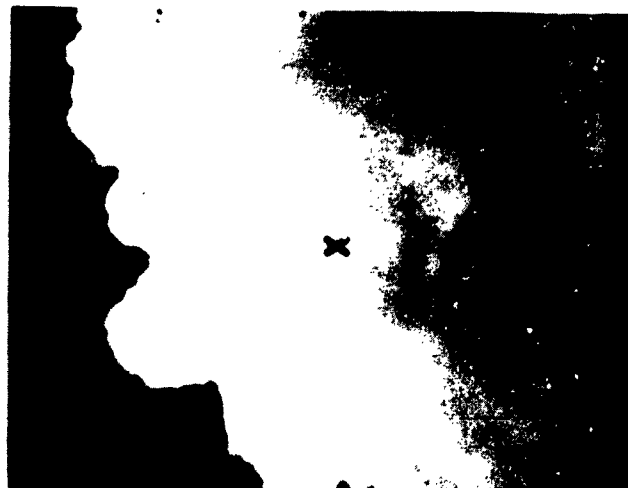


Figure 1-32



**27 sec BEFORE PENETRATION**



**6 sec BEFORE PENETRATION**

**C-130 16 mm NOSE TIME-LAPSE PHOTOGRAPHS OF CLOUD  
PENETRATION AT 5891 sec (1016 EST) DURING RUN NUMBER  
5 (ALT. 9.9 kft) OF FLIGHT 242 7 AUG. 1963**

**Figure 1-33**

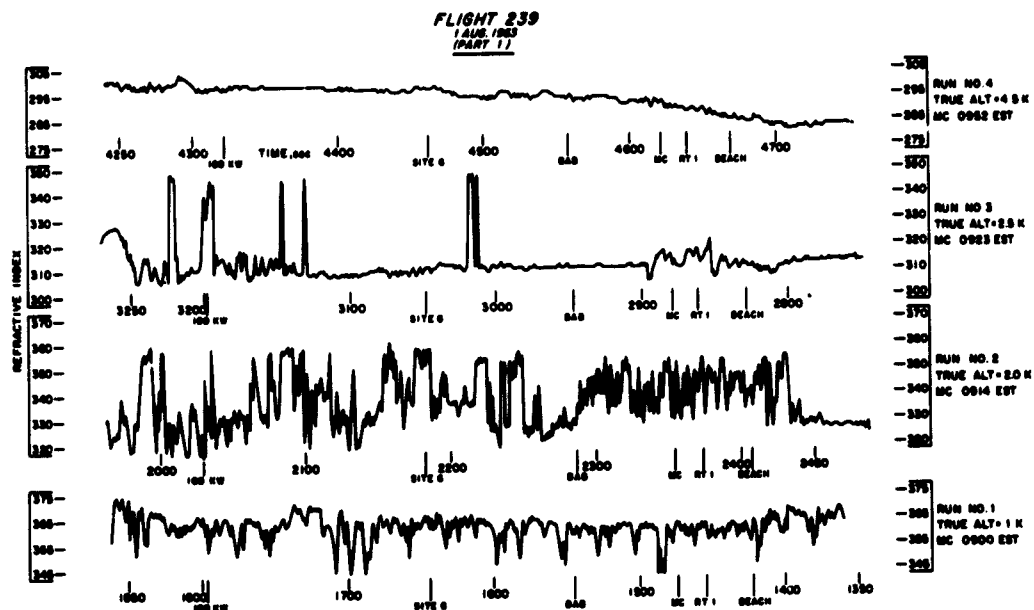


Figure 1-34 (a)

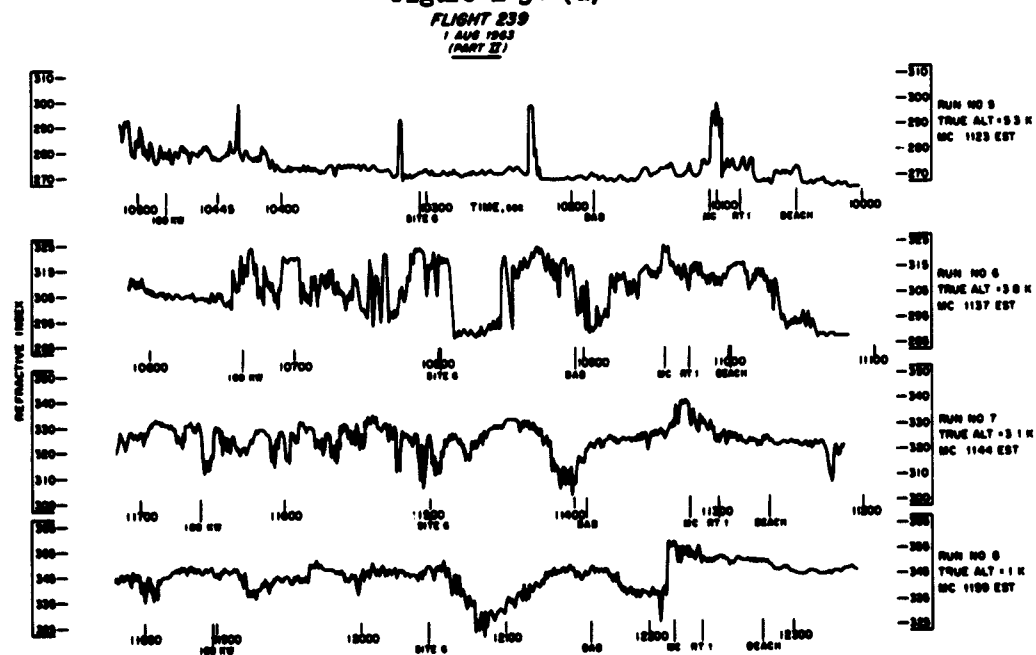
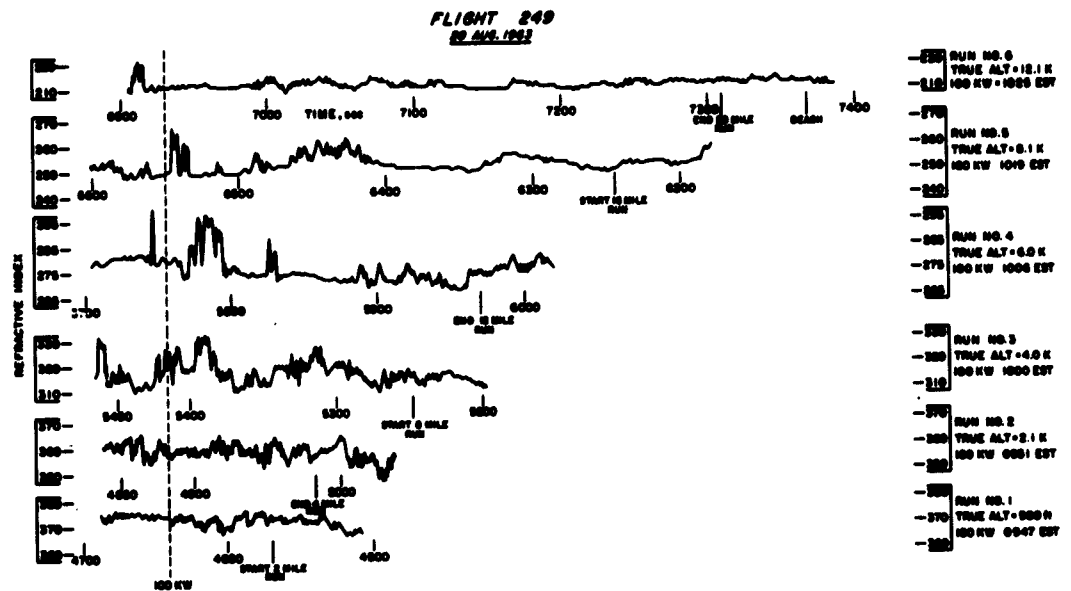


Figure 1-34 (b)



**Figure 1-35**

above 4 degrees. This procedure allowed a fairly quick coverage of six altitudes. Here again, the progression of  $\Delta N$  amplitude variation runs from small and short-scaled at 900 feet to large-scaled at mid-cloud altitude. The ambient air is apparently moist because, at the low level of cloud top (12,000 feet), the  $\Delta N$  values are again low.

Meteorological conditions over the MISTRAM area in daytime summer has been described and, to a certain extent, a refractive index climatology has been stated. To compare the meteorology with measured interferometer noise and errors, however, requires special analysis techniques not as yet invented. One attempt at a solution involving the description of the refractive index atmospheric roughness by power spectra has been considered. Range and range rate errors can then be computed from an atmosphere so described. A later paper by the National Bureau of Standards on this approach is included in these proceedings. As an input to such an approach, several power spectra were computed by Electromagnetic Research Corp. from the aircraft passes. Two spectra from the first case described in this paper are shown in Figure 1-36. The original data for passes 1 and 3 are shown in Figure 1-10. It was not considered appropriate to calculate spectra of data where the "square" wave cloud is a predominate feature. A different approach is under consideration, as mentioned earlier, for this part of the atmosphere. These spectra should be considered as first trial runs because of the limited sample of data.

The spectra on the time scale of the aircraft can be translated into the time scale for a line-of-sight sweeping through the indicated heights. Note that a pressure altitude of 3710 feet is equal to a true altitude of 4000 feet, and a pressure altitude of 800 feet is equal to a true altitude of 900 feet. The frequency as seen from an aircraft can be translated into wave length terms with respect to a stationery point. This scale is given at the bottom of Figure 1-36

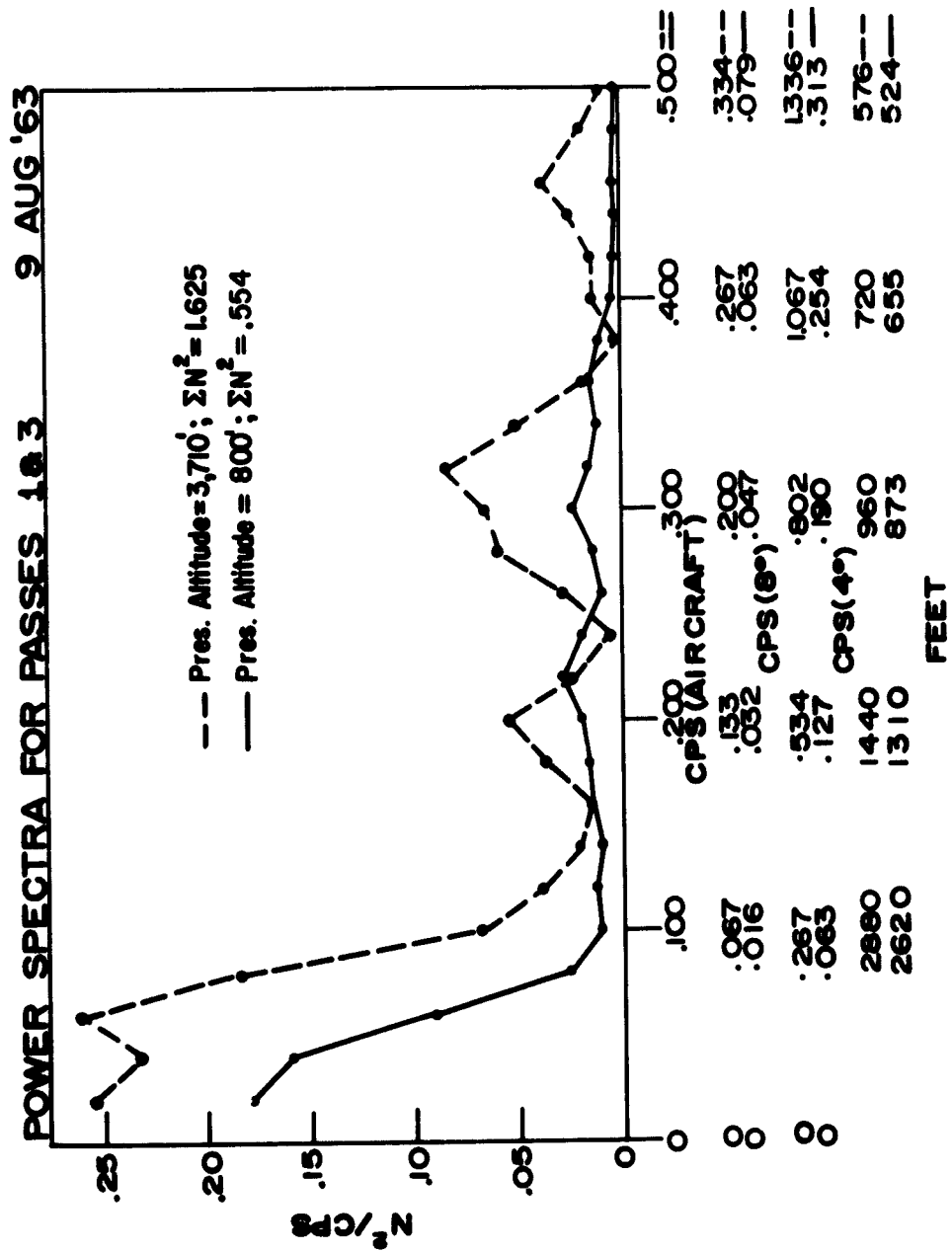


Figure 1-36

for the two cases. A discussion of these spectra, the manner of their derivation, and a note on their significance is given in a separate report.<sup>[2]</sup>

A different approach to the derivation of range and range rate errors from meteorological data has been started as part of this effort. For the case of the cumulus cloud-dominated atmosphere, (and probably clear-cut two-layer atmospheres), vertical cross sections through which the line-of-sight passes are constructed and  $N$ , or rather  $\Delta N$ , isolines drawn. The data on such a cross section are introduced into the memory of a computer and integrations along lines-of-sight carried out. The result gives the deviations from a local atmospheric range bias correction due to the atmosphere's large cloud scales of fluctuation. Range rate error is computed from differences between the range error for each integration along a specific angle. Range rate error for the case where the inland station line-of-sight sweeps through clouds while the coastal station does not, is equal to lateral rate error for this particular case.

An initial attempt at following the above procedure was made using the facilities of Mr. Ming Wong, AFCRL, and his contractor, Electronic Associates, who have an analog-digital computer arranged to process ray-tracing problems. The cross section supplied to the computer is shown in Figure 1-37. This figure does not include a section used for 90 to 100K, which has one area at a low level of excess  $N$  with values up to 17N units. Grid points were taken every 500 feet horizontally and vertically. It is assumed that the very sharp cloud gradients measured by the aircraft are somewhat smoothed in the process of determining the difference between two integrations along a line-of-sight by the cauliflower scale roughness (about 500 feet) of the cumulus cloud edge.

The whole cross section for August 9 was not given to the computer. A section from 90 to 125K feet was used. This section was repeated a number of times beyond the 120K distance until all rays





passed through the 18,000-foot level. Integration of  $\Delta N$ s was carried out along rays for every degree from 10 to 0 degrees, and for every 0.1 degree from 8 to 5 degrees. The results appear in Table 1-2 and Figure 1-38. The general increasing range error, really a bias error, is of course, due to the fact that most of cross-sectional  $\Delta N$  data are on the positive side. It is assumed that the refractive index standard is computed from a radiosonde that rises through undisturbed atmosphere.

The range rate errors computed from the range differences are subject to the normal computational "noise" involved in a differencing procedure. Presumably  $\pm 0.01$  foot difference changes are not meaningful. The larger changes are perhaps meaningful as they exhibit persistence.

It should be emphasized that this is the result of a first trial of this procedure for translating certain scales of refractive index roughness into range and range rate numbers. Several of the cross sections shown earlier in this paper will be reduced in a manner similar to the above trial.

Details of the analytical work have been published in a CRL report,<sup>[1]</sup> and the program of instrumentation measurement and analysis being accomplished at AMR, is well-covered in a memorandum report.<sup>[3]</sup>

Table 1-2

Results of the Integration of Nds and  $\Delta Nds$  from Sea Level to 18,000 Feet Along lines-of-Radio-Sight for Elevation Angles from 10 to 1 degrees. Values Obtained at h=18,000 ft.

Elevation Angle (deg)	$\int_0^{18k} ds$ (ft)	(dh/dx) Slope at 18k	$\int_0^{18k} Nds \times 10^{-6}$ (ft)	$\int_0^{18k} \Delta Nds \times 10^{-6}$ (ft)
10.0	101,300	0.1808	25.6	0.01
9.0	112,500	0.16260	30.8	0.05
8.0	126,500	0.14520	31.9	0.10
7.9	128,800	0.14348	32.2	0.11
7.8	129,600	0.14174	32.5	0.12
7.7	131,300	0.14000	32.9	0.11
7.6	133,000	0.13836	33.4	0.12
7.5	134,700	0.13664	33.9	0.12
7.4	136,800	0.13460	34.4	0.12
7.3	138,300	0.13318	34.8	0.13
7.2	140,200	0.13146	35.2	0.14
7.1	142,100	0.12980	35.6	0.14
7.0	144,100	0.12806	36.2	0.15
6.9	146,100	0.12636	36.7	0.15
6.8	148,200	0.12466	37.1	0.18
6.7	150,300	0.12294	37.2	0.19
6.6	152,500	0.12128	38.2	0.21
6.5	154,800	0.11960	38.8	0.21
6.4	157,100	0.11790	39.4	0.22
6.3	159,500	0.11602	40.0	0.22
6.2	162,000	0.11552	40.6	0.23
6.1	164,500	0.11288	41.2	0.22
6.0	167,100	0.11122	41.9	0.22
5.9	169,900	0.10954	42.6	0.22
5.8	172,600	0.10788	43.3	0.22
5.7	175,500	0.10614	44.0	0.21
5.6	178,500	0.10450	44.8	0.22
5.5	181,600	0.10284	45.4	0.22
5.4	184,800	0.10112	46.3	0.24
5.3	188,000	0.09946	47.1	0.29
5.2	191,400	0.09786	48.0	0.32
5.1	195,000	0.09626	48.9	0.35
5.0	198,500	0.09470	49.8	0.36
4.0	243,900	0.07850	61.2	0.56
3.0	313,400	0.06348	79.1	0.94
2.0	428,400	0.05010	111.3	1.55
1.0	644,400	0.03974	172.4	2.39

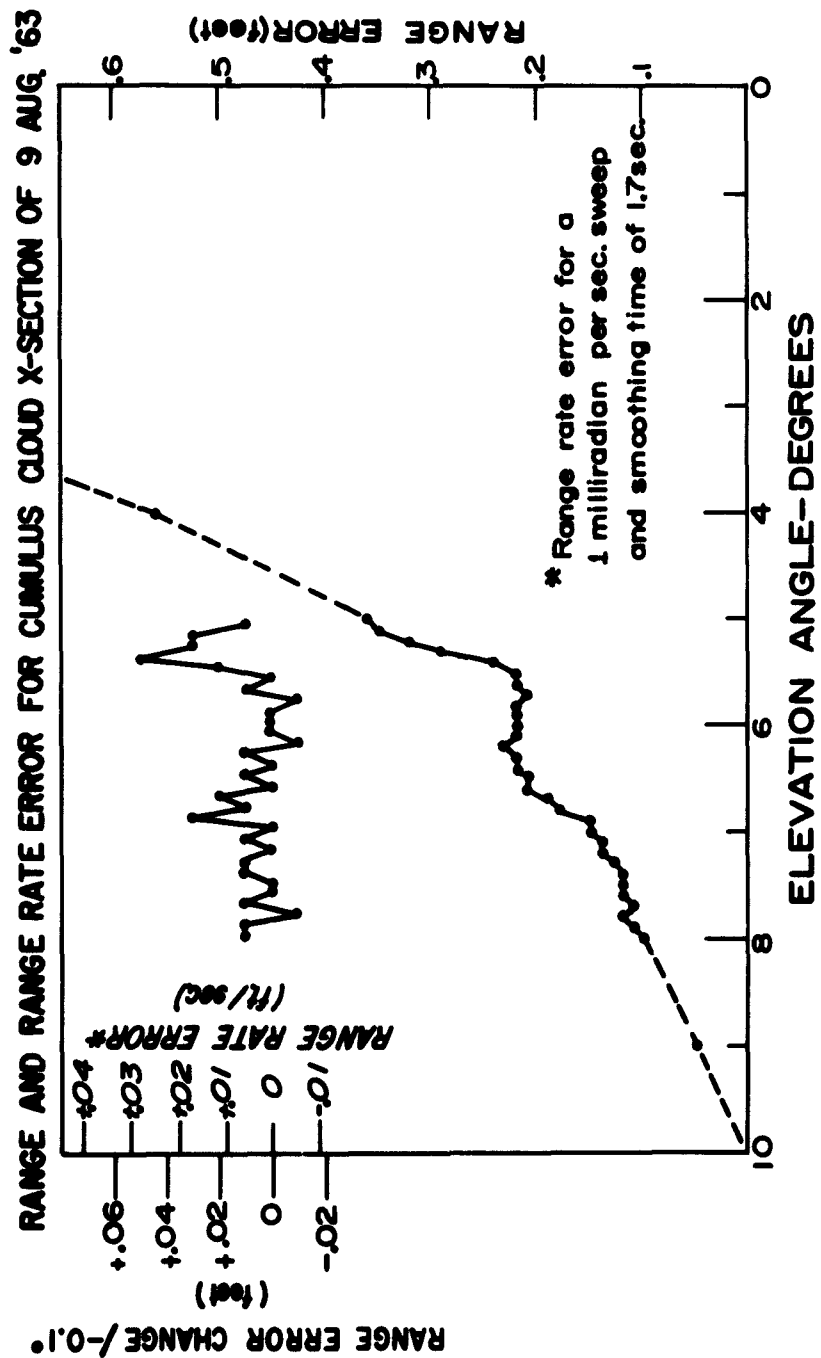


Figure 1-38

#### REFERENCES

1. Cunningham, R.M., Vickers, W.E., and Fain, C.G., "Effects of Clouds and Moist Layer Roughness on Range Rate Errors of Radio Interferometer Tracking," AFCRL-63-706.
2. Cunningham, R.M., Plank, V.G., and Campen, C.M., Cloud Refractive Index Studies, AFCRC-TR-56-210, ASTIA AD-110259, October 1956.
3. Ringwalt, D.L., Memorandum Report to AFCRL-11/3, Electromagnetic Research Corp., November 7, 1963.

## THE MITRE LINE INTEGRAL REFRACTOMETER

J. F. Sullivan

The MITRE Corporation  
Bedford, Massachusetts

The main portion of the report on The MITRE Line Integral Refractometer effort will concentrate on the preliminary experimental data obtained by operating the equipment during six weeks in October and November (1963) in the Lake Winnepesaukee region of New Hampshire. A discussion of the experimental technique and experimental results will be presented by Mr. Richardson during the latter part of the present session. Since the concept of the refractometer is relatively new to many of you, I will present introductory material at this time on the phenomenon involved in our technique, on what we are doing, and what has to be done to achieve our ultimate goals.

The purpose of this effort is to evaluate experimentally the feasibility of direct real-time measurement of the tropospheric effects on radio propagation. This technique is ultimately expected to provide the possibility for an improved means of correction to increase the precision of radar range measurements. Radar range measurements of the straight line distance between two points in the atmosphere are inferred from the determination of the transit time of propagation. The equation

$$R \approx S = c\Delta t - \int_C N ds \quad (1-1)$$

indicates the parameters affecting such a measurement,

where

C is the transmission path,

R is the distance to be determined,

S is the arc length of the radio wave,

$\Delta t$  is the transit time,

c is the velocity of light, and

$\int N ds$  is the atmospheric refractivity integrated over the arc C.

The effects of the atmosphere are evidenced in two ways: first, the atmosphere decreases the propagation velocity of the electro-magnetic wave; second, refractivity gradients result in the bending of the rays and hence, the straight line distance differs from the arc length. However, this bending effect, for any reasonable atmospheric path, is negligible compared to the slowing effect on the waves due to the presence of the material atmosphere. This slowing effect is reflected in the equation by a single quantity  $\int N ds$ , the refractivity integrated over the path.

Refractivity is a point function in the atmosphere which varies with both time and all three dimensions of space. Refractivity at any point in the clear air of the troposphere can be expressed as the sum of two primary terms:

$$N_{TOTAL} = A N_{HOH} + B N_{DRY} \quad (1-2)$$

The first term shown in Equation (1-2) is that due to the water vapor constituent; it is directly proportional to the water vapor partial pressure and inversely proportional to the temperature. The second term is the contribution of the refractivity due to the dry constituents in the atmosphere (oxygen, nitrogen, etc.). This "dry" contribution depends only on the density of these constituents at a point. The total refractivity is the sum of these two terms.

The correction that should be made to the distance measurement is related to the integrated value of this point function over the specific path and at the time that a distance measurement is being made. This correction is conventionally accomplished by utilizing a static atmospheric model based on average atmospheric conditions and sample measurements of refractivity at one or more points. This conventional technique is limited in accuracy by departures of the actual atmosphere from the assumed model and in utility by the complexity of calculations necessary for all but the simplest of models. The MITRE technique makes use of a direct measurement of the integrated refractivity along a particular path. In a metric measurement system utilizing this correction technique, the only computation necessary is a simple weighted subtraction.

The principle that we are employing in order to make this measurement depends on the presence of molecular absorption lines in the microwave frequency region of the spectrum. The presence of the lines in the troposphere is most readily observed by the absorption that occurs in propagation at or near frequencies corresponding to the lines. The first lines that are of any consequence in our approximations are the absorption line due to water vapor at 22 gc, and a group of lines due to oxygen at about 60 gc.

There is a small dispersity, or change in refractivity with frequency, associated with this absorption. The refractivity increases and then decreases in the vicinity of this 22 gc water line and returns to a lower level at frequencies above 22 gc. The effect of changes in the density of water vapor on the dispersion curve is illustrated by the lower dotted line of the curves in Figure 1-1(a). The whole level of refractivity shifts, and the small differential refractivity ( $\delta$ ) decreases almost in proportion to the change in level. The relationship is expressed by the equation indicating that the ratio of  $\delta$  to  $N_{\text{HOH}}$  is constant:

$$\frac{\delta}{N_{\text{HOH}}} = K \quad (1-3)$$

This is not quite the case since there are weak temperature effects. The equations on the right in Figure 1-1(a) indicate how this atmospheric phenomenon can be used to make a measurement of the integrated refractivity. Expressions relating the arc length, transit time and integral of refractivity at each of two frequencies about the water vapor line can be written if geometrical optics are assumed:

$$s_1 = c \Delta t_1 - \int_{C_1} (N_1) ds \quad (1-4)$$

The arc lengths at the two frequencies are equal for all practical purposes since the differential dispersion is so small, and path lengthening due to bending is of the second order. One can, therefore, subtract the differential transit time of two waves, one above and one below the frequency of the water vapor absorption line, to obtain the differential shift in phase integrated over the entire path in question:

$$\Delta t_1 - \Delta t_2 = \frac{1}{c} \int_C (N_1 - N_2) ds = \frac{1}{c} \int_C \delta ds \quad (1-5)$$

Since there is a proportionality between this shift and the total refractivity at all points of the path, one can infer, from the change differential transit time measurements, the integrated refractivity due to the presence of water vapor in the path at the time:

$$\Delta t_1 - \Delta t_2 \propto \int_C N_{\text{HOH}} ds \quad (1-6)$$

As indicated earlier, there are many gases involved in the refractive effects of the dry part of the atmosphere. However, for any point in the troposphere, the analysis of samples taken from the atmosphere reveal that there is a fairly constant mixing ratio of the dry constituents of the atmosphere; hence, the effect of one element can be used as a measure of the effect of all the dry constituents. In the MITRE system, it is planned to use dispersion measurements around the oxygen line to indicate the magnitude of the second term of the total refractivity equation.



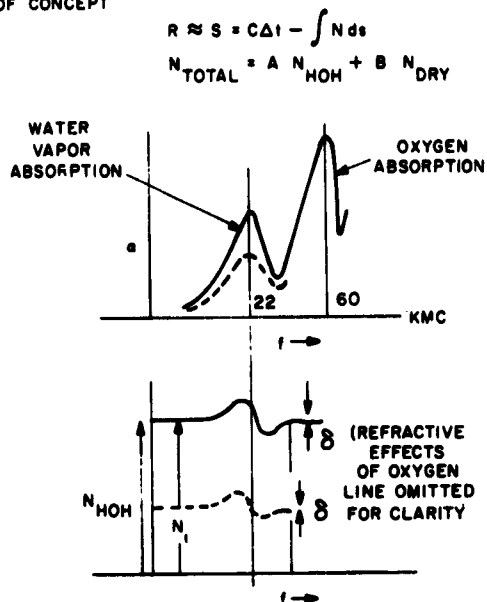
At this time, we will consider the size of the dispersion effects involved in the measurements. Typically, the value of  $N_{\text{HOH}}$  amounts to something like 60N units of refractivity, while the corresponding shift across the 22 gc line is about 0.03N unit. This results in a differential path length of about 500 microns over an 18-kilometer path and a differential transit time in the order of 2  $\mu\text{sec}$  in a total transit time of 50  $\mu\text{sec}$ . In order to make a valid measurement of such a small magnitude, it is necessary to determine whether or not it is possible to build apparatus stable enough to make measurements of these minute differential transit times, and whether the atmosphere itself can support these measurements.

To answer the first question we have developed, under MITRE in-house sponsored research activity, a prototype model of a water vapor line integral refractometer. The stability of the device has been tested in the laboratory. The signal was attenuated through a ridged waveguide with satisfactory results. To provide answers to the second question, the apparatus has been installed in vans and operated over a 13-mile path across Lake Winnepesaukee. Preliminary results of these tests are very promising and indicate that the technique can be exploited with today's state-of-the-art in electronic instrumentation.

Figure 1-1(b) shows a block diagram of the apparatus. The equipment has been set up and will be available for inspection tomorrow. Personnel will be stationed in the vans to answer detailed questions with regard to the specific design considerations and construction details. However, we will now cover some of the most pertinent features of the design. A 750-mw continuous wave (c.w.) klystron is used for the source of fundamental 15.6-gc radio frequency power. A varactor frequency doubler, located as near as possible to the horn of the cassegrainian parabolic antenna, is excited with the fundamental signal to obtain two coherent electromagnetic waves (15.6 and 31.2 gc) at the antenna. This energy traverses the path and is

# LINE INTEGRAL REFRACTOMETER

## REVIEW OF CONCEPT



$$S_1 = C\Delta t_1 - \int N_1 ds$$

$$\frac{S_1 - S_2 = C\Delta t_2 - \int N_2 ds}{\Delta t_1 - \Delta t_2 = \frac{1}{C} \int N_1 - N_2 ds = \int \delta ds}$$

$$\frac{\delta}{N_{HOH}} = K$$

$$\therefore \Delta t_1 - \Delta t_2 \propto \int N_{HOH} ds$$

Figure 1-1 (a)

## IMPLEMENTATION

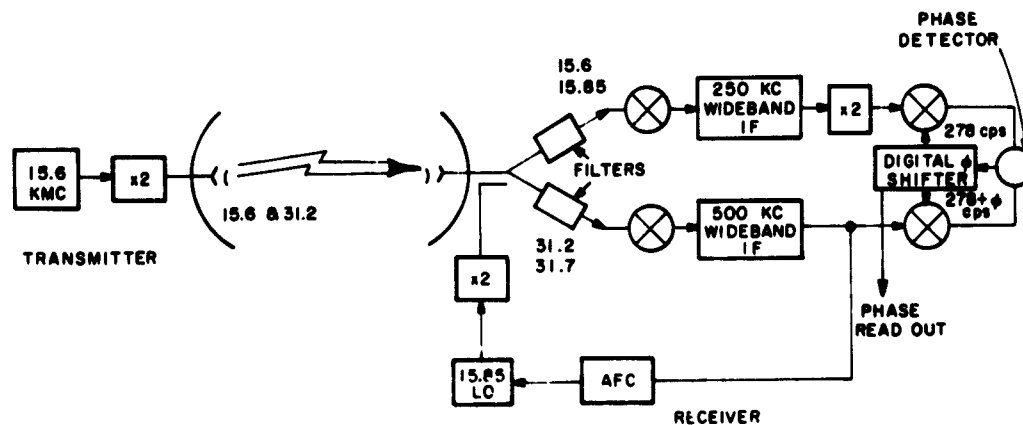


Figure 1-1 (b)

detected by a system utilizing a similar antenna in the receiver. A local oscillator signal is combined with the received signal in a ridged waveguide directional coupler located as near the horn as physically possible. The local oscillator signal consists of fundamental and second harmonic waves generated in the same way as in the transmitter. This fundamental signal is controlled in frequency to be 250 kc away from the transmitted fundamental. The four signals present after this injection are then split into two pairs and fed into crystal mixers. This process results in two IF frequencies; one at 250 kc to carry the phase information of the lower transmitted frequency, and one at 500 kc IF to carry the information on the higher frequency. The 250 kc signal is doubled and the phase of the two are then compared.

The comparison is made by a "digital phase shifter" which inserts a second local oscillator signal of 278 cycles into one arm, and "coherent" signal of 278 cycles into the other arm. The phase of the second signal is controlled by the digital unit. A phase detector-servo combination varies the output of the digital phase shifter until a null is achieved in the phase detector; the amount of phase shift required to achieve the null is the measure of differential transit time. The digital phase is recorded both in digital and analog forms.

These are the essentials of the device that we have developed. A number of unique designs of microwave components was required, as well as some imaginative solutions to problems that arose in the video portions of the apparatus. The system has performed very well, but some residual problems remain in regard to the "resetability" of the device and thermal stability. We believe that further refinements, which are in progress, will improve the equipment.

In addition to apparatus development, our current program includes further testing (Figure 1-2). An additional receiver for the water vapor refractometer will be completed soon in order to make it possible to study baseline effects. This study will yield information

#### DEVELOPMENT PHASE

1. Additional H<sub>2</sub>O, Receiver
2. Higher Frequency Oxygen Instrument

#### TEST PHASE

1. Local Testing
  - a. Calibration ( $\phi$  vs  $\int Nds$ )
  - b. Spectral Analysis (Confirmation of Statistics)
  - c. Environmental Investigations (P,T,LWC)
  - d. Operational Experience
2. Critical Evaluation
  - a. Comparison with Independent Technique
  - b. Real Time Analysis

FIGURE 1-2

LINE INTEGRAL REFRACTOMETER PROGRAM PLAN

of importance on angular refractive variations which affect trilateration or interferometric systems.

We are also in the process of developing a higher frequency instrument for measurement of the dispersion by oxygen. The long procurement lead time for a suitable klystron has delayed somewhat this portion of the program; we are currently awaiting delivery of this klystron.

The development program is being conducted in parallel with a test program. We are evaluating whether this concept is, in fact, a reasonable one. In such an evaluation, it is necessary to determine not only whether an apparatus stable enough to support the measurement can be built, but also whether the atmosphere itself can support these minute differentials. The first phase of this testing can be performed locally. We have just completed a very short series of preliminary local tests during the past month or so. These tests will not only provide insight as to the reasonableness of our measurements, but will enable us to plan and provide for a complete set of experiments to obtain the needed data.

However, in order to perform a critical evaluation of the refractometer, we eventually intend to operate it in parallel with the 9.4-gc phase-measuring instrumentation of the National Bureau of Standards (NBS). This equipment provides an independent measure of the identical function that we are attempting to measure. This type of comparison, over a fixed path, is the best way we can think of to evaluate the system without having an extremely detailed knowledge of the atmospheric path. If the two measurements compare in real time, we will have a fairly solid quantitative indication of the performance. We had originally planned to perform this comparison early next year in conjunction with the atmospheric tests being made by NBS in Hawaii.

The purpose of the local testing is to make sure, before we attempt the critical evaluation, that we conduct sufficient preliminary

tests of the performance of our system to determine if there are any unforeseen difficulties.

In the month of local testing, we have gathered a great deal of data. From a quick look at the raw data, it looks quite promising. However, there are some disturbing fluctuations that we have not had time to analyze fully. We think, at least from this quick look, that we will probably want to delay somewhat the plans that we had for operating the units next to the NBS equipment in Hawaii early in 1964.

A number of additional tests, which can be performed at local test sites, are needed to confirm the validity of the concept. We should, for instance, gather more data by operating the apparatus over a fixed path and take simultaneous atmospheric measurements of the water vapor content of the path. The atmosphere is frequently stable enough over a horizontal path so that little or no variations of the humidity are measurable with the meteorological equipment we have available. Over such a path, one can readily calculate the integral of refractivity by multiplying the refractivity measured at any point by the path length. The differential phase measurement can then be compared with the calculated  $\int N ds$  value. If this procedure is repeated for a wide range of water vapor content conditions, the "constant" of proportionality can be determined and compared with that theoretically calculable from the quantum mechanical theory of the behavior of the water vapor molecule.

The above approach is useful for stable atmospheric conditions. However, measurements taken during unstable conditions can be utilized to develop the statistics of the variations and to make spectral analyses of the phase data acquired. The statistical analysis results are useful for comparison purposes with the statistics of the troposphere already generated by NBS. Comparisons of statistics are not very conclusive, since one can get the same

kind of statistics for two phenomena that are not necessarily correlated. Eventually, The MITRE Line Integral Refractometer equipment should be operated in parallel with the NBS apparatus and comparisons made in real-time.

Also, there are some environmental investigations that are a further object of our local tests. For example, the exact shape of the dispersion curve near the 22-gc line is dependent upon the pressure of the other gases in the environment. Since the quantity of interest is the amount of water vapor, variation of differential dispersion with pressure due to other constituents effect the results. At frequencies far enough away from the absorption line, the measurement is relatively independent of pressure; however, the residual pressure sensitivity of the measurements should be investigated. In addition, we would like to experimentally determine the temperature sensitivity previously mentioned. While both of these effects are expected to be small, some correction for them may be in order to obtain the most accurate data.

Another environmental factor which we want to investigate is the effect of liquid water in the path. The equations shown assume clear air conditions. The resonant phenomena do not occur in condensed vapor; since the water molecules are not free to rotate in the same manner, the droplets of liquid water will not exhibit the same dispersion. Hence, an appreciable amount of water in the path is expected to be detrimental to the measurement. It is necessary to confirm quantitatively what can be expected under such conditions. These tests will provide the opportunity to gain additional operational experience with the apparatus, in addition to developing and refining our techniques for making calibrations.

These are the objectives of our local tests. As I have previously indicated, we expect that it will be necessary to do some further critical local testing before we engage in the comparison phase of the evaluation.

#### REFERENCE BIBLIOGRAPHY

1. Bean, O.E., Design Considerations for a Line Integral Refractometer, MITRE Working Paper W-4954, 1962.
2. Bickel, S.H., Near Field Phase Shift for Line Integral Refractometer, MITRE Working Paper W-06808, 1964.
3. Bridge, W.M. Microwave Instrumentation for an Oxygen Refractometer, MITRE Working Paper W-6576, 1963.
4. Report of Ad Hoc Panel on Electromagnetic Propagation. AF AFSC:103; 1962.
5. Richardson, H.M., Refractive Index and Dispersion for Air at 22.2-gc and 60-gc, MITRE Working Paper W-4968, 1962.
6. Richardson, H.M., An Estimate of the Magnitude of Microwave Dispersion in Clouds and Rain, MITRE Working Paper W-5234, 1962.
7. Sullivan, J.F., A Line Integral Refractometer, MITRE Working Paper W-4967, 1962.
8. Sullivan, J.F., Problems in Range Electronic Tracking and Trajectory Measurements, MITRE Working Paper W-4984, 1962.



## TESTING OF THE LINE INTEGRAL REFRACTOMETER

H. M. Richardson

The MITRE Corporation  
Bedford, Massachusetts

A path across Lake Winnepesaukee in New Hampshire was utilized to check out and calibrate the first version of the water vapor line integral refractometer. This site was chosen over several others considered because of the extent of terrain clearance, achievable uniformity of atmosphere, and proximity to MITRE.

A path about ten miles in length is required due to the small magnitude of the dispersion. The system will function over a greater distance, but the longer path is rather inconvenient to handle. A line-of-sight path for a microwave beam, one over which the main lobes for the transmitter and receiver clear the terrain, was necessary in order to reduce the bias and fluctuation effects that multipath would introduce in phase. We wanted atmospheric conditions that were as uniform in temperature, pressure, and humidity as possible, but that were variable from day to day and from season to season. In New England, the weather, in terms of mixing ratio, changes quite markedly from August to October. During this period, changes over a range of from 8 g/kg to 1 g/kg can be expected. In 1962, the mixing ratio varied from as little as 1 g/kg to as much as 15 g/kg.

The sites inspected included the top of the Gaither building at MITRE, Reservoir Hill at Hanscom Field, Boston Hill, Mount Wachusett, Monadnock Mountain, Ossipee Mountain, Belknap Mountain, Mount Mansfield

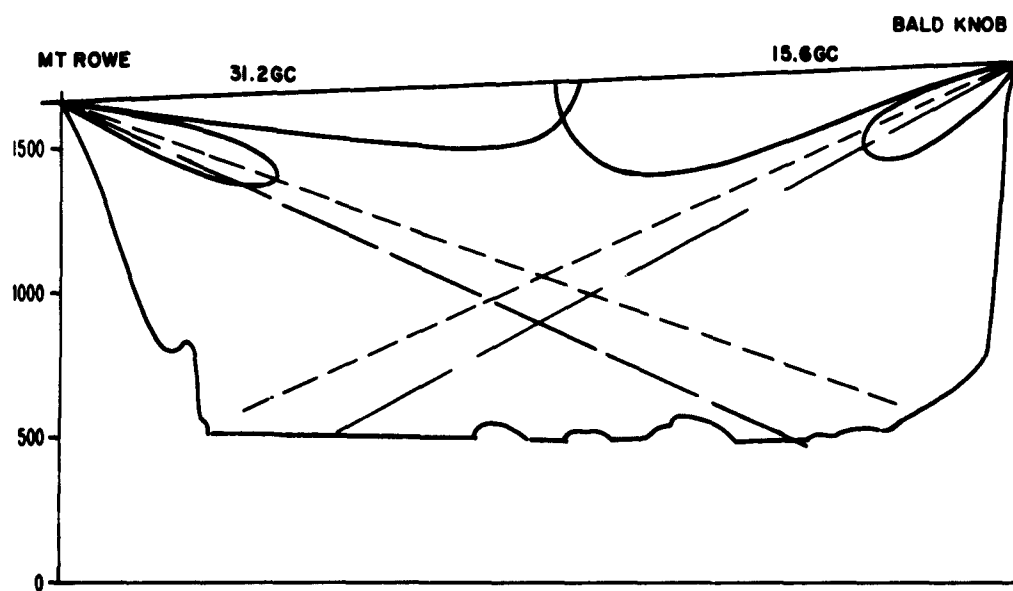
in Vermont, White Face Mountain in New York and Mount Washington. The path finally selected runs from the Bald Knob side of Ossipee Mountain across Lake Winnepesaukee to Mount Rowe in the Belknap Mountain area. The path clears the lake by something like 1200 feet and is about 13 miles long.

Mirror images of each antenna pattern should be added at both ends of the path in Figure 1-1 to complete the illustration of the dual frequency, "congruent" antenna patterns on the site profile and antenna pattern.

The path as viewed from the transmitter on Bald Knob toward Mount Rowe is shown in Figure 1-2. The transmitter is located on the Bald Knob site and the antenna is located in the truck (Figure 1-3). Normally, a 0.004 inch of polyethylene plastic weather window is used during the measurement runs. The path as viewed from the receiver site on Mountain Rowe and the position of the receiver truck are shown in Figures 1-4 and 1-5, respectively. The reference transmitter, which was originally located in the distant foreground at the time of the picture, has since been moved to a position nearer (about 97 feet) the receiver. The limited amount of meteorological gear shown was utilized to obtain some end-point weather data. Figures 1-6 and 1-7 are views of the inside of the transmitter and receiver vans respectively. The two antennas are identical (down to the feed), and can be seen in the operating position.

One requirement for the tests was that the condition of uniform mixing ratio exists. Inversions or ducts are certainly facts of life, but again if the operating days are properly selected, one does not have to pay much attention to this effect in terms of calibration of the device with respect to humidity.

The question of humidity from the lake was of some concern. Our weather staff looked into what research had been done on the amount the water content of an air mass might change as a dry air mass flows



**SITE PROFILE AND ANTENNA PATTERNS**

**Figure 1-1**



Figure 1-2



Figure 1-3



Figure 1-4

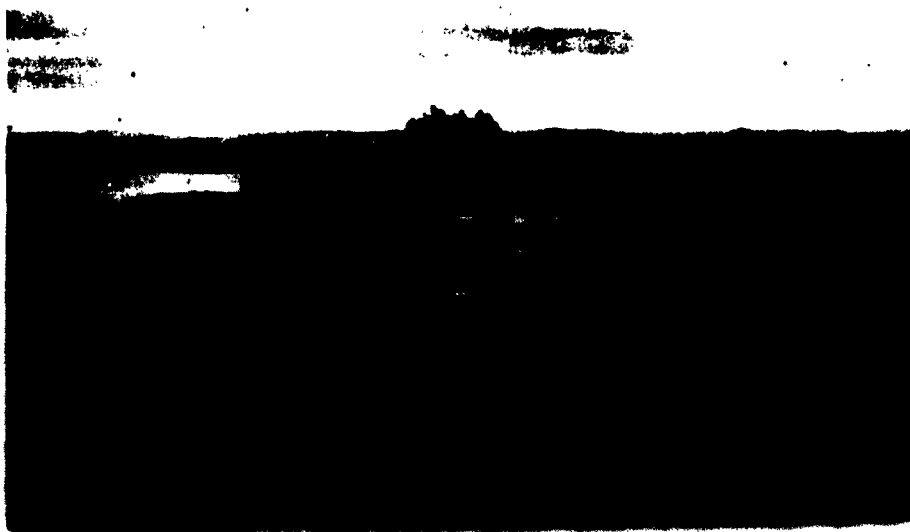


Figure 1-5

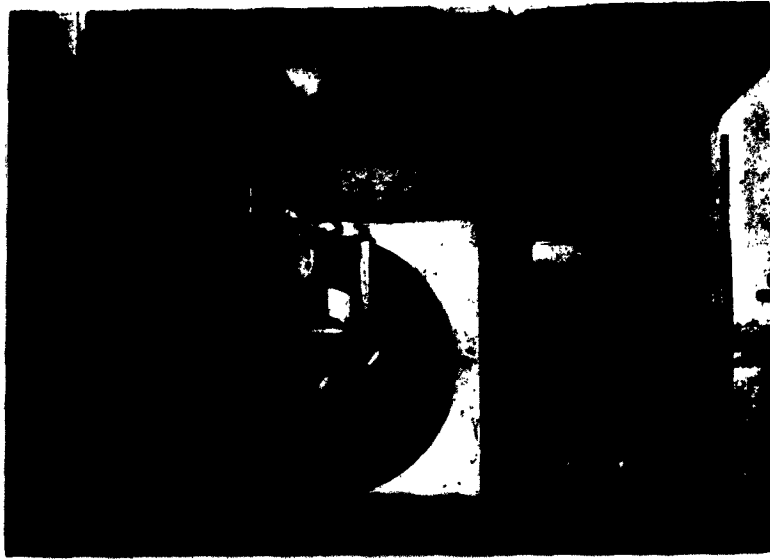


Figure 1-6



Figure 1-7

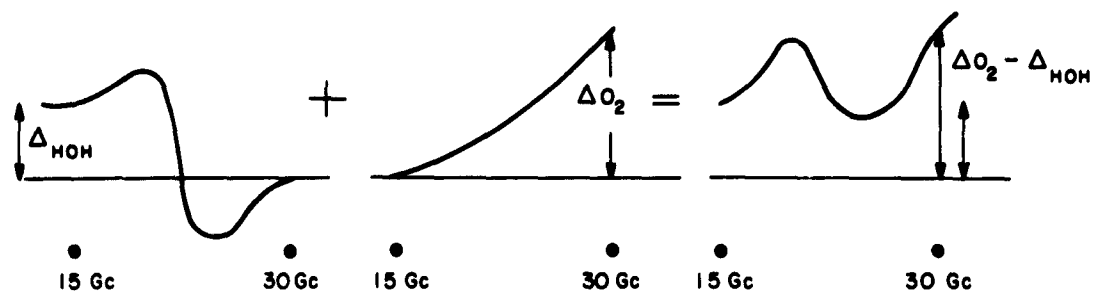
over water. Measurements made in 1944, when an air mass blowing offshore was warmer than the water by about 4 degrees, indicated that the humidity changed less than 10 per cent at an elevation of 600 feet and a distance of 40 miles from the shore. It was concluded that there would be little or no effect from vertical diffusion of water vapor into the path when there was a reasonable cross wind.

The test plan was to observe the weather and to schedule operations accordingly. Data on the medium were obtained by flying a Tripacer aircraft equipped with a limited amount of instrumentation along a course parallel to the microwave path. The phase data were given a preliminary check in the field prior to their normal reduction processing on the 7090 computer in Bedford.

The dispersion over the frequency range due to both the absorption of the water vapor at 22 gc and oxygen at about 60 gc is illustrated in Figure 1-8. The sum in this figure is related to what the equipment sees, i.e., the difference of dispersion caused by relatively stable oxygen and the quite variable water vapor. The dispersion due to oxygen is roughly equal to that of water vapor (approximately 0.03N unit), and is in the opposite direction.

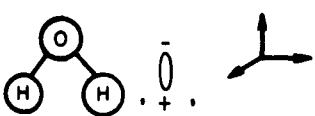
The first equation in Figure 1-9 was used to estimate the dispersion for water vapor. The water molecule has two hydrogen atoms separated by an angle of about 100 degrees. It has a permanent electric dipole moment, and three principal moments of inertia; hence, it is an asymmetric rotor. The dipole moment matrix elements for this 22 gc transition are somewhat complicated, but the operation has been performed.

The oxygen molecule has two electrons Figure 1-10. They are not balanced in alignment, but are parallel. Oxygen is magnetic, has a permanent magnetic dipole, and has one moment of inertia. The electron orientations couple with the end-over-end rotations of the molecule, which are



## MICRO DETAIL OF INDEX OF REFRACTION

Figure 1-8



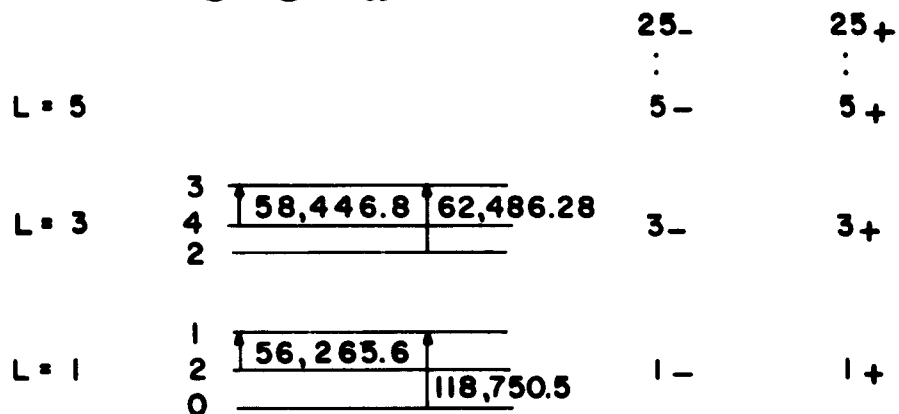
$$1. \quad n^2 - 1 = \frac{8\pi N}{\sum e - \frac{W_e^0}{KT}} \sum_{\ell, \ell'} \frac{\nu(\ell, \ell') \left| \frac{PE^0(\ell, \ell')}{h} \right|^2 e^{-\frac{W_e^0}{KT}} \cdot f}{\left[ \nu(\ell, \ell')^2 - \nu^2 \right]}$$

$$2. \quad f = 1 - \frac{\nu \Delta \nu^2}{2\nu_0^2} \left[ \frac{\nu_0 + \nu}{\Delta \nu^2 + (\nu_0 - \nu)^2} + \frac{\nu - \nu_0}{\Delta \nu^2 + (\nu + \nu_0)^2} \right]$$

1. CHAPTER XIII, ELECTRIC AND MAGNETIC SUSCEPTIBILITIES, VAN VLECK (1932)
2. CHAPTER 13, MICROWAVE SPECTROSCOPY, TOWNES AND SCHAWLOW (1955)
3. VOL. 13, RADIATION LABORATORY SERIES, CHAP 8 (1951)  
BACKGROUND FOR HOH DISPERSION

Figure 1-9





1. PHYSICAL REVIEW 121, PG.152, PRECISE MEASUREMENT OF MICROWAVE ABSORPTION FREQUENCIES, ETC, ZIMMERER AND MIZUSHIMA (1961)
2. PHYSICAL REVIEW 97, PG. 937, THEORY OF THE FINE STRUCTURE OF THE MOLECULAR OXYGEN GROUND STATE, TINKHAM AND STRANDBERG (1955)

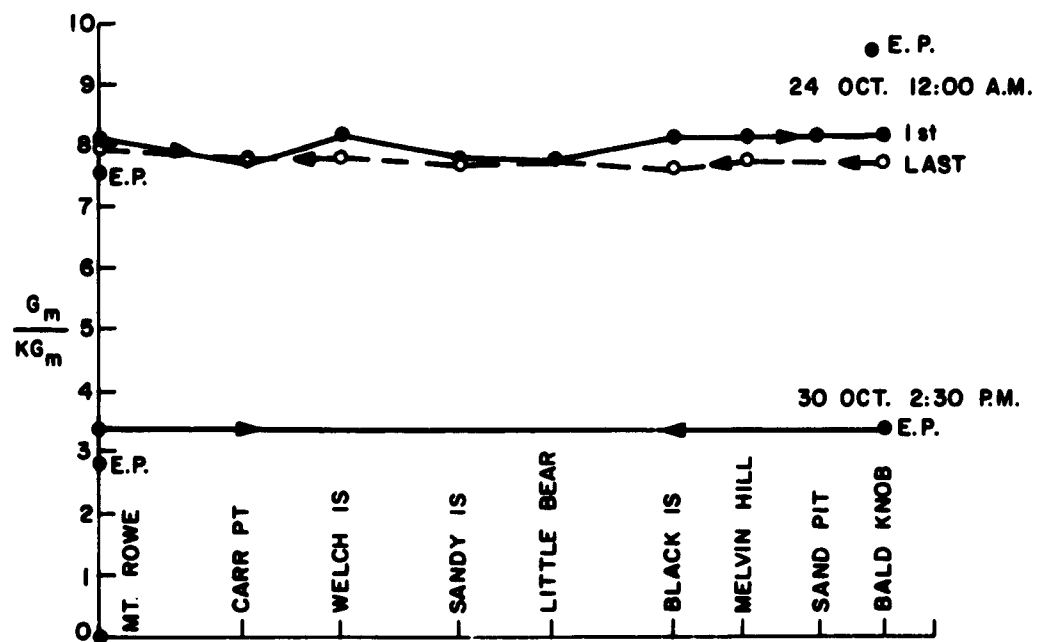
## BACKGROUND FOR O<sub>2</sub> DISPERSION

**Figure 1-10**

characterized by quantum numbers associated with different frequencies. Most of the transitions lie in the region between 56 and 60-gc. The dispersion is obtained by summing over 25 lines.

Some of the data obtained by utilizing the airborne sling psychrometer are shown in Figure 1-11. The heavy line represents the first pass on October 24 from Belknap to Bald Knob; the dashed line is for the last portion of the flight which consisted of a total of three round trips over the path. The water content was estimated at 8 g/kg based on a psychrometric chart. On October 30, a very different set of conditions was encountered. It was much cooler and much windier (about 15 mph crosswind). The end-point readings are indicated on the graph; they appear to be better on the cold dry day than on the wet day.

Figures 1-12, 1-13, and 1-14 show actual analog traces of differential phase versus time. The amplitude of a 1-degree increment in the upper noise trace (Figure 1-12) is indicated by the small double pointed arrow. The sample exhibits approximately 2 degrees peak-to-peak variation during the 45 seconds of record reproduced. The arrows ending on the other two broad tracers in Figure 1-12 indicate the magnitudes of 1-db fluctuations in the IF signal and correspond to amplitudes of the 31.2-gc and the 15.6-gc carrier signals. On October 25, the variations in amplitude are a small fraction of 1-db. The phase fluctuations are somewhat larger than might be expected from data given by other workers (NBS) for single carrier phase fluctuation, and hence, larger than might be expected for the difference in phase of two carrier frequencies in a portion of the spectrum where dispersion is about one part in ten thousand.



## PRELIMINARY HUMIDITY VS PATH

Figure 1-11

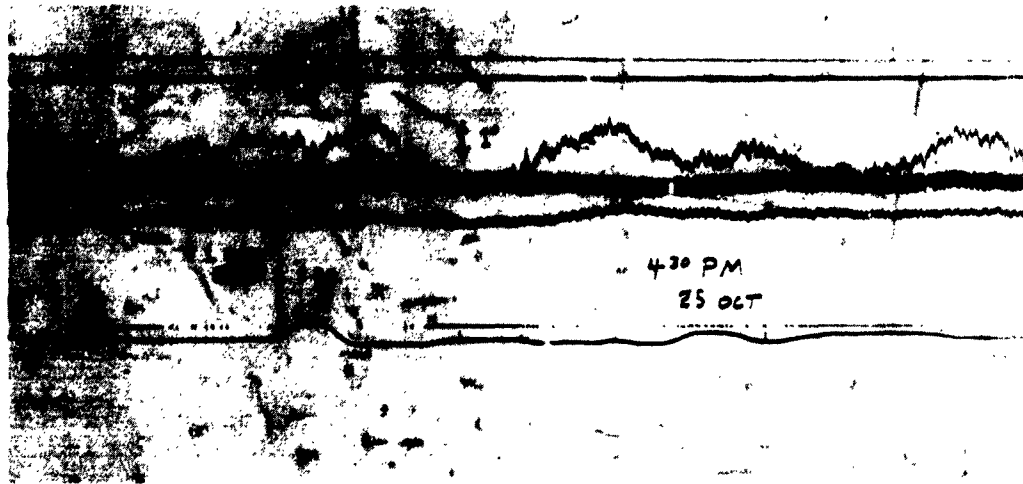


Figure 1-12



Figure 1-13

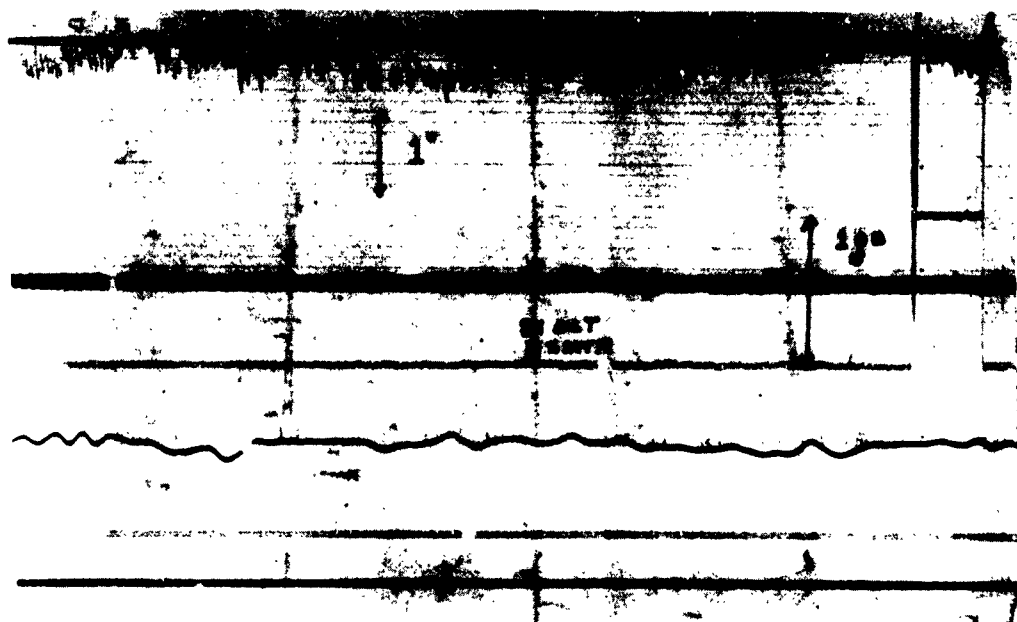


Figure 1-14

As perplexing as this result is, the fluctuations earlier in the afternoon were much larger, as shown in Figure 1-13. The largest amplitude noise trace is that of differential phase, with peak-to-peak variation a bit less than 15 degrees. At this time, the amplitudes of the signals were fluctuating about 1 db, with a significant amount of correlation between amplitudes and phase. However, the record shows some lack of correlation. These two records represent extreme conditions in a short period of time; a quick look at the records reveal that 3- to 5-degree fluctuations are most common.

A full explanation of these results is not available at this time, but it is known that some of the phase is due to amplitude sensitivity of the receiver at low power levels. It may also be postulated that the angle of arrival (shimmer) of the signals on the dual-lobe structure characteristic could cause such effects.

The short-term stability of the apparatus is illustrated in (Figure 1-14) where the differential phase read out is the second trace from the top and the two broad traces near the middle are amplitude monitors. A 1-db change in level is shown for the 15.6 gc channel with negligible change in phase, on the right side of the figure.

It is obvious that some averaging is necessary for comparison of the phase with humidity measurements. The averaged differential phase versus average humidity graph shown in Figure 1-15 is based on fifteen cases taken during the interval of October 15 through 31. The slope of the line compares quite favorably with that predicted by theory, i.e., the differential phase shift per  $\text{gm/m}^3$  averaged over the path is as anticipated. These parameters are plotted versus time in Figure 1-16.

Only two power spectra have been run as of this presentation and are so preliminary that they are not included in this publication. This work is continuing.

# DIFFERENTIAL PHASE VS WATER DENSITY

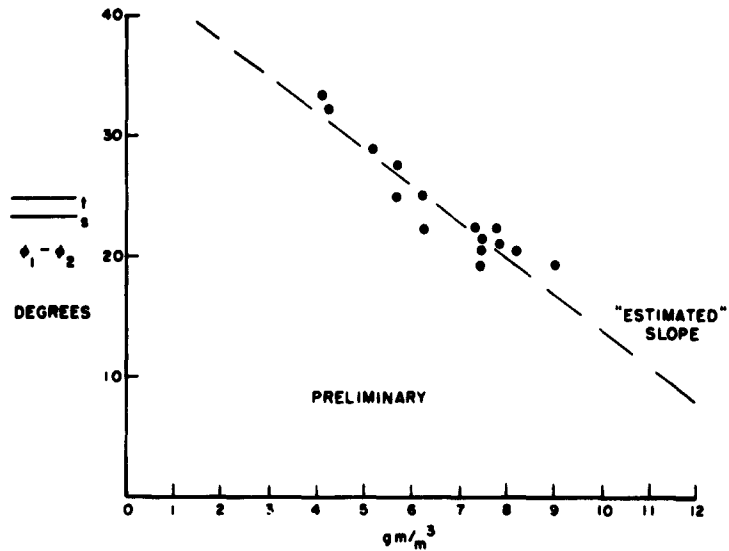


Figure 1-15



## HUMIDITY VS TIME DIFFERENTIAL PHASE VS TIME

Figure 1-16

In conclusion, it appears that the dispersion due to water vapor is measurable and consistent with theory for dynamic refractive effects. It should be pointed out that the horizontal path utilized for the measurements reported in this paper is probably the most sensitive condition one would ever encounter, and that a slant path, characteristic of tracking systems, would greatly decrease the effect. Plans are underway to make measurements on a slant path, and results of the two conditions will be compared.



COMMENTS BY KENNETH A. NORTON

made at

The MITRE Meeting

At the recent meeting at The MITRE Corporation, I mentioned a paper which I had prepared for the U.R.S.I. meeting in Japan. A copy is presented elsewhere in this Section. The discussion of the correlation of apparent range variations measured simultaneously on two radio frequencies begins on page 1-188 this was the theory applied to the explanation of the spectra obtained by Sullivan and Richardson with The MITRE Line Integral Refractometer.

Subsequent to the meeting, E.C. Barrows used the results obtained in his paper to obtain the spectra shown in Figures 1-1, 1-2, 1-3 and 1-4. Three spectra are shown in each figure. Figure 1-1 shows, with the path parameters used with the line integral refractometer, i.e., 20.3-km path length and 1-meter diameter antennas, (a) the spectra of variations of path length  $R_{e1}$  measured at a frequency  $\nu_1 = 15.6 \times 10^9$  c/sec, (b) the spectra of  $R_{e2}$  measured at a frequency  $\nu_2 = 31.2 \times 10^9$  c/sec, and (c) the spectra of the difference  $R_{e2} - R_{e1}$ . To fit these spectra to those observed experimentally by Sullivan and Richardson, the magnitude of  $W(f)$  can be raised or lowered, since the magnitude shown on this graph represents a median of the values observed by Thompson and Janes at the National Bureau of Standards (NBS), and the curves can be shifted to the right or left to fit the effective mean wind velocity normal to the path since all of the curves shown are for an assumed velocity of 2 m/sec. Note the small difference in the expected spectra for 15.6 and 31.2 gc/sec; the small

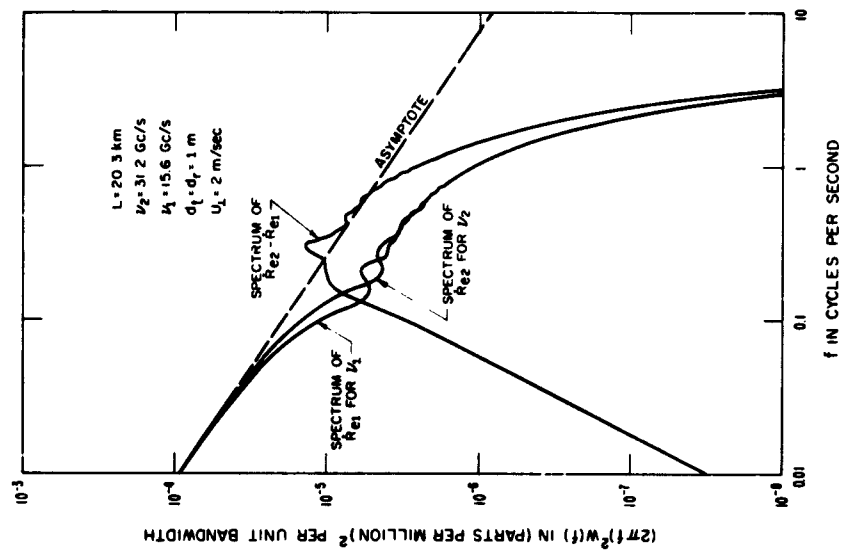


Figure 1-1

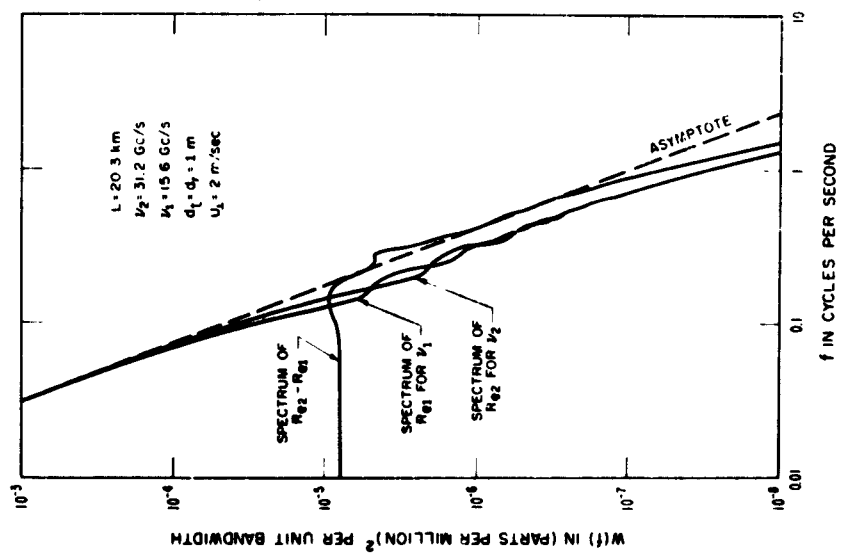


Figure 1-2

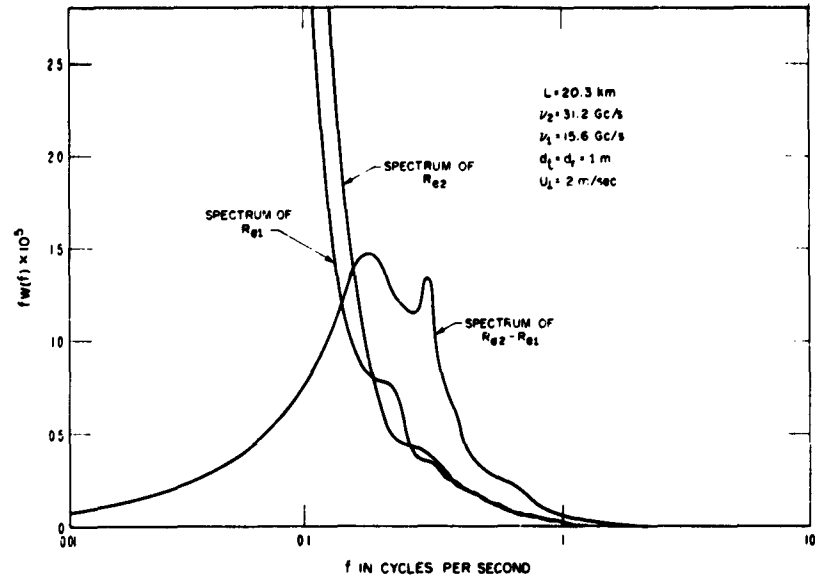


Figure 1-3

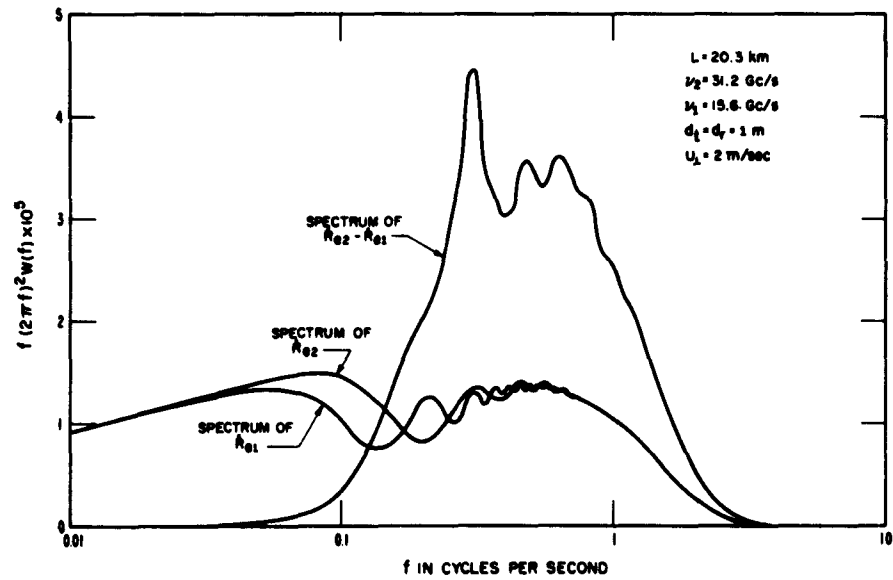


Figure 1-4

difference as shown on this graph arises solely from the fact that geometrical optics can be used at higher fluctuation frequencies (Equation 1-11) in proportion to  $\sqrt{\nu}$  and no allowance was made for the fact that  $\Delta R_{e2}$  will be slightly larger than  $\Delta R_{e1}$  since  $\nu_2$  is near the water vapor absorption line. The dashed asymptote in Figure 1-1 has the slope  $f^{-8/3}$ , which would be expected by geometrical optics in accordance with the Obukov-Kolmogorow theory of homogeneous turbulence and the use of isotropic antennas. The difference between the dashed and the solid curves illustrates the smoothing achieved by the 1-meter diameter antennas and includes a drop by one-half which follows from the use of wave optics.

Figure 1-2 shows the same three spectra for range rate which were obtained from the spectra in Figure 1-1 simply by multiplying by the factor  $(2\pi f)^2$ .

Figures 1-3 and 1-4 show the range and range rate spectra on a linear scale after multiplying by  $f$ , and illustrate the relative contributions to the total variance by different spectral regions since:

$$\sigma^2 = \int_{\ln f = -\infty}^{+\infty} fW(f)d(\ln f)$$

We may conclude from the above analysis that The MITRE Line-Integral Refractometer may very well provide a powerful means for correcting in real-time for that large portion of those changes in  $R_e$ , and thus also in  $\dot{R}_e$ , which are caused by fluctuations in water vapor along the propagation path. Figure 1-12 on page 1-180 of this Section shows that, for an assumed wind speed of 2 m/sec normal to the path, most of the variance of  $R_e$  (after appropriate correction by  $N_g$ ) occurs in the fluctuation frequency range from  $10^{-5}$  to  $10^{-3}$  c/sec while most of the variance of the  $N_g$  corrected  $R_e$  occurs (see Figure 1-13, page 1-183) for  $f > 10^{-4}$  c/sec and (Equation 1-12, page 184) for 1-meter diameter antennas for

$f < 0.52$  c/sec but for 10-meter diameter antennas for  $f < 0.052$  c/sec. Since it is evident in Figure 1-3 that most of the variance of  $(R_{e2} - R_{e1})$  occurs (for an assumed wind speed of 2 m/sec) at fluctuation frequencies greater than  $10^{-2}$  c/sec and (see Figure 1-4) since most of the variance of  $(\dot{R}_{e2} - \dot{R}_{e1})$  occurs for  $f > 10^{-1}$  c/sec it does appear that The MITRE Line-Integral Refractometer holds promise as a useful means for improving either radio guidance or tracking instrumentation. Note that in the radio guidance application, the midpoint of the propagation path will move through the atmosphere at speeds ranging from 100 to 1000 m/sec so that all of the fluctuation frequencies mentioned above will be larger in such an application by a factor ranging from 50 to 500.

In my paper, I emphasize the proven utility of the Bean, Cahoon and Thayer linear regressions on  $N_s$ , such as those shown on Figures 1-2 and 1-3, for bending and range corrections. These are not only simpler but better than those derived from an exponential model. On page 1-182 of the attached report, I point out that  $N_s$  corrections to  $\Delta R_e$  measurements should be made only after filtering out the high frequency variations of  $N_s$  by averaging, or other more sophisticated means. If these are not filtered out, the corrected values will be worse than the uncorrected values.

## A SUMMARY OF TROPOSPHERIC PHASE STABILITY MEASUREMENTS

Dr. M. C. Thompson

National Bureau of Standards  
Boulder, Colorado

### INTRODUCTION

In baseline tracking systems, the variability of phase velocity of electromagnetic signals in passing through the atmosphere enters as a quasi-random error. The slower variations in atmospheric characteristics, resulting from diurnal, seasonal, and more or less erratic air mass changes, can produce errors of the order of tens of centimeters in apparent range. In many cases, this type of error can be corrected by conventional meteorological observations. In addition, the general atmospheric turbulence introduces a higher frequency error, essentially random in nature, which cannot, at this time, be corrected. In all cases observed in our work, the magnitudes of these more rapid error components are small compared with the systematic components.

Generally then, it appears that by using appropriate supplementary measurements one can reduce the errors from long-term changes, and that the higher frequency errors tend to become smaller as the frequency increases. This suggests that there may be some frequency at which the residual error peaks. The definition and description of this residual error spectrum is one of the important questions we wish to study in connection with tracking system design.

In a typical tracking configuration, there are three paths which contribute to these errors. Two of these are the ground-to-missile paths which are generally several hundred kilometers in length and

sweep through the atmosphere as the missile progresses. The third is the ground-to-ground link which completes the measuring system. This path is normally about ten kilometers long, is located within a few hundred meters of the ground, and is stationary (spatially).

The research programs carried out at the National Bureau of Standards (NBS) have included both types of propagation paths. The actual measurement programs have included configurations simulating ground-to-ground path and air-to-ground paths. In the latter category, various antenna arrangements and baseline lengths have been studied. Most of these experiments have been performed using 9.4 gc but in some cases, 100 or 1000 Mc signals were used simultaneously.

Four generally different geographical areas have been used to date: the eastern foothills of the Colorado Rocky Mountains, Cape Kennedy, Maui, and Eleuthera. Thus, the paths have included land, water and mixed terrain and, in Colorado, all seasons of the year.

Most of the results of these measurement programs have been presented in NBS reports listed in the bibliography.

#### CURRENT ACTIVITIES

In the present program being conducted for the Air Force Electronic Systems Division (ESD), primary emphasis is placed on determining experimentally the dependence of atmospheric errors on baseline length and orientation. Other problems being investigated include the "bias" or slowly varying errors in range and angular position, and the extent to which various refractive index data can be utilized in correcting these errors. The dependence of atmospheric tracking system noise on antenna aperture size is also being investigated. This dependence is expected to be most noticeable at the high-frequency end of the fluctuation power spectrum, and hence, should be most important in velocity measurements. Finally, the value of refractometer data to serve as predictors of atmospheric tracking system noise is being studied.

During the summer of 1963, experimental measurements were made at Boulder. These were designed for study of the problem areas, and to serve as a preliminary pilot study for more extensive measurements now being undertaken in Hawaii. The dependence of angular position errors on baseline length were studied with three orthogonal antenna arrays. Azimuth angle variations were recorded using baselines 1.5, 32, 215 and 384 meters in length. Elevation angle variations were measured with horizontal baselines 76, 239 and 516 meters in length and vertical baselines 1.2, 7.6 and 28 meters long. A mountain-top target, at a distance of 15.5 km and elevation angle of 44 milliradians, was used in all cases. Atmospheric refractive index measurements were made using airborne, tower-mounted and ground-based refractometers. Comparative recordings were made of range noise from two antennas 46 centimeters and 3 meters in diameter.

Preliminary data analysis has yielded estimates of rms angular position and range difference variations as a function of baseline length for all three baseline orientations. Subsequent analyses will examine the power spectra of these variables and of the metric range data from the antenna size experiment. They will also study the relative utility of the various refractive index variables.

In many actual tracking problems, the propagation paths sweep through the atmosphere as the target proceeds along its trajectory. This modifies the effect of atmospheric structure as it appears in the output of the tracking system. Proper methods for translating the results of the geometrically stationary experiments to the moving target problem are being studied from a theoretical standpoint.

A second phase of the experimental measurement in Maui is being carried out under the sponsorship of the Air Force Aeronautical Systems Division (ASD). In this phase, the lower terminal (near sea level) will serve as the target while the series of normally displaced stations along the rim of Haleakala will simulate a synthetic array looking toward earth. Because of the usual variations of turbulence



with altitude, it is anticipated that the atmospheric phase noise in such a system will exhibit significantly different characteristics from the normal ground-based configuration.

The work which we have just begun, or are just now initiating in Hawaii is very similar to the work we did there in 1956, except that we have taken some pains to obtain a wider variety of data containing configurations of ground units and the ground antennas. We will be operating azimuth arrays and arrays in-line with the target position and on vertical baselines, simultaneously. We will have the supplementary meteorological data and the refractive index data. We will have also light aircraft equipped with refractometers for obtaining a variety of measurements in the general vicinity of the path. One technique still in the experimental stage is that of flying the aircraft essentially along the propagation path. There are some limitations to how far the pilots will cooperate in this, but so far we have had pretty good luck in getting close to the path. The results to date have been indecisive, but we plan to continue using this approach to some extent during these new Maui measurements. We are also planning on a certain amount of general flying, probably in a ladder-type flight plan, to get some general idea of the spectral distribution of the turbulence at different levels in the vicinity of the path.

The additional portion of the work being planned for Hawaii is being done for ASD, and is of sufficient interest to warrant a brief discussion. In the conventional arrangement for this baseline tracking problem, the antennas on the ground are spaced by some amount and the target is moving overhead. The inverted case will be investigated by displacing the antennas along the rim of the mountain and looking down through atmosphere at a beacon which is fixed essentially at sea level. This will not produce exactly the same kind of results as the case where the turbulence in the atmosphere is distributed uniformly with height. Therefore, one would expect to see a different amount of noise.

The reason for the difference in effect is that in the one case, the baseline is located in the place where the biggest intensities of turbulence are located and, therefore, for separations of 100 meters or so, the correlation is less except for the long-term fluctuations. If the baseline is located at the top, the short-term fluctuations will tend to be more highly correlated since the paths are converging at the bottom of the atmosphere. For this condition, 2000 feet out of the total 80,000-foot path will be very close to each other and in the most dense part of the atmosphere.

At the request of ESD, a comprehensive literature review has been made concerning problems of optical refraction in the atmosphere, of errors from such refraction, and of possible means of reducing, or compensating for, such errors.

This review is nearly completed. It contains 23 subchapters, dealing with subjects such as refraction in plane and spherically stratified media, refractive index variations, radio refraction, scintillation, and coherence problems. More than 400 original publications and reports have been read, abstracted, and incorporated into this report. It will contain over 200 pages and about 26 illustrations.

Main emphasis in the report has been placed on the effects of atmospheric refraction on the propagation of electromagnetic radiation at optical frequencies. We distinguish systematic or normal refraction from random refraction. The former can be deduced from stratified layer models which allow a prediction using various types of atmospheric models; the latter normally requires analysis by statistical methods. Numerous aspects of random refraction, that is, scintillation, in its widest sense, are discussed. It is believed that further efforts should be centered around better instrumentation for the detection and accurate quantitative determination of atmospheric conditions which produce random refraction.

## BOULDER, COLORADO MEASUREMENT RESULTS

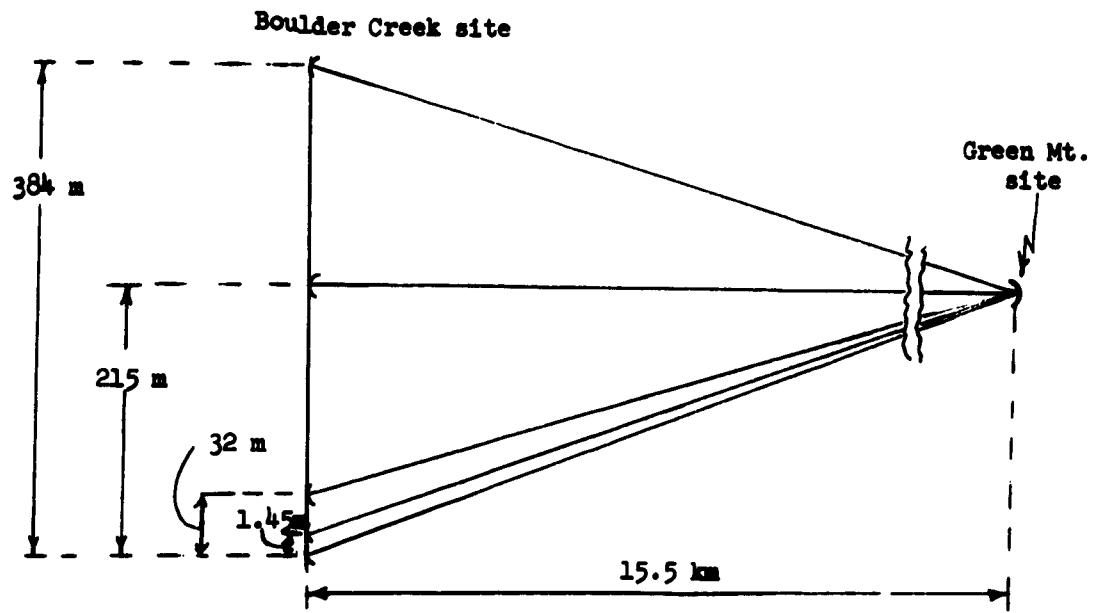
H. Janes

National Bureau of Standards  
Boulder, Colorado

The work we did this summer was designed to clarify the relationship between the baseline length and the magnitude of angular errors (azimuth and elevation angles), and also to compare variations in apparent range in our 10-mile path over Boulder with corresponding variations in refractive index. We have pointed out that there was some question of the value of making measurements with an airplane flying up and down the path, and we were attempting to gather data that would clarify that problem. We also made measurements to determine the results on antenna aperture size by using a 10-foot dish and an 18-inch dish side by side and comparing the range variations as seen by these two aperture sizes. In addition, we wanted to check out the measurement system and be certain that everything would operate properly when we unloaded our gear at Maui.

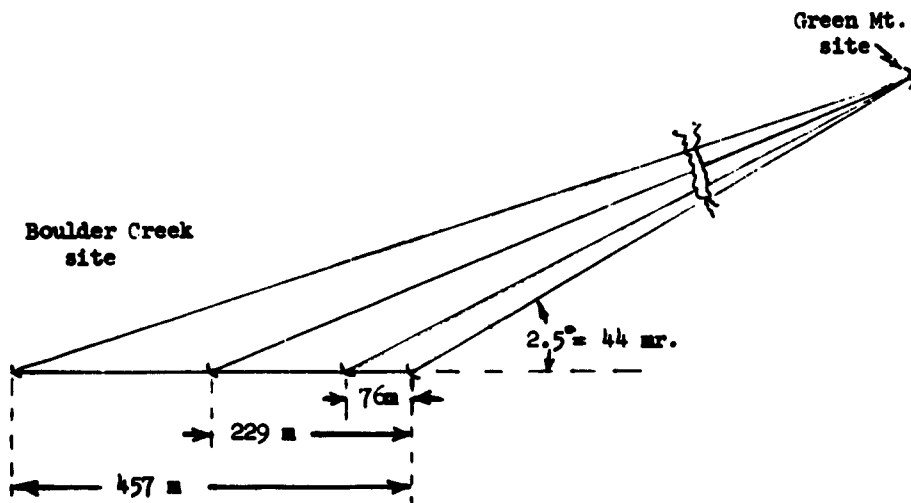
Figure 1-1 shows the arrangement we used at Boulder Creek this summer. Azimuth baselines ranging in length from 1.45 to about 380 meters and a target 15.5 kilometers away were used. These baselines were operated simultaneously. The statistics of the apparent azimuth variations in the location of this target are being analyzed as a function of these various baseline lengths.

Elevation angle fluctuations using the in-line baseline ranging from 76 to 457 meters, (Figure 1-2) were investigated. The elevation angle to the target is about 44 milliradians, which is not a very steep angle but is probably down in the limiting case of most



BOULDER CREEK "AZIMUTH" BASELINE LAYOUT

Figure 1-1



BOULDER CREEK "IN - LINE" BASELINE LAYOUT

Figure 1-2

operational targets. For the vertical baseline a 30-meter tower provided facilities for making measurements on vertical baselines ranging from 1.2 to 28 meters.

Figure 1-3 contain examples of the long-term variations on apparent azimuth measured. For the different baseline lengths (as one would expect in terms of millimeters of range difference), the longer the baseline, the larger the fluctuation. The long-term variations in azimuth angles for the normal baseline and the variations on the in-line horizontal baseline (which are really fluctuations in the elevation angle) are also shown in Figure 1.3. The different baselines used, 76, 239, 516 meters, etc., are noted in this Figure. It can be seen that a trend in one baseline length, shows up proportionately in the others.

The Figure also shows some results obtained from our vertical baseline. We did not have room on the tower for as many choices as in the horizontal case. The Figure gives a very crude idea of very long-term variations. I should point out that the analysis currently being conducted will look at the short-term variations, which are at least as important as these slow variation errors in apparent angle. The comparison of simultaneous vertical and horizontal baseline errors (Figure 1-4), using the tower and in-line elevation angle measuring baseline simultaneously, indicates that the two are roughly correlated. I should also point out that one of these should be drawn upside down, because actually as the refractive index at the ground changes, the two baselines behave in opposite directions; the vertical baseline shows errors in one direction and the horizontal baseline shows errors in the opposite direction. The baselines were chosen to be roughly comparable in effective length; in other words the shadow cast by the vertical baseline as seen from the target was similar in length to the horizontal baseline.

The rms fluctuations versus baseline length taken from the previous graphs for normal, in-line, and vertical baselines are

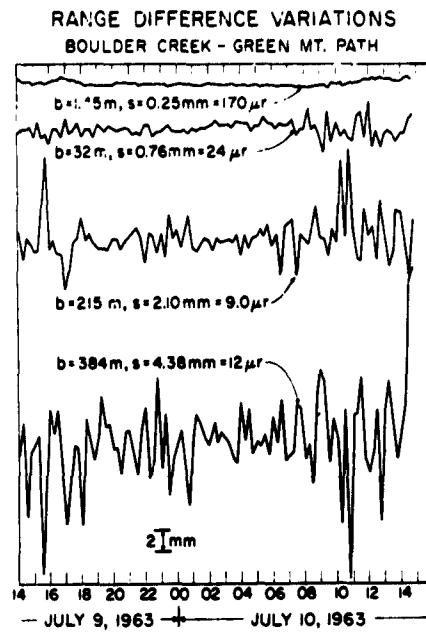


Figure 1-3(a)

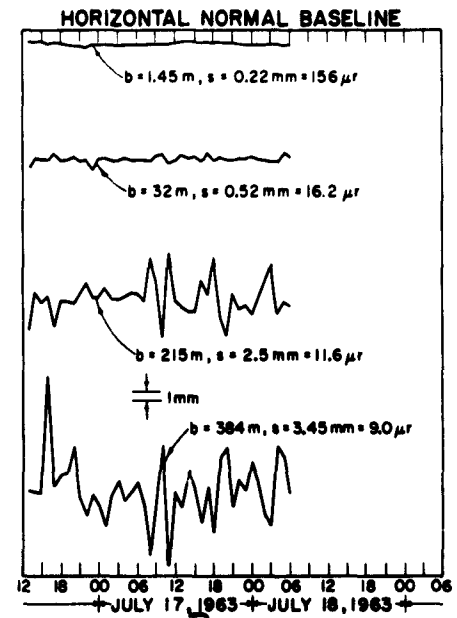


Figure 1-3(b)

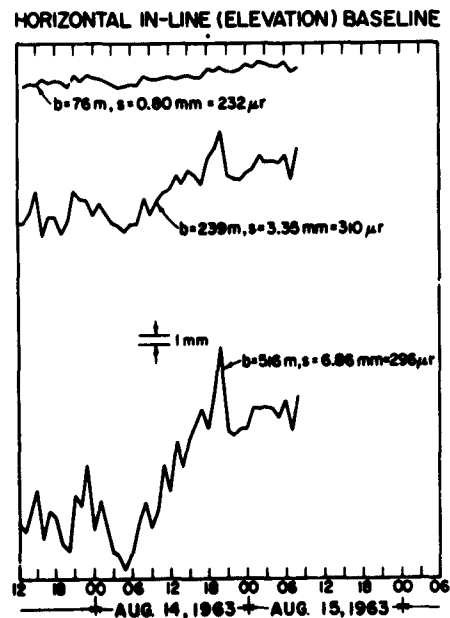


Figure 1-3(c)

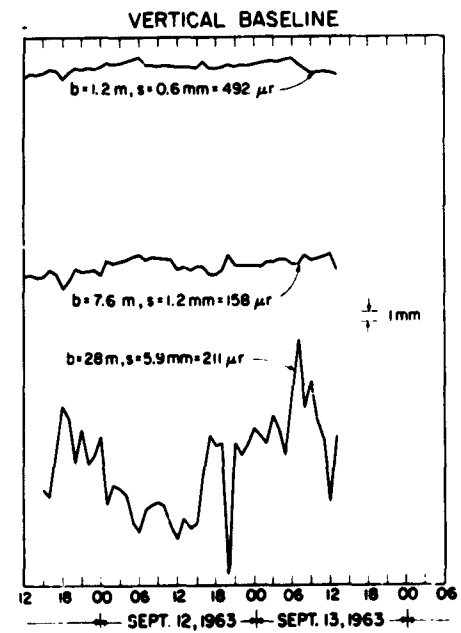


Figure 1-3(d)

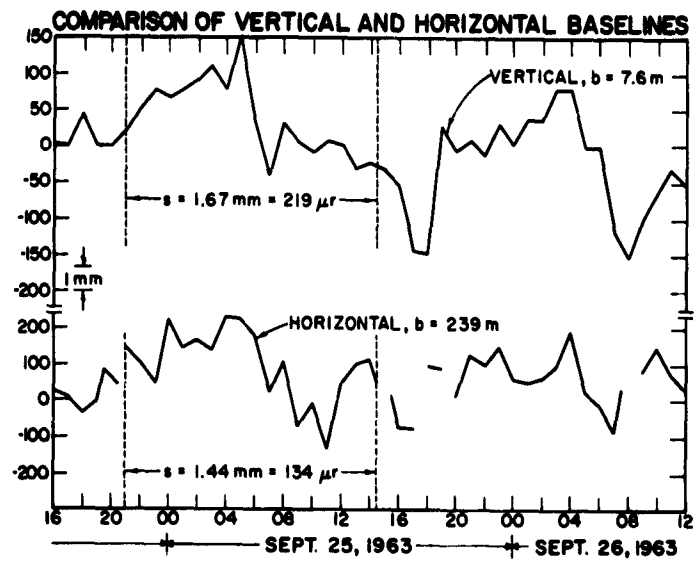


Figure 1-4(a)

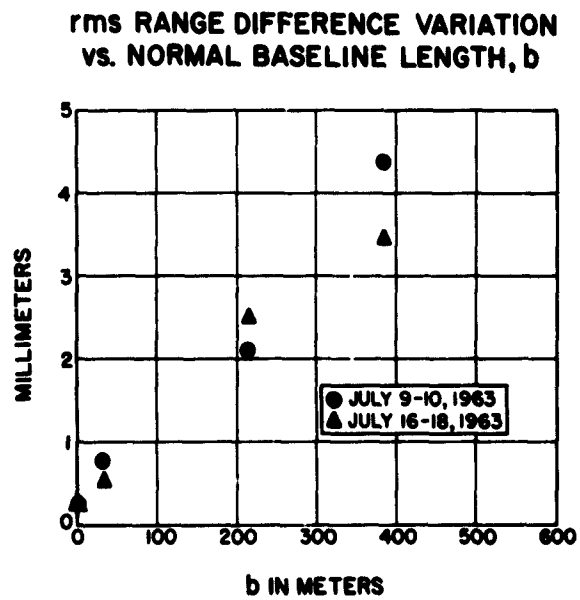


Figure 1-4(b)

shown in Figure 1-5. As can be seen, the range difference increases with baseline length; fortunately, the error in terms of micro-radians decreases with increasing baseline length. This is true at least for the relatively short baselines investigated thus far; at Maui we plan also to use longer baselines. The elevation angle variation Figure shows that there is not much dependence of actual angular error on baseline length. The rms fluctuations over a two-day period are shown in Figure 1-6. These results are based on two days' worth of data without smoothing or any processing and simply computing the rms fluctuations about the two days' sample means. The circles indicate the vertical baseline case. There is quite a dramatic increase in the range difference fluctuations as a function of the vertical baseline length.

(Q) Does this show that you get more range error the longer the baseline?

(A) In terms of millimeters of range difference, yes. It is necessary to divide by the baseline length to get an estimate of angular errors.

(Q) Is this error due to noise?

(A) This is really noise.

(Q) Noise increases with baseline?

(A) That is right ~ except in the case of the in-line baseline. Apparently the noise expressed in terms of microradians did not increase. These values have nothing to do with absolute angular errors; they are simply the noise fluctuations with time about a sample mean; in this case, a two-day mean. We did not measure in any absolute errors.

This plot compares the angular error for the vertical and horizontal in-line baselines, where, in the case of the horizontal



**rms AZIMUTH ANGLE VARIATION  
vs. BASELINE LENGTH, b**

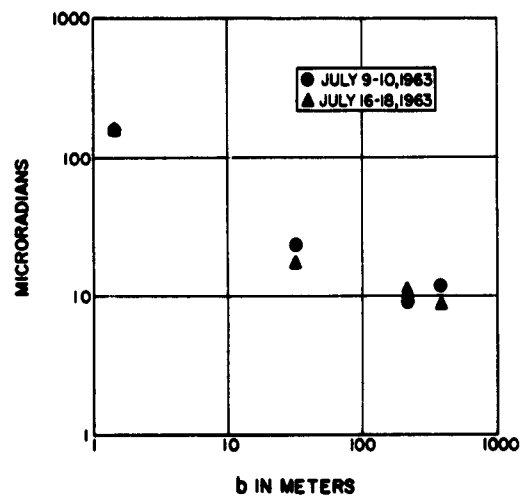


Figure 1-5(a)

**rms RANGE DIFFERENCE VARIATION  
vs. IN-LINE BASELINE LENGTH, b  
AUGUST 13-15, 1963**

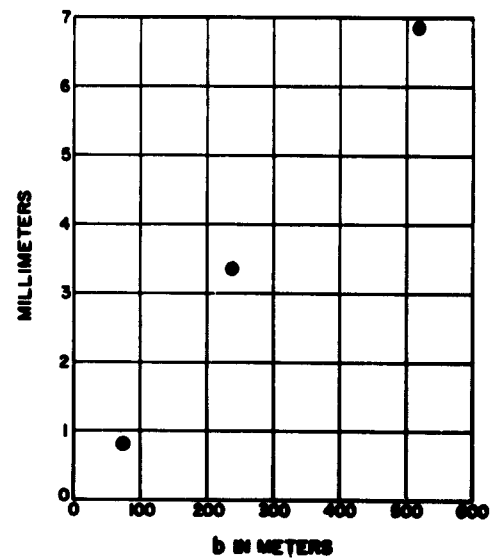


Figure 1-5(b)

**rms ELEVATION ANGLE VARIATION  
vs. IN-LINE BASELINE LENGTH, b  
AUGUST 13-15, 1963**

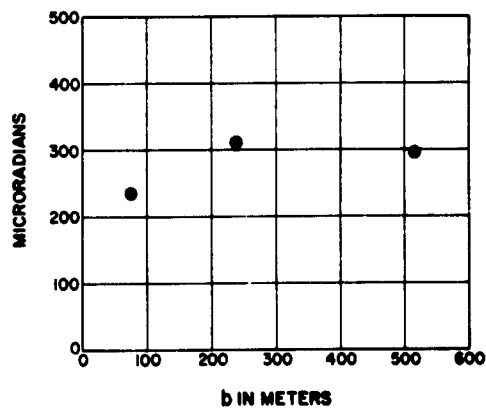


Figure 1-5(c)

**rms RANGE DIFFERENCE VARIATION  
VS. VERTICAL BASELINE LENGTH  
SEPT. 11-13, 1963**

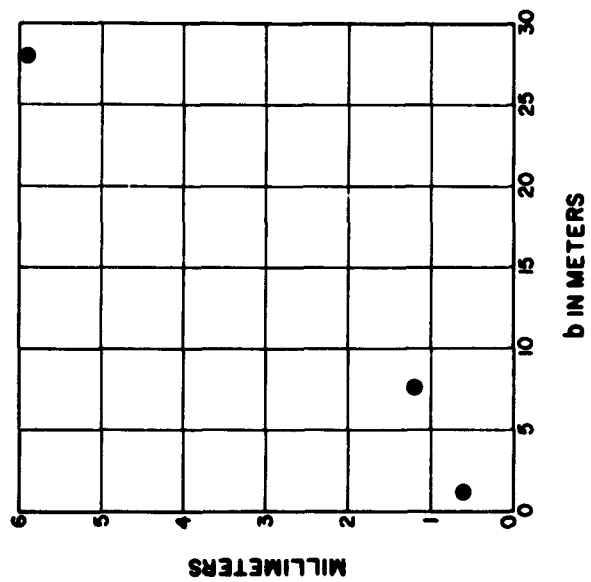


Figure 1-6(a)

**rms ELEVATION ANGLE VARIATION  
VS. BASELINE LENGTH  
SEPT. 11-13, 1963**

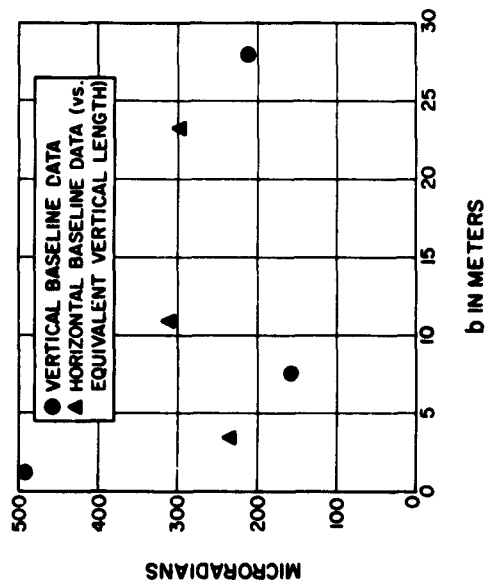


Figure 1-6(b)

data, the baseline length is transformed into the equivalent vertical dimension for comparison purposes.

Notice the point for the shortest baseline in the vertical case. It was, relatively speaking, a little bit noisier than the rest. The analysis that we will be performing will consist of breaking these angular position variances into their spectral components in order to better handle the problem of extrapolating these results to other baseline lengths. Figure 1-7 is my conception of what the spectra should look like as a function of baseline length. This, of course, is highly idealized. We plan to extend what was done in Boulder, in our Hawaii measurements. There will be more space for laying out baselines since they will be situated on an abandoned Naval Air Station. We will be able to extend the normal or azimuth baselines to 1800 meters without any difficulty. For the in-line horizontal baselines we have complete latitude up to 1200 meters, but we are still restricted to the same 30-meter tower for the vertical baseline work. The mountain which will be used for the target site has a gradual slope and is more or less flat on top (Figure 1-8). The whole profile from the mountain peak down to the base is a very smooth curve; there are two runways, one of which is about 6000 and the other about 8000 or 9000 feet long, for our baselines. The reasonably uniform and simple foreground conditions minimize multipath effects. Views of the Hawaiian test site are shown in Figure 1-9.

# Range and Range Difference Spectra\*

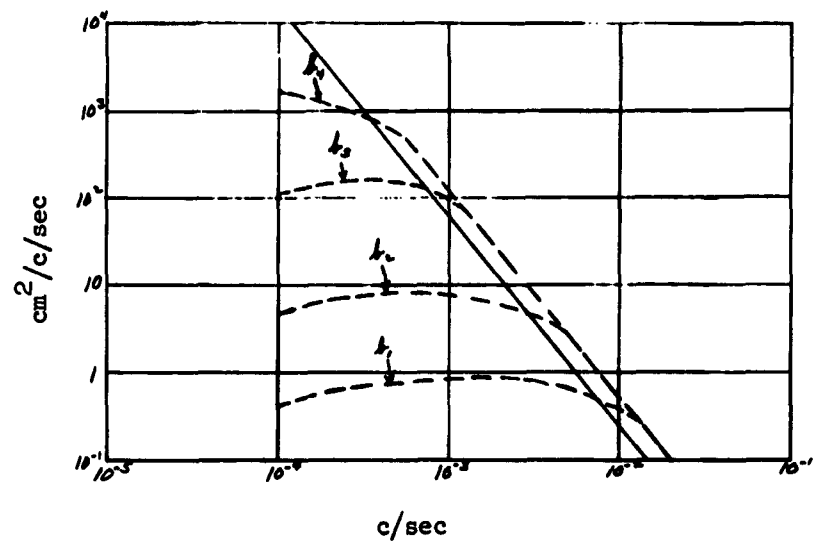
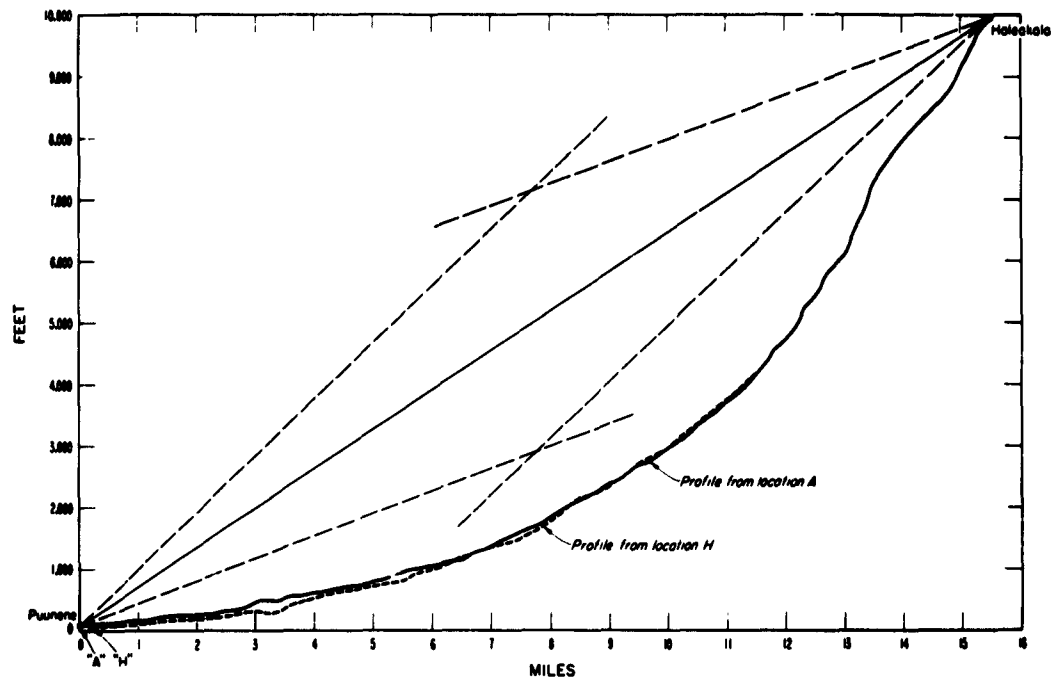


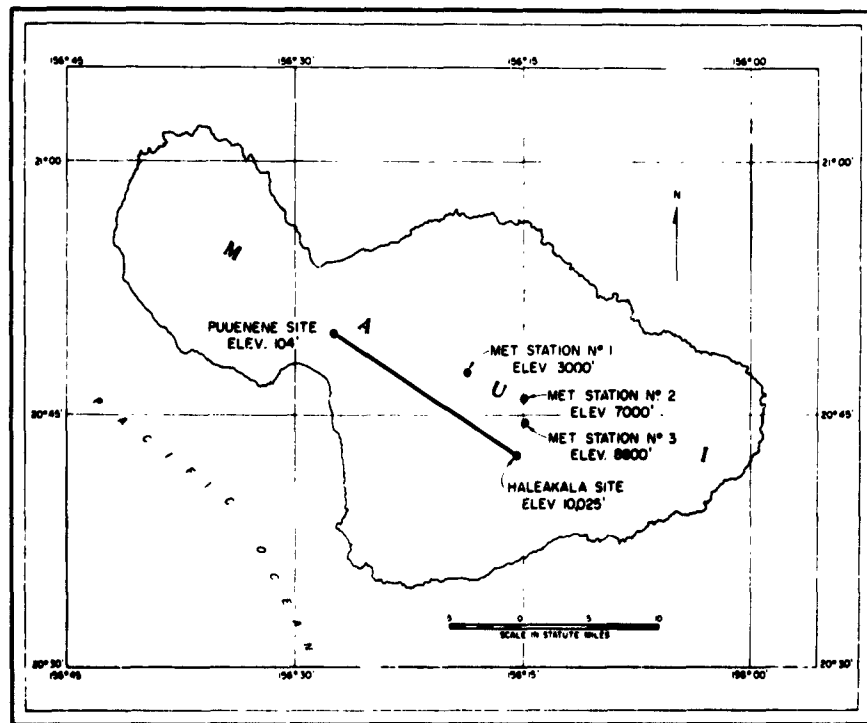
Figure 1-7

\*Range —————  
Range Difference - - - - -



Profile of Haleakala-Puunene path showing half-power beam-widths of 0.514 Mc/s antennas.

Figure 1-8(a)



Location of propagation paths used in Maui experiments.

Figure 1-8(b)



Elevated End Location of the Haleakala Crater -- Puunene Measurement Site

Figure 1-9(a)

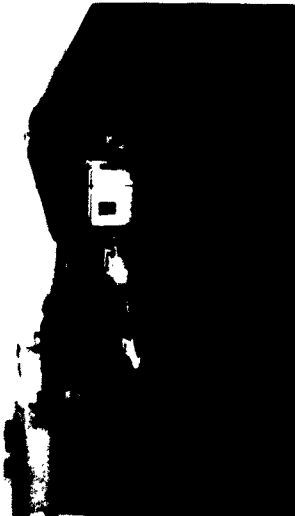


Figure 1-9(b)



Baseline and Antennas at Puunene, Maui

Figure 1-9(c)

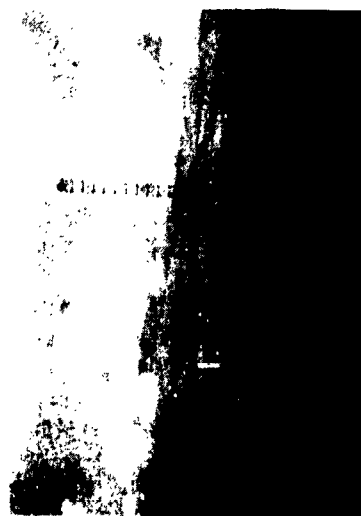


Figure 1-9(d)

## OPTICAL SCINTILLATION - REVIEW OF THE LITERATURE

Jurgen R. Meyer-Arendt and Constantinos B. Emmanuel

National Bureau of Standards  
Boulder, Colorado

### INTRODUCTION

This literature review on optical scintillation has been prepared on request by the United States Air Force Electronics Systems Division (ESD), Hanscom Field, and The MITRE Corporation. The National Bureau of Standards (NBS) report to be issued in 1964 is concerned with problems of regular and random optical refraction in the atmosphere, with errors arising from such refraction, and with possible means of reducing, or compensating for, such errors. The following subjects are included: refraction in plane and spherically stratified media, refractive index variations, radio refraction, scintillation as a function of aperture size, zenith distance, and a variety of meteorological conditions, contrast reduction, refraction, diffraction, and autocorrelation analysis of scintillation, coherence problems, and suggestions as to what further theoretical and experimental efforts should be undertaken. The Table of Contents (Figure 1-1) indicates the organization of the report. The NBS report number can be obtained by writing to Dr. Meyer-Arendt.

### RECOMMENDATIONS FOR FURTHER RESEARCH

In contrast to radio frequencies, the ionosphere is no barrier to optical telecommunication. Some degradation of optical signals, however, is likely to take place in the lower atmosphere. The problem on hand, then, is whether, and if so, how, it may be possible to

A	Regular Refraction
A-1	Introduction
A-2	Refraction in a Plane Stratified Medium
A-3	Refraction in a Spherically Stratified Medium
A-4	Optical Refractive Index and Refractive Index Variations
A-5	Radio Refraction
B	Random Refraction
B-1	Light-Optical Scintillation, Definitions
B-2	Stellar Shadow Bands
B-3	Scintillation and Seeing
B-4	Physiological and Psychological Factors Related to Scintillation
B-5	Scintillation as a Function of Circular Aperture Size
B-6	Scintillation as a Funtion of Zenith Distance
B-7	Scintillation as a Funtion of Site Elevation and Latitude
B-8	Color Scintillation
B-9	Frequency Range of Scintillation
B-10	Terrestrial Scintillation
B-11	Scintillation and Meteorological Conditions
B-12	Contrast Reduction
B-13	Refraction Theory of Scintillation
B-14	Diffraction Theory of Scintillation
B-15	Analysis of Turbulence Element Fluctuation
B-16	Radio Star Scintillation
B-17	Coherence
B-18	Recommendations for Further Research
C	References

FIGURE 1-1

TABLES OF CONTENTS OF NBS REPORT BEING PREPARED UNDER THIS TASK



(a) reduce and/or (b) utilize such degradation which may result from optical, systematic as well as random, refraction.

The first alternative would mean that ways be sought to enhance the accuracy at which positions can be determined as a function of space and time. The requirements for accuracy are given if the position of a space vehicle or other object is to be determined to the highest degree obtainable or if high-precision geodetic measurements are to be conducted. The second alternative, the better utilization of atmospheric phenomena, would relate to weather-forecasting, to the prediction of light and radio propagation through the atmosphere, and to similar tasks.

Several means to achieve these goals follow directly from the preceding discussions. A telescope of large aperture will smooth out the dancing and pulsation of the image of a celestial object, thus giving a time-average of the position of that object. Sufficiently long exposure times have about the same effect. Observing the object at longer wave lengths, such as near the red end of the spectrum (provided the system has no serious aberrations for just such wave lengths), will, in the presence of atmospheric turbulences, enhance the distinctness of stellar image.

Extensive theoretical work has very much improved our capabilities of accurately predicting, and subsequently correcting for, atmospheric refraction effects which otherwise induce serious errors in the localization of celestial and terrestrial objects. We only refer to the development of models of the atmosphere by Gerrard (1961), Strand (1953), Hamilton (1956-57), and to the discussion of atmospheric models in Chapter A-3 of the NBS Report to be issued. This approach related only to systematic changes, and hence to systematic or regular refraction in the atmosphere. Random perturbations, by their very nature, cannot be assessed in such a way. But these are just the errors which remain after the usefulness of regular refraction models has been exhausted and which at this state

seem to require the major effort of research and development.

Similarly, our knowledge of the actual variations of the physical state of the atmosphere is rather limited and we are forced to make generalizations by approximation. Whenever actual conditions, prevailing at a given point in space and time, are required to be known, such generalizations, of course, will not suffice for the purpose on hand. The most direct way of solving this problem is to carry out actual measurements, for instance, of the refractive index along the path of a missile or along the line of sight of an astronomical or geodetic determination. This is not easy, although not impossible, and often rather expensive. Direct measurements from airplanes Overcash (1951), from sounding rockets, or from satellites, as proposed by Jones, Fischbach, and Peterson (1962), are some of the possibilities. Anderson, Beyers, and Rainey (1960) confirm that errors in ranging and tracking through the atmosphere are not primarily due to the instrumentation, but to meteorological conditions which, at the present time, cannot be monitored and corrected for properly.

Only if we are able to determine actual pressures, humidities, temperatures, and perhaps other parameters in a given cross section, can we hope to correct for random perturbations. It is believed, that not only are better theoretical models needed, but also better means for specifically determining the unpredictable fluctuations and other complex parameters which are encountered in the field. To this end, a series of specific research areas are proposed and outlined below:

#### Analytical Studies of Atmospheric Models

Atmospheric models have been refined to a high degree of usefulness. However, there seems to be a need for models that take into account the wave-length dependency of refraction; that is, dispersion. This is especially true at low-elevation angles and in the ultraviolet and infrared. Furthermore, models are needed which

not only are based on horizontal stratification, but which assume as well inhomogeneities in the horizontal dimensions. Work of this kind will involve a statistical evaluation of such phenomena.

#### The Continuous Determination of Water Vapor Pressure in The Atmosphere

Such determinations could be made using a combination radio and light optical refractometer. The radio component of the system would be used to record and to continuously monitor the absolute refractive index and refractive index variations which may change as a function of space and/or time. The light optical system component would be used to determine air density variations. The subtraction of these from the radio data will yield the relative water pressure, without being dependent on any (infrared) absorption phenomena.

#### Construction of a Scanning System for Monitoring the Lateral Excursions of a Light Beam Passing Through a Turbulent Medium

The problem is to record continuously in space and time the lateral deviations of a highly collimated beam of light which might be produced by passing the beam through nonhomogeneous media of various kinds.

#### The Development of Schlieren Systems for Optically Probing the Atmosphere

Main emphasis in this area is placed on the development, calibration, and utilization of novel schlieren systems which are suitable for optical determination of refractive index variations  $\partial n / \partial x$  in representative cross sections through the atmosphere.

Schlieren systems as such are by no means new. Foucault (1859) was the first to use a schlieren technique for testing large quartz mirrors (Foucault's knife-edge test). Topley (1864) realized their significance. His first schlieren detectors contained

a triangle to block out the light. But Topler soon recognized that it is only one edge that is needed. Since then, a half plane or knife-edge is used most commonly as the light stop, but a variety of other elements such as slits, wires, grids, and colored sector plates can be used for the same purpose.

Further advances have been made by many authors, most notably Schardin (1942), Barnes and Bellinger (1949), Burton (1949), Prescott (1951), and Wolter (1956). The theory has been treated exhaustively by Sommerfeld (1954), Wolter (1957), Temple (1957), Reisman and Sutton (1961), Toraldo di Francia (1954), Rossi (1957), Smart (1960), and Baker, Meyer-Arendt, and Herrick (1963). Requiére and Giroux (1962) have increased the sensitivity of schlieren systems by using a ruby laser.

Schlieren systems can be built which not only give a faithful, two-dimensional image of refractive or reflective perturbations which constitute "schlieren" and which cause deviations of light, but which at the same time yield directly quantitative schlieren indications that make unnecessary any secondary densitometric evaluation of the schlieren image. One type of such a novel system is what we have called a two-grid non-complementary schlieren system. Two-grid systems of this kind have definite advantages. They contain in place of the slit and the knife-edge two Ronchi grids but these grids need not be complementary to one another; they only have to be parallel (Baker, Meyer-Arendt, and Herrick 1963). This makes the instrument rather easy to align. Even more important, it allows a by far higher light throughput, making the system easy to operate even with weak light sources.

Although schlieren systems are primarily used to record refractive index gradients, it is anticipated that absolute refractive indices can also be recorded. One way of doing this is by employing the moiré fringe effect in connection with the calibration system to be described later.

If schlieren techniques are to be applied to an "optical sounding" or probing of the atmosphere, clearly another feature would be highly desirable. In a conventional schlieren system, the field under investigation is located inside the optical system. This requirement makes it difficult to examine refractive index gradients that are located at a great distance from the observer. A new type of a schlieren system has been developed by one of the authors of this report in which the sampling field is outside the optical system proper. Figure 1-2 shows two block diagrams in which these two principal types of schlieren systems are compared with one another.

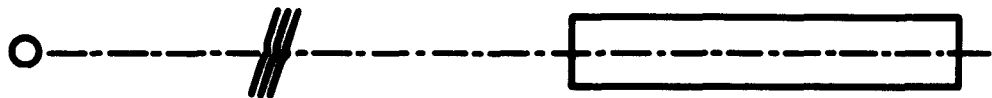
This new type of a system, which might be called a "forward-looking schlieren detecting instrument" or, for short, a "schlieren telescope" is basically an astronomical telescope with a Ronchi grid placed between the eyepiece and the image plane. Optical inhomogeneities in the sampling field produce distortions of the grid shadow pattern from which the density gradients can be determined.

Figure 1-3 presents a schematic arrangement of the optical components in a telescopic schlieren detecting system. (1 + 2) = light source + collimator (an artificial star is not needed when observations are made using the sun, moon, or a real star as the light source); (3) = field containing refractive inhomogeneities; (4) = objective lens of telescope; (5) = eyepiece; (6) = Ronchi grid, and (7) = image plane showing distortions of the shadow line pattern.

The Ronchi grid has 53 lines/cm and is positioned about halfway between the eyepiece and the photographic film. The grid is placed in a rotatable mount and can also be moved back and forth along the optic axis. Generally, the rulings in the grid are inclined at an angle of 45 degrees with the principal gradient in the object field. In preliminary investigations by Meyer-Arendt, Herrick, and Emmanuel (1963) the test objects, tiny flaws in a glass plate, were placed at a distance of 24.51-meters from the telescope objective,



CONVENTIONAL SCHLIEREN SYSTEM



SCHLIEREN TELESCOPE

Figure 1-2

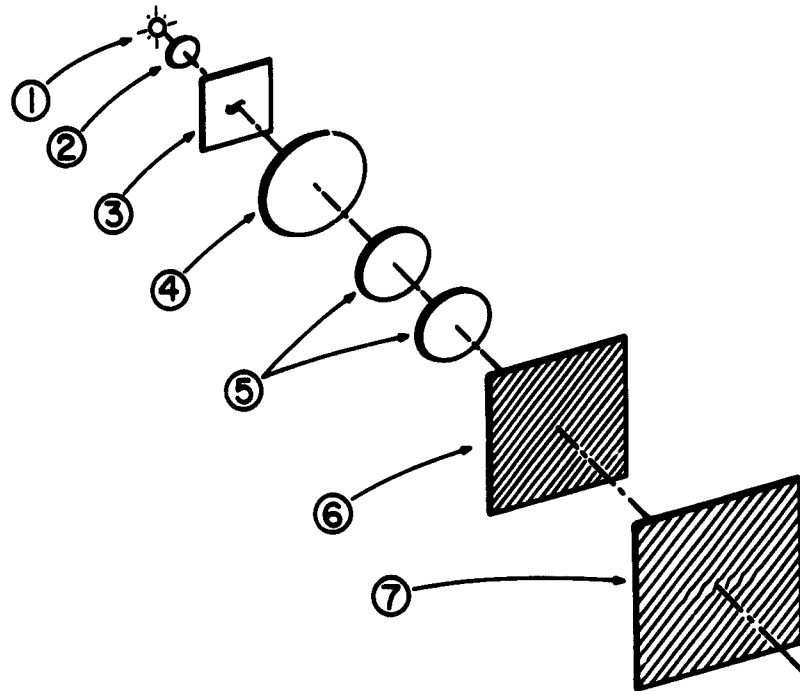


Figure 1-3

although there seemed to be no principal reason why they could not be placed much farther away.

The range of the system depends only on the focal length of the telescope which is part of the system. The sensitivity for measuring refractive gradients was better than 10N-units/millimeter (the length dimension as measured in the plane of the image) and seems sufficient for detecting refractive gradients in the troposphere. The response time depends on the characteristics of the electronic components necessary and hence, is considerably shorter than that of any more mechanical probe which has to be placed in, or moved to, proper positions.

How well the height of the perturbations can be determined using a single instrument can only be inferred from the focal discrimination capability of the telescope which in turn is a function of the size of the aperture and from experiments made by Kantrowitz and Trimpi (1950). That the sensitivity will be sufficient can be seen from studies by Bruch and Clastre (1948) where the undulation, or "boiling", of a solar limb could be related to the movements of air parcels near the tropopause. Optical soundings of the atmosphere were also described by Bellemin (1923) and Boutet (1950).

#### Development of a Multiple-Axis Telescope

The character of atmospheric turbulences can be assessed with a high accuracy by using a dual telescope. Two types of such instruments have been used: (1) large-aperture telescopes screened off except for two small holes or a rectangular slot in front of the objective lens, or (2) a tandem of two relatively small-aperture telescopes. The tandem system is more economical and, if supplemented by a third telescope, completely sufficient to detect all (horizontal) movements of turbulences in space. A height discrimination of the turbulent layers, furthermore, is possible (a) by the focal discrimination provided by the telescope and (b) by using rather narrow



acceptance cones for light entering each component telescope. If the finite distance between the three component axes is known, cross-correlation functions between any two telescopes can be obtained which, in turn, give the probability that certain inhomogeneities will be at a given height.

#### Development of a High-Precision Calibration Device for Schlieren Systems

It is obvious that a quantitative interpretation of schlieren patterns requires a reliable calibration method. Schardin (1942) had introduced for this purpose the "normal schlieren," that is, a lens of known diameter and focal length which is placed in the schlieren field. Such standards, and similarly wedges used as standard schlieren, are customarily evaluated by densitometry of the photographic records made or by direct photoelectric photometry.

#### Assessment of Image Deterioration in a Turbulent Atmosphere by Means of a Pulsed Laser

It is conceivable that continuous wave (c.w.) lasers do not yield enough energy for propagation and image deterioration studies over very long paths. If this is so, pulsed lasers will be required, necessitating photographic recording. A laser beam may be spatially modulated by inserting two-dimensional patterns of varying spatial frequency, for instance a Siemens star or sun-burst pattern or a variable-density or checkerboard modification of such a pattern. The deterioration effect produced by turbulence can then be directly read from the size of the blurred center inside of such a pattern.

#### Image Deterioration Studies Using C.W.-Lasers.

C.W.-lasers would permit continuous analyses of turbulence phenomena varying with time. It is proposed to use transfer functions as an established analytical means to express the character and degree

of such turbulence-induced image deterioration. The logical choice, if a cw-laser can be used as the light source, is to record which spatial frequencies pass through a medium of a given degree of turbulence. Varying spatial frequencies could be provided by means of a rotating sector or a rotating drum, in a way similar to that described by Murata (1960), Meyer-Arendt (1963), and Shannon and Newman (1963). Further theoretical details are found in Perrin (1960) and Smith (1963).

#### Depolarisation Effects of Atmospheric Turbulences on Light Signal Transmission

Many details are known about the state of polarization of skylight, of light passing through turbid media, and of stellar spectra. With the advent of signal transmission at optical frequencies, however, it seems desirable to investigate more fully the degree of depolarization which a direct, linearly polarized bundle of light undergoes while passing through a turbulent medium.

The degree of depolarization, in principle, can be determined by passing the light through two Glan-Thompson prisms or other polarizers. The first polarizer is used to obtain linearly polarized light. Rotating the second polarizer in the same path and recording the intensity of the light passing through gives the intensity as a function of azimuth. From this relationship the degree of depolarization can be deduced.

It would seem practical to perform a systematic study concerning the spectral dependence of the depolarization effect. This information about the spectral dependence of the effect will permit extrapolation for spectral ranges which otherwise might not be easily accessible but which are of considerable interest in the field of laser communication technology.

RESIDUAL RANGE AND RANGE RATE ERRORS  
DUE TO THE TROPOSPHERE

Eugene C. Barrows

Central Radio Propagation Laboratory  
Boulder Laboratories  
National Bureau of Standards

This communication gives some of the results of a paper [Barrows, 1964] in which electrical range fluctuations arising from tropospheric refractive index variations are studied theoretically. It gives theoretical expressions for the variances in uncorrected error in range  $R$  and range rate  $\dot{R}$  of a rocket or satellite. It also gives an expression for the frequency spectrum of electrical path length fluctuations which is valid when the fluctuation frequency is much greater than the vehicle velocity normal to the path divided by the range  $R$ . The frequency spectrum is expected to be useful in deciding how best to filter the received signal. However, one would never want to filter frequencies small enough to compare to those describing the actual vehicle trajectory. Nevertheless, in the above-mentioned paper, the frequency spectrum is given for the smaller fluctuation frequencies, which is also of interest in the design of radio guidance systems.

Let  $\Delta R_e(t)$  represent the stochastic or random fluctuation from the corrected statistical mean  $R_e(t)$  of the vehicle-to-receiver electrical path length at the time  $t$ . A typical way to correct  $R_e(t)$  is to use appropriately filtered surface values of refractive index at or near the time  $t$ . Let dots represent time derivatives, and  $\langle \rangle$

represent an ensemble average. Then the variances sought are

$$\sigma_R^2 \equiv \langle [\Delta R_e(t)]^2 \rangle, \quad (1-1)$$

and

$$\sigma_{\dot{R}}^2 \equiv \langle [\Delta \dot{R}_e(t)]^2 \rangle. \quad (1-2)$$

Also, the wanted frequency spectrum is defined by

$$W(f) \equiv \int_{-\infty}^{\infty} d\tau \cos(2\pi f\tau) \left\langle \Delta R_e\left(t - \frac{\tau}{2}\right) \Delta R_e\left(t + \frac{\tau}{2}\right) \right\rangle \frac{1}{R_e^2(t)}. \quad (1-3)$$

These quantities will be given in terms of the wave number spectrum

$$S(\vec{k}, \vec{r}) \equiv \frac{1}{\pi^3} \int d^3 r' \cos(2\vec{k} \cdot \vec{r}) \left\langle \Delta n(\vec{r} + \vec{r}', t) \Delta n(\vec{r} - \vec{r}', t) \right\rangle \quad (1-4)$$

of the refractive index fluctuations  $\Delta n(\vec{r} \pm \vec{r}', t)$  from the corrected mean in the vicinity of  $\vec{r}$  at a time  $t$ . An accurate determination of the wave number spectrum can only be obtained from spaced refractometer measurements since the wave number spectra obtained by using Taylor's hypothesis on single-point refractometer frequency spectra are not reliable at low fluctuation frequencies. Also,  $\sigma_R^2$  and  $W(t)$  will be expressed in terms of the local effective drift velocity

$$\vec{U}(\vec{r}, t) \equiv -\vec{U}_p(\vec{r}, t) + \vec{U}_n(\vec{r}, t), \quad (1-5)$$

where

$\vec{U}_p(\vec{r}, t)$  is the path sweep velocity at  $\vec{r}$  at time  $t$ , and

$\vec{U}_n(\vec{r}, t)$  is the actual local drift velocity of the random refractive index structure at  $\vec{r}$  at time  $t$ .

The term  $\vec{U}_n(\vec{r}, t)$  is usually negligible in the present application.

The expression found for  $\sigma_R^2$  is

$$\sigma_R^2 = R \int_{-1}^1 dz \int_0^\infty dk_\perp k_\perp A(k_\perp, t) \left[ 1 + \cos\left(R\lambda k_\perp^2 \frac{1-z^2}{8\pi}\right) \right] \\ \times \int_{-\infty}^\infty dk_\parallel \frac{\sin[R(1-|t|)k_\parallel]}{k_\parallel} \int_0^{2\pi} d\phi S\left(\vec{k}, \vec{R} \frac{t}{2}\right) \quad (1-6)$$

where

$$A(k_\perp, t) \equiv \frac{2J_1\left(\frac{1+t}{4} k_\perp d_t\right)}{\frac{1+t}{4} k_\perp d_t} \frac{2J_1\left(\frac{1-t}{4} k_\perp d_r\right)}{\frac{1-t}{4} k_\perp d_r} \quad (1-7)$$

Here,  $\lambda$  is the radio wave length,  $d_t$  and  $d_r$  are the antenna diameters,  $J_1$  is the Bessel function, and the origin of  $\vec{r}$  is chosen as the center of the path. Also,  $\vec{k}_\parallel$  and  $\vec{k}_\perp$  are the components of  $\vec{k}$  parallel and normal to  $\vec{R}$ , and  $\phi$  is the angle between  $\vec{k}_\perp$  and  $\vec{U}_p$ . Note that in Equation (1-6)  $k_\parallel \lesssim 1/R$ .

Also, the expression for  $\sigma_R^2$  is

$$\sigma_R^2 = \frac{R^2}{2} \int_{-1}^1 dz \int_0^\infty dk_\perp k_\perp A(k_\perp, z) \left[ 1 + \cos\left(R\lambda k_\perp^2 \frac{1-z^2}{8\pi}\right) \right] \\ \times \int_{-\infty}^\infty dk_\parallel \int_0^{2\pi} d\phi S\left(\vec{k}, \vec{R} \frac{z}{2}\right) \int_{-1+|z|}^{1-|z|} dz' e^{iRk_\parallel z'} \left( \vec{k} \cdot \frac{\vec{U}_+ \vec{U}_- + \vec{U}_- \vec{U}_+}{\vec{U}_+ + \vec{U}_-} \right)^2 \quad (1-8)$$

where

$$\vec{U}_{\pm} = \vec{U}\left(\vec{R} \frac{\mathbf{z} \pm \mathbf{z}'}{2}, t\right)$$

If

$$\vec{U}\left(\vec{R} \frac{\mathbf{z}}{2}, t\right) \cong -\vec{U}_p\left(\vec{R} \frac{\mathbf{z}}{2}, t\right) \equiv -\vec{V}(t) \frac{1-\mathbf{z}}{2}, \quad (1-9)$$

Equation (1-8) becomes

$$\begin{aligned} \sigma_R^2 &= \frac{1}{4} V^2(t) R \int_{-1}^1 d\mathbf{z} \int_0^{\infty} dk_{\perp} k_{\perp}^3 A(k_{\perp}, \mathbf{z}) \left[ 1 + \cos\left(R\lambda k_{\perp}^2 \frac{1-\mathbf{z}^2}{8\pi}\right) \right] \\ &\times \int_{-\infty}^{\infty} dk_{\parallel} \left\{ \left[ (1-\mathbf{z})^2 + \frac{2}{R^2} \frac{\partial^2}{\partial k_{\parallel}^2} + \frac{1}{(1-\mathbf{z})^2 R^4} \frac{\partial^4}{\partial k_{\parallel}^4} \right] \frac{\sin[R k_{\parallel} (1-|\mathbf{z}|)]}{k_{\parallel}} \right\} \\ &\times \int_0^{2\pi} d\phi \cos^2 \phi S\left(\vec{K}, \vec{R} \frac{\mathbf{z}}{2}\right). \quad (1-10) \end{aligned}$$

Here again,  $k_{\parallel} \gtrsim 1/R$ .

Finally, the expression for  $W(f)$  for  $f \gg U_{\perp}/2\pi R$  is

$$\begin{aligned} W(f) &\cong \frac{2\pi^2}{R} \int_{-1}^1 d\mathbf{z} \int_{-\infty}^{\infty} dk_{\perp} \frac{1}{U_{\perp}} A^2\left(\sqrt{k_{\perp}^2 + \left(\frac{2\pi f}{U_{\perp}}\right)^2}, \mathbf{z}\right) \\ &\times \left\{ 1 + \cos\left[R\lambda \frac{1-\mathbf{z}^2}{8\pi} \left(k_{\perp}^2 + \left(\frac{2\pi f}{U_{\perp}}\right)^2\right)\right] \right\} \frac{1}{2} \sum_{\pm} S\left(\vec{K}_1 \pm \frac{\vec{U}_{\perp}}{U_{\perp}} \frac{2\pi f}{U_{\perp}}, \vec{R} \frac{\mathbf{z}}{2}\right); \quad (1-11) \end{aligned}$$

where

$\vec{k}_1$  is in the direction of  $\vec{U} \times \vec{R}$ , and

$\vec{U}_1$  is the component of  $\vec{U}(\vec{R} \frac{z}{2}, t)$  normal to  $\vec{R}$  and is given approximately by Equation (1-9).

The range rate spectrum is obtained by multiplying  $(2\pi f)^2$  by Equation (1-11).

The conditions for the validity of the preceding expressions are as follows:

- (a) Geometrical optics are valid for an atmosphere with refractive index  $\langle n(\vec{r}, t) \rangle$ . That is,  $\langle n(\vec{r}, t) \rangle$  changes relatively slightly over a distance of a wave length and there is a unique ray path connecting each point in space to each antenna.
- (b)  $f \ll \sqrt{(\Delta n)_{\text{rms}}} f_s$ , where  $(\Delta n)_{\text{rms}}$  is the rms value of the refractive index fluctuation which is  $\approx 10^{-6}$  in the lower troposphere, and  $f_s$  is the radio signal frequency.
- (c) There is no significant ground reflection, or specular reflection from elevated layers.
- (d)  $\lambda \ll R$ .
- (e)  $f \ll U/\lambda$ . Ordinarily, this condition is violated only deep in the antenna cut-off region, where the spectrum is probably negligible.
- (f)  $d_t + d_r \ll$  both  $R$  and  $\ell_\perp$ , where  $\ell_\perp$  is the smallest distance in a direction normal to  $\vec{R}$  over which either the effective drift velocity  $\vec{U}$  or the wave number spectrum  $S(\vec{k}, \vec{r})$  change by a significant amount, meaning a reasonable fraction. This condition is probably always met.

- (g) Either  $\ell_1 \gg w_g$ , where  $w_g = \sqrt{R\lambda} + fR\lambda/U$ , or else the inhomogeneities in  $\vec{U}$  and  $S(\vec{K}, \vec{r})$  are distributed in space approximately in accordance with some distribution function which itself changes only slightly for  $\vec{r}$  distances normal to  $\vec{K}$  which are  $\gtrsim w_g$ , so that averages along the various paths in the "scatter region" will be approximately the same. This latter condition is probably usually met. If one of these assumptions is not met then the modified formulae to be used are given in the original paper.
- (h) For  $W(f)$  and  $\sigma_R^2$ , it must be assumed that the fluctuations at any location are due predominantly to an effective local drift of the refractive structure. The original paper gives a more general expression which is valid when such is not the case. Note that the diurnal changes can be approximately associated with an effective westward wind velocity of once daily around the earth, and except for the diurnal and annual fluctuations and their overtones, the fluctuations on a non-moving path appear to be associated with the ordinary wind velocity. Also, the effect of a self or internal motion can be largely approximated by an averaging over wind velocities.
- (i) The wind is not predominantly nearly parallel to  $\vec{K}$ , which is always true in the present application. For other applications the proper formula is given in the original paper.
- (j) The antennas are parabolic dishes.  $A(k_1, z)$  can be computed from a general expression given in the original paper, if such is not the case.



As mentioned earlier,  $S(\vec{k}, \vec{r})$  should be determined from spaced refractometer measurements and the values so determined can then be used directly in the above formulas which can then be evaluated numerically. For illustrative purposes a reasonable simple form in which to cast  $S$  is

$$S(\vec{k}, \vec{r}) = S_0 k^{-n}. \quad (1-12)$$

Using this form for  $S$ , the  $k_{\perp}$  integrand of (1-6) has the following general behavior: for  $k_{\perp} \ll 1/R$ , it is approximately  $\propto k_{\perp}^{2-n}$ ; at  $k_{\perp} \approx 1/R$ , it becomes  $\propto k_{\perp}^{1-n}$ ; at  $k_{\perp} \approx 1/\sqrt{R\lambda} \ll 1/(d_t + d_r)$ , it oscillates and drops by a factor of  $1/2$  and then continues the  $k_{\perp}^{1-n}$  dependence, and finally, at  $k_{\perp} \approx 1/(d_t + d_r)$ , the antenna smoothing takes over and the  $k_{\perp}$  power is decreased by from 1 to 4 making the  $k_{\perp}$  integrand  $\propto k_{\perp}^{-n}$  to  $k_{\perp}^{-3-n}$ , the former value holding for a single antenna and the latter for two antennas of equal diameter. Equation (1-11) for  $W(f)$  has a similar behavior in  $f/U_{\perp}$  for its permitted range, as is expected. Again, the  $k_{\perp}$  integrand in (1-10) for  $\sigma_R^2$  is roughly  $k_{\perp}^2$  times the  $\sigma_R^2$  integrand in (1-8). Also, the range rate spectrum, which is  $(2\pi f)^2$  times  $W(f)$ , behaves roughly as the  $k_{\perp}$  integrand in (1-10), as is expected. In the complete paper, formulas are given in which  $n$  and  $S_0$  are slowly varying functions of both  $\vec{r}$  and  $\vec{k}$ .

No graphs are currently prepared for the above space vehicle tracking formulas. However, the attached graphs for a stationary path and constant  $\vec{U}$  may be helpful. Equation (1-12) was used for  $S$ , with  $n = 11/3$ . It is expected that the spectra and  $k_{\perp}$  integrands for the moving paths will be very comparable in its gross features.  $W(f)$  and  $(2\pi f)^2 W(f)$  are given in parts per million squared per unit bandwidth. The ordinate values may change with geographical location, time of day, and season by a factor of 100 or more.

**NOTE:** The abscissa on Figure 1-6 should be  $F(U/\pi\lambda)$  instead of  $F(U/2\pi\lambda)$ .

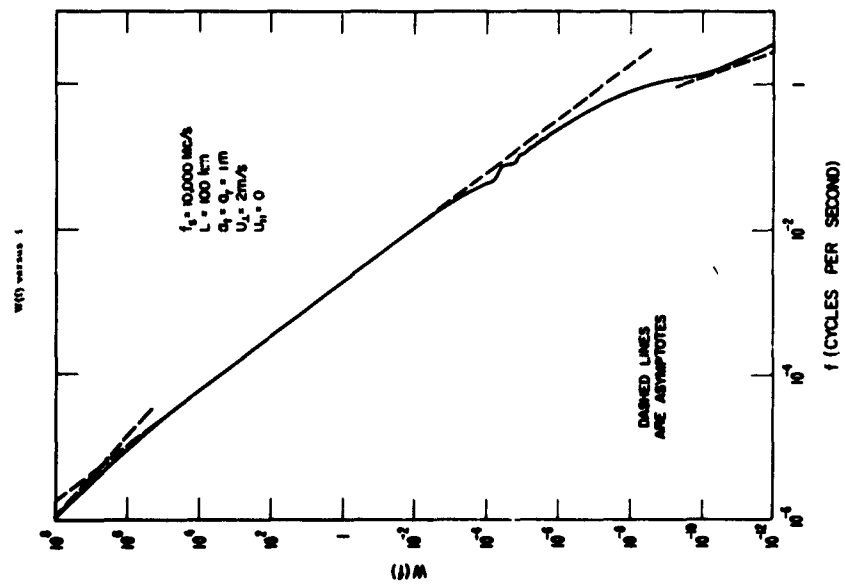


Figure 1-1

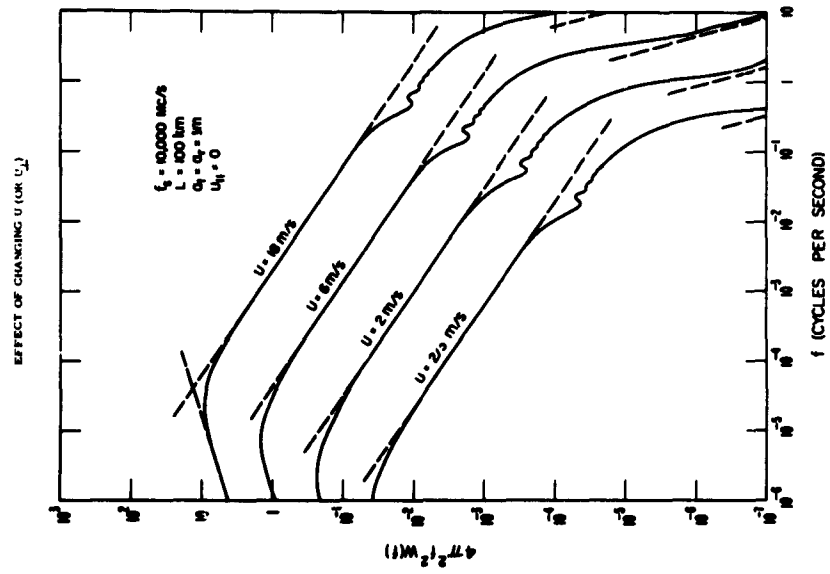


Figure 1-2

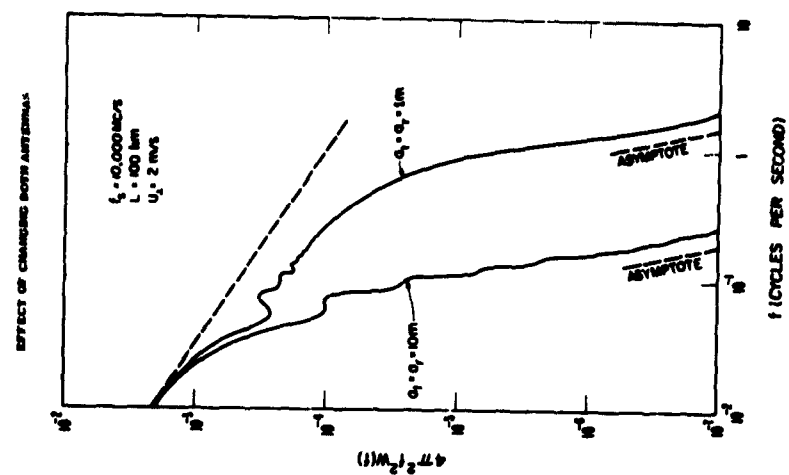


Figure 1-5

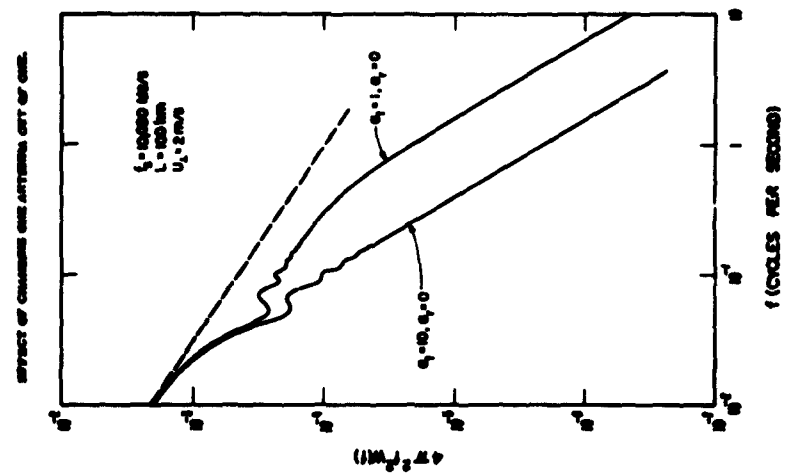


Figure 1-4

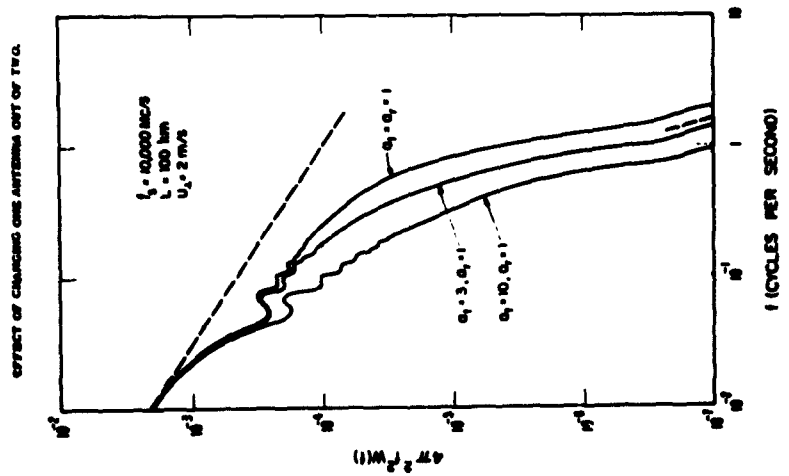


Figure 1-3

Figure 1 is a log-log plot showing the normalized power spectrum  $4\pi^2 f^2 W(f) \times 10^4 (2/U)^{5/3}$  on the y-axis versus the normalized frequency  $f/(U/2\pi L)$  on the x-axis. The y-axis ranges from 0.001 to 0.5, and the x-axis ranges from 0.05 to 100. The plot displays several curves for different values of the ratio  $u_{II}/U$ , ranging from 0.0 to 1.0000. The curves show a broad peak at low frequencies and a series of sharp, narrow peaks at higher frequencies. The parameters are  $f_s = 10,000$  Mc/s and  $L = 100$  km.

1-152

## REFERENCES

1. Barrows, Eugene C. (to be published in 1944), Electrical Range Fluctuations in the Troposphere.

## EFFECTS OF TROPOSPHERIC REFRACTION IN EARTH-SPACE LINKS

Invited Paper by Kenneth A. Norton for the XIVth General  
Assembly of U.R.S.I., held in Japan, September, 1963

### INTRODUCTION

This paper is a survey of the current state of knowledge of tropospheric refraction phenomena. Of necessity, some selection of topics has been made since it would be impractical to describe in detail all aspects of this problem. Emphasis will be given to the basic scientific aspects of tropospheric refraction and only passing mention made of the applications. Methods of measuring and methods of predicting tropospheric refraction variables will be discussed, and it will be shown that excellent progress has been made in recent years in the accurate prediction both of the magnitudes of the variables involved and their variances. It is convenient to consider separately the bending of the radio waves in the vertical and horizontal directions.

### REFRACTION IN A HORIZONTALLY HOMOGENEOUS ATMOSPHERE

Since the atmosphere tends to be horizontally homogeneous, most of the bending occurs in the vertical direction and this will be considered first. Figure 1-1 illustrates the nature of tropospheric refraction and defines the variables which describe its magnitude for the usual case in which the refractive index may be considered to decrease more or less monotonically with height above the surface. A radio wave leaving the earth at an elevation angle  $\theta_0$  and traveling a horizontal distance  $d$  to a target point at an altitude  $h_t$  and height above the surface  $(h_t - h_g)$  will be refracted or bent

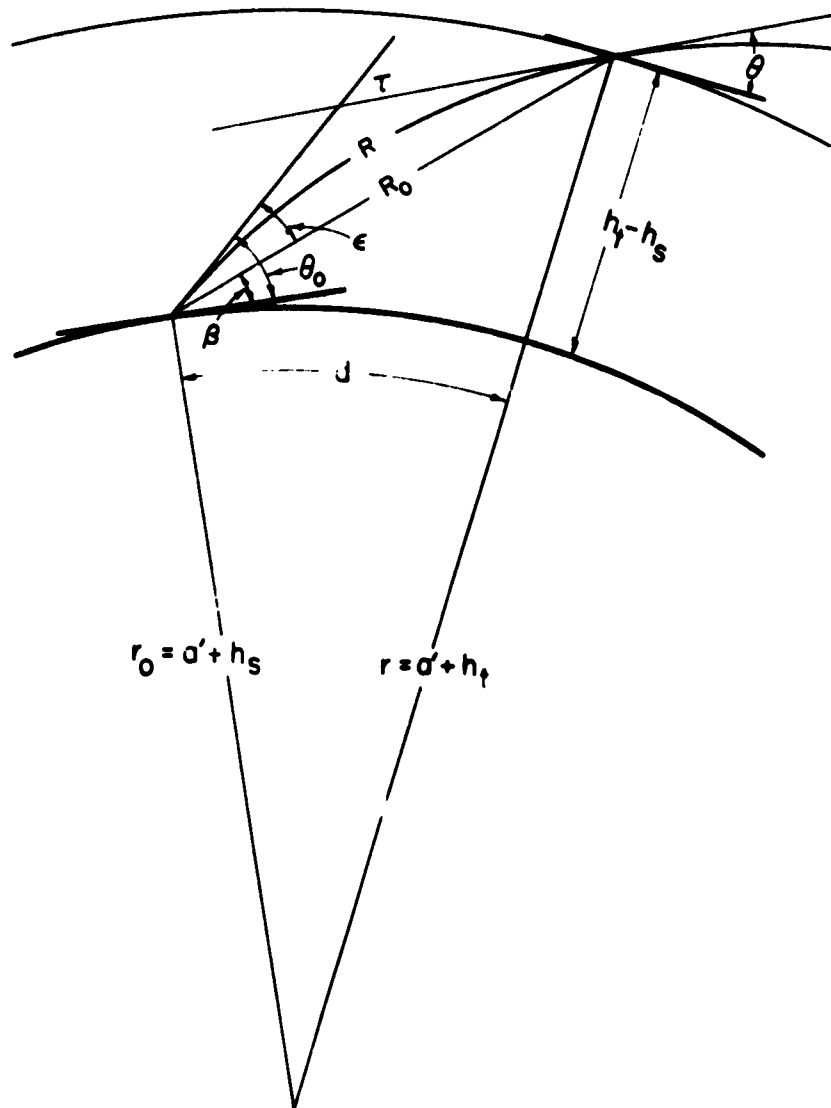


Figure 1-1

downward by the angle  $\tau$ , will travel along the curved path of length  $R$  to a target point having the true angle of elevation  $\beta = \theta_0 - \epsilon$  and true slant range  $R_0$  from the point of origin. The initial radio ray elevation angle  $\theta_0$  is the apparent elevation of the target and  $\epsilon$  is the error in such a radio determined elevation angle.

The apparent range to the target point as determined by radio waves is the integral of the radio refractive index  $n$  along the curved path of length  $R$ :

$$R_e = \int_0^R n \, dR . \quad (1-1)$$

Radio techniques may be used to measure directly the apparent elevation angle  $\theta_0$  and the apparent range  $R_e$  of the target point and the general problem of tropospheric refraction is to predict its horizontal range  $d$  and altitude  $h_t$  using only these two measured variables.

To a first approximation, we may consider that the radio refractive index of the atmosphere will be horizontally homogeneous in spherical shells surrounding the earth at the same large heights above sea level. At the lower altitudes, these shells will have different heights above the local terrain and this will tend systematically to introduce some horizontal inhomogeneity, but the gradients of refractive index in the horizontal direction will usually be small in comparison to those in the vertical direction. There are, in addition, other causes for horizontal inhomogeneities in the refractive index, but none cause large systematic variations. It is also approximately valid to assume that the refractive index  $n$  decreases monotonically, and, in fact, very nearly exponentially, with height above the surface.



When measured data are available on the variation of  $n$  with height above the surface and when the assumption of horizontal homogeneity is reasonable, Snell's law may be used to trace rays through the inhomogeneous atmosphere and thus compute the relations between the measured variables  $\theta_0$  and  $R_e$  and the predicted variables  $d$  and  $h_t$ . This technique was first used extensively for radio refraction by Schulkin [1952] and has since been used by Bean and Cahoon [1957] who showed (a) that the total bending  $\tau$  for a radio wave passing entirely through the atmosphere is linearly related to the value  $n_s$  of the refractive index of the atmosphere at the surface, and (b) established empirically the dependence on initial elevation angle  $\theta_0$  of the values of  $a(\theta_0)$  and  $b(\theta_0)$  in the following regression relation:

$$\tau = a(\theta_0) + b(\theta_0) N_s \quad (1-2)$$

Here the refractivity  $N_s = (n_s - 1) \times 10^6$ .

Anderson [1958] has described a modification of Schulkin's method which uses graphical methods to simplify some of the steps involved. However, ray-tracing calculations are currently made on high-speed computers and the use of such graphical aids is then unnecessary.

Fannin and Jehn [1957] also studied the elevation angle errors due to atmospheric refraction by tracing rays through a set of profiles intended to be representative of the various climates encountered in the United States.

The existence of the simple relation (1-2) suggests that the variation of  $n$  with height above the surface must be well-defined in terms of the surface value  $n_s$  alone and indeed, Bean and Thayer [1959] later established that this was, in fact, the case to a very good degree of approximation. Thus, they developed the Central Radio

Propagation Laboratory Exponential Reference Atmosphere which is a function of the single easily measured parameter  $N_s$ , the surface value of the radio refractivity. Using this model atmosphere, it is possible to calculate  $\epsilon$  and  $\Delta R_e \equiv R_e - R_0$  for given values of  $N_s$ ,  $\theta_0$ , and  $h$ , and this provides a complete and very useful solution to the problem of the prediction of radio refraction in terms of the easily measurable surface value of the radio refractive index.

Naturally, the refractive index of the actual atmosphere at a particular time and location does not decrease with height from its value at the surface in exactly the same way as the CRPL Exponential Reference Atmosphere, and small improvements in radio refraction prediction relative to those using the model atmosphere have been achieved in the following ways. In the first place, a CRPL Standard Atmospheric Radio Refractive Index Profile Sample was established which was intended to be representative of arbitrary conditions of location, climate and weather. This was done by choosing thirteen radiosonde stations representative of the major geographic and climatic types of the world, and then choosing from each station six N-profiles of particular types, two or which are typical of the extremes of monthly mean conditions for that location, and the other four of which are typical of some of the variations which are found at that location. The result is a sample of 77 N-profiles [Bean, Cahoon and Thayer 1960] which has been found, over a period of years, to be a sound cross section of general refractive conditions. By tracing rays through each of these 77 profiles, it is possible to obtain 77 values of  $\epsilon$  and  $\Delta R_e$  for selected values of  $\theta_0$  and  $h_t$ . These values are then fitted by least-squares to a linear function of  $N_s$  which results in the prediction equations:

$$\epsilon = a_1(\theta_0, h_t) + b_1(\theta_0, h_t) N_s, \quad (1-3)$$

$$\Delta R_e = a_2(R_e, h_t) + b_2(R_e, h_t) N_s. \quad (1-4)$$

Figure 2 shows the 77 values of the elevation angle error  $\epsilon$  expressed in milliradians as obtained by tracing rays through these 77 profiles for initial ray elevation angles  $\theta_0 = 0$  degree, 34.9 mr (2 degrees), 100 mr (5.73 degrees), and 400 mr (22.9 degrees). The straight lines on this figure represent least-squares fits to these points, and are considered to represent the best currently available predictions of elevation angle error using the single parameter  $N_s$ . The dashed lines represent the predictions obtained using the CRPL Exponential Reference Atmosphere; these latter predictions are evidently as good as those obtained from the Standard Sample for  $\theta_0$  greater than 2 degrees. The Standard Sample contained 13 profiles with surface ducts and roughly half of the sample had large surface gradients; this is the reason that this Standard Sample is believed to represent, for initial elevation angles  $\theta_0 < 2$  degrees, a significantly better basis for prediction than the CRPL Exponential Reference Atmosphere.

Figure 3 shows similar data and prediction curves for  $\Delta R_e$  expressed in meters and in this case for several apparent target ranges  $R_e$  with corresponding approximate values of apparent elevation angles  $\theta_0$ . The 77 ray-traced values of  $\Delta R_e$  are shown only for the apparent target range  $R_e = 1000$  km. For other values of  $R_e$  the variance of the points about the prediction line is smaller approximately in proportion to  $(\Delta R_e)^2$ ; in fact the standard deviation of the points about the regression lines is approximately equal to 1.44 per cent of the values of  $\Delta R_e$  predicted for  $N_s = 300$ .

The variance of the 77 ray-traced values of  $\epsilon$  is of interest since this represents a measure of the unpredictable component of the elevation angle error. The upper curves in Figure 4 show the standard deviation of the computed values of  $\epsilon$  for the Standard Sample about its means value, i.e., the predicted value of  $\epsilon$  in

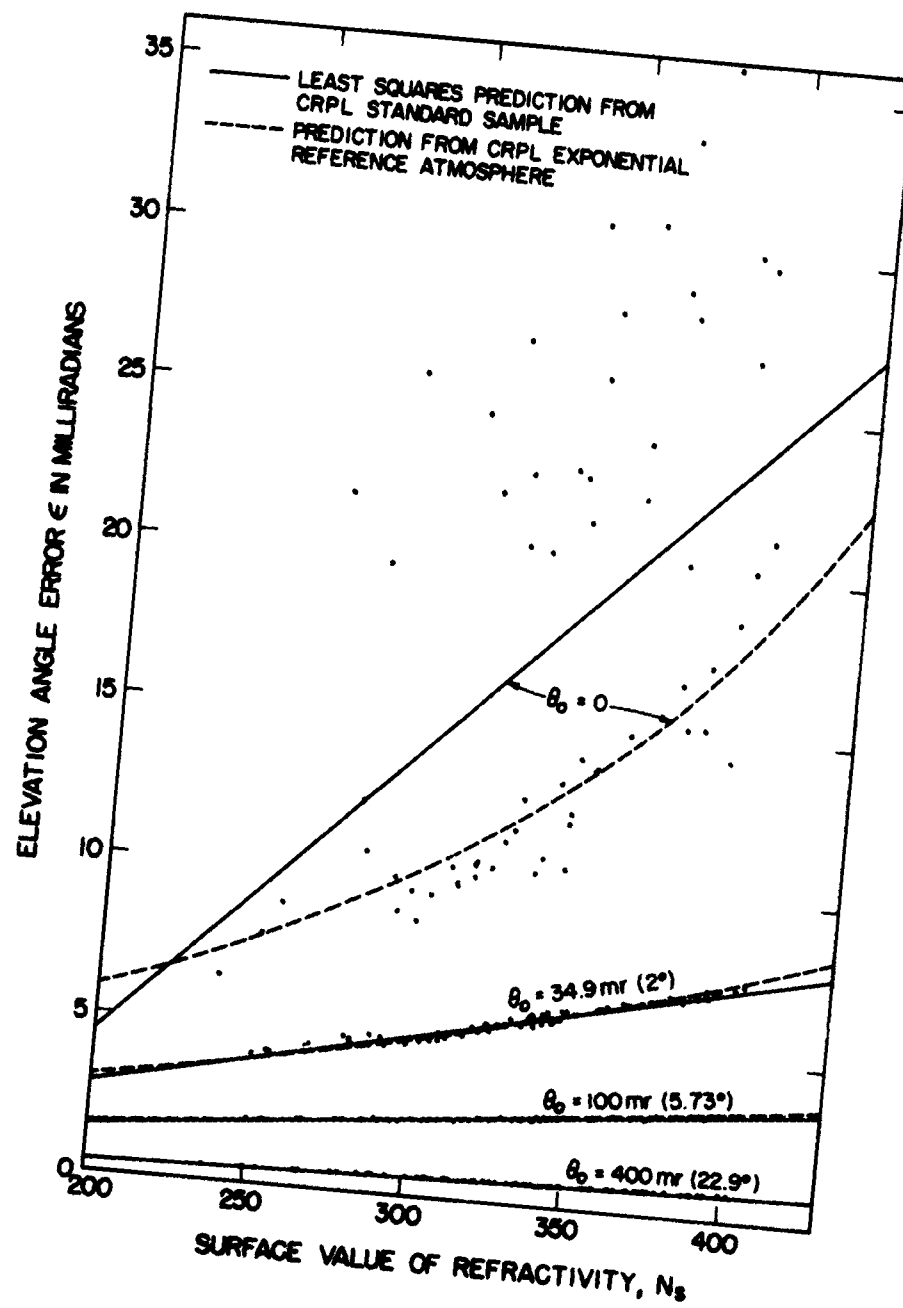


Figure 1-2

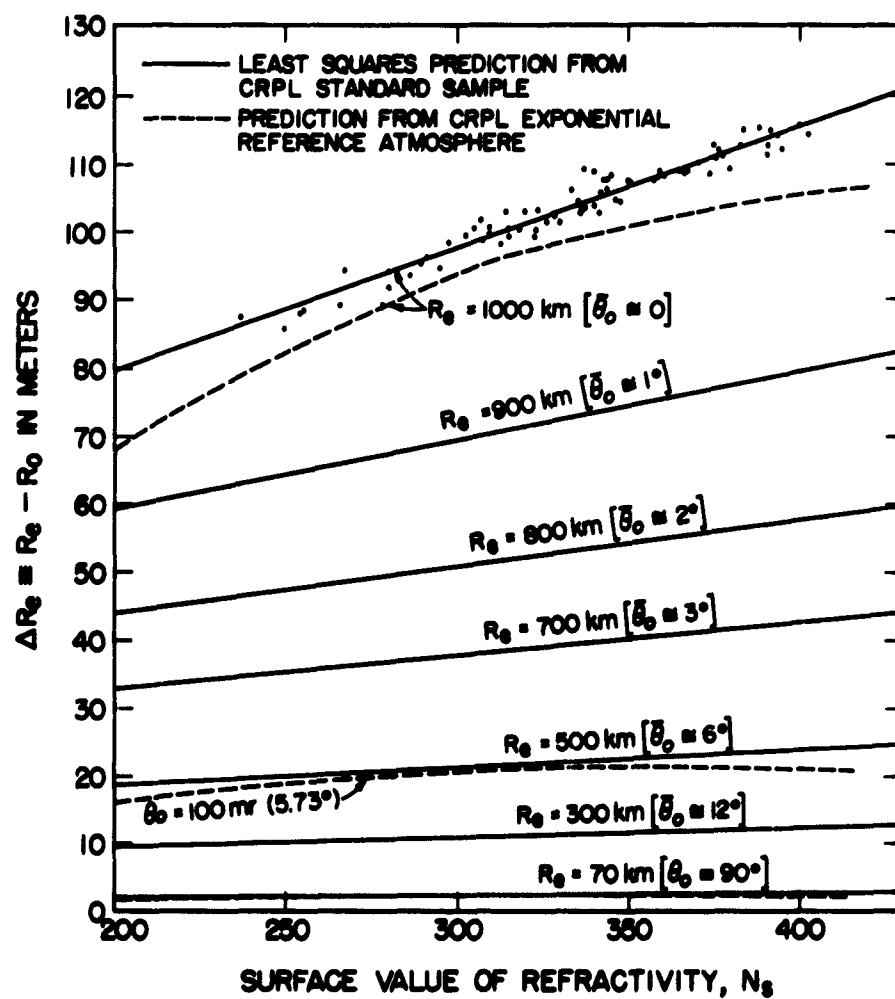


Figure 1-3

the absence of a knowledge of  $N_s$ , while the lower curves in Figure 4 show the standard deviation of  $\epsilon$  about the regression lines on Figure 2, i.e., the predicted values of  $\epsilon$  for given values of  $N_s$ . The ordinate in Figure 4 is the standard deviation expressed in microradians, and the abscissa is the tangent of the initial elevation angle  $\theta_0$  of the ray, i.e., the apparent elevation angle of the target. For elevation angles less than about 2 degrees, surface ducts have an increasingly large influence on the results and the standard deviations are given with and without these profiles; surface ducts will practically never trap radio waves leaving the surface at elevation angles greater than 10 milliradians [Bean, 1959] and surface ducts occur less than 13 per cent of the time, even in the tropics [Bean, 1959], so that ray-tracing is feasible in most cases.

The dotted curves in Figure 4 give estimates of the standard deviation of  $\epsilon$  arising from horizontal inhomogeneities which were neglected in the particular method of ray-tracing used; these estimates were obtained from the measurements of the apparent position of the sun made with the Collins Radio Company radio sextant [Iliff and Holt, 1962; Anway, 1963]. A new analysis is currently underway at CRPL to determine quantitative estimates of the influence of horizontal inhomogeneities on the standard deviation of  $\epsilon$  by using a more accurate method of ray-tracing through a horizontally inhomogeneous atmosphere. This new method allows for slight tilts in the iso-n contours which occur at random and with magnitudes which tend to decrease exponentially with altitude.

The solid curves on Figure 5 show the standard deviation of the computed values of  $\Delta R_e$  relative to its mean value for the Standard Sample, i.e., the predicted value of  $\Delta R_e$  in the absence of a knowledge of  $N_s$ . The standard deviations are divided by  $R_e$  and given in parts per million; values are shown for three target ranges  $R_e = 10$  km, 100 km and 1000 km. The dashed and dotted curves on

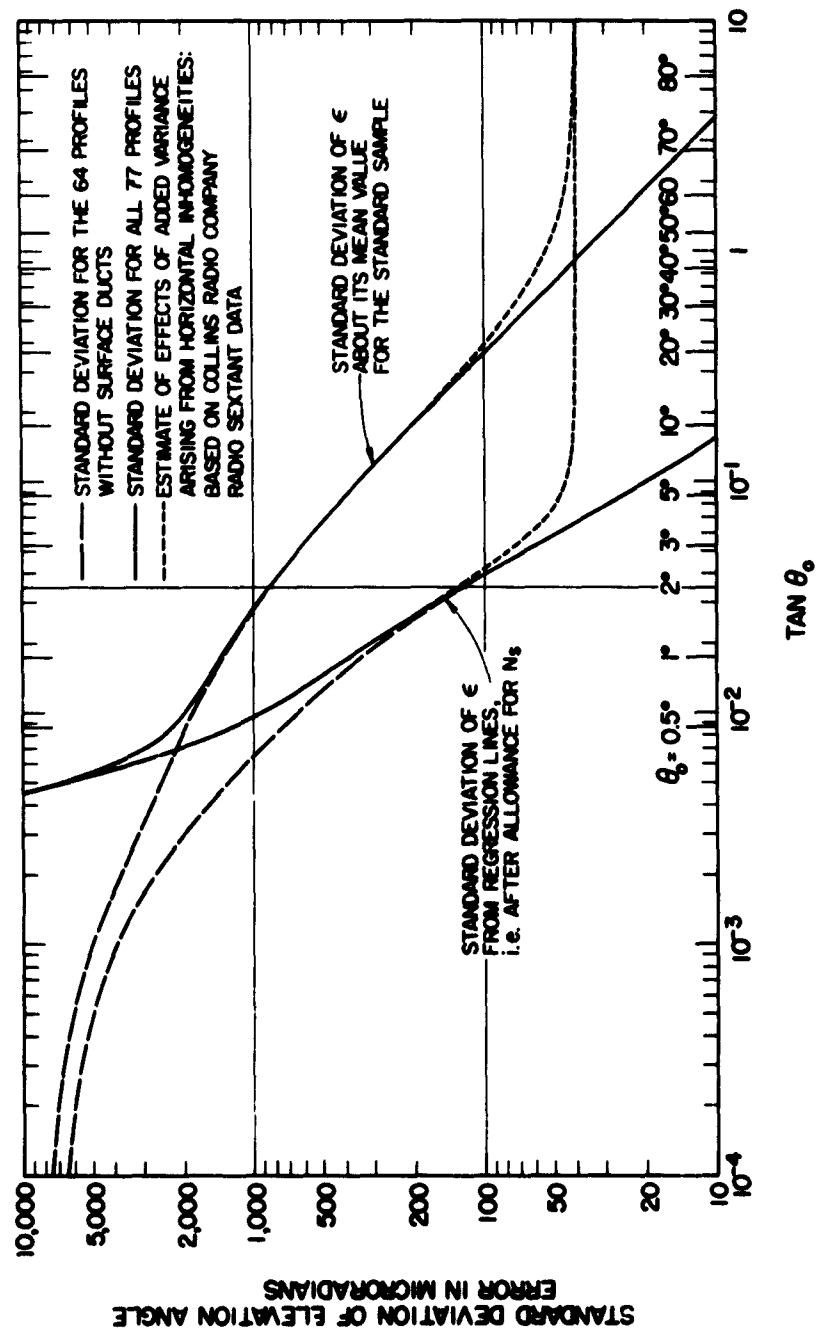


Figure 1-4

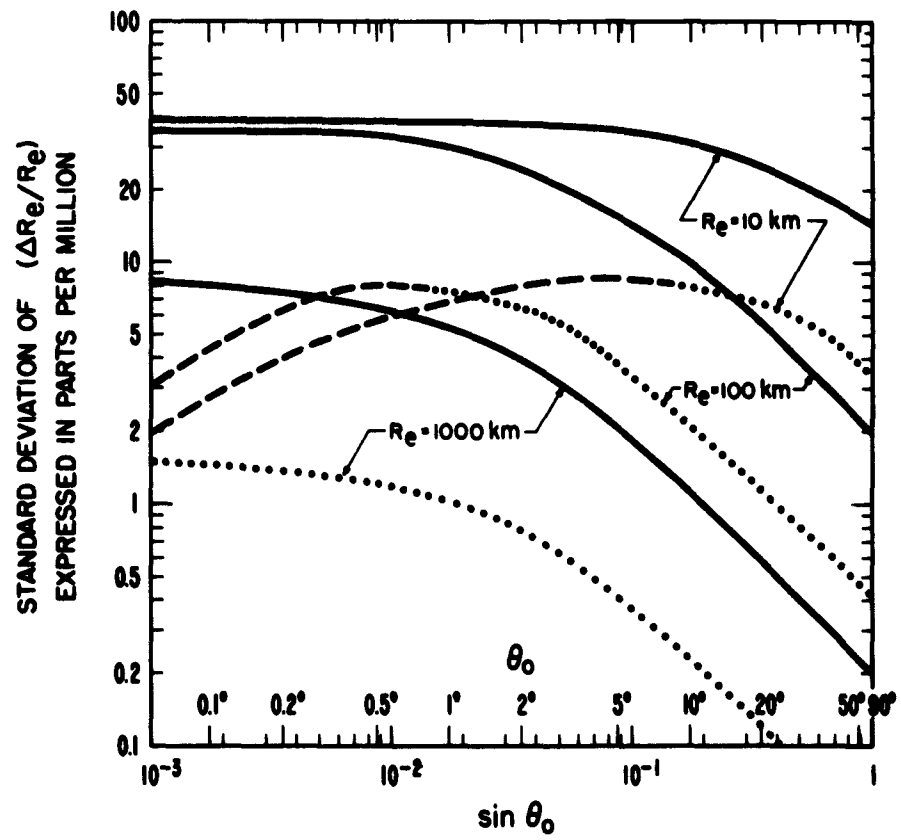


Figure 1-5



Figure 5 give corresponding computed standard deviations of  $\Delta R_e$  about the regression lines in Figure 3, i.e., relative to the predicted values of  $\Delta R_e$  for given values of  $N_s$ . The true standard deviations of  $\Delta R_e$  will be larger than those shown by the dashed portions of the curves shown in Figure 5, since the effects of horizontal inhomogeneities were not included in the ray-traced computed values of  $\Delta R_e$ . Other methods of estimating these standard deviations at very low apparent elevation angles will be discussed later in this summary.

The mean value  $\overline{\Delta R_e}$  for the Standard Sample can also be estimated from the values given by the solid curves shown in Figure 5, since it is approximately 10 times these values, the actual ratio  $\left\{ \overline{\Delta R_e} / \sigma_{\Delta R_e} \right\}$  varying from 8.6 for a target height  $h_t - h_s = 0.2$  km up to 12.3 for a target height  $h_t - h_s = 10$  km, and then decreasing to 12.1 for target heights  $h_t - h_s \geq 70$  km. As an example, consider a target at an apparent elevation angle  $\theta_o = 2$  degrees and at an apparent radio range  $R_e = 100$  km; in this case,  $\sigma_{\Delta R_e} = 23 \times 10^{-6} R_e = 2.3$  meters and  $\overline{\Delta R_e} \approx 23$  meters for the Standard Sample. It is important to note that there are, at present, no electromagnetic methods available for directly measuring  $\Delta R_e = R_e - R_o$  and that it is often difficult, if not impossible, to use other metrological methods such as steel tapes. Consequently, the predictions of  $\Delta R_e$  in terms of measured meteorological parameters represent the only currently available means for correcting the apparent radio ranges  $R_e$  to their true values  $R_o$ . Note that  $\Delta R_e$  may be divided into an electrical component  $\Delta R_N \equiv R_e - R$  associated with the changes in refractivity along the curved path  $R$  plus a geometrical component  $\Delta R_g \equiv R - R_o$  associated with the bending of the radio waves. It has been shown by Bean and Thayer [1963] that the geometrical component  $\Delta R_g$  is usually a very small fraction of  $\Delta R_e$ , ranging from less than  $0.0004 \Delta R_e$  for  $\theta_o \geq 30$  degrees to  $0.27 \Delta R_e$  for a zero elevation angle.

## INFLUENCE OF THE INITIAL GRADIENT

For small initial elevation angles, say  $\theta_0 < 10$  milliradians, the initial gradient of the refractive index has a large influence on the bending and thus, in those cases where a knowledge of this initial gradient is available, it is desirable to make use of this information in addition to the surface refractivity for predicting the bending. Bean and Thayer [1959a] have developed a method for using this initial gradient information for predicting the bending, and Bean, Thayer and Cahoon [1960] have shown that the rms errors in predicting  $\tau$  is reduced substantially, when  $\theta_0 < 10$  milliradians, by the use of the initial gradient in the first 100 meters of the atmosphere as a predictor in addition to the use of  $N_s$ .

## EFFECTS OF HORIZONTAL INHOMOGENEITIES

Since the refractivity of the atmosphere is almost horizontally homogeneous, bending of the radio waves in azimuthal directions is quite small. Bean and Cahoon [1959] studied this horizontal bending in air masses near frontal and land-sea interfaces where such bending is expected to be most important. Even under these conditions they found the effects to be relatively small and, in fact, essentially negligible for all except the lowest elevation angles. Also, at heights greater than one kilometer above the surface, horizontal inhomogeneities were found to be negligible. Adamsson [1962] has made similar studies in Sweden in connection with the effects of this azimuthal bending on radar performance. Although the effects of horizontal inhomogeneity may be extremely small, they are not always negligible, and the dotted curves on Figure 4 show that the residual, unpredictable effects of these horizontal inhomogeneities are of a greater magnitude than the unpredictable component of the bending in the vertical plane for elevation angles greater than 5 degrees. Martin and Wright [1963] have recently reported their studies of ray-tracing in a horizontally inhomogeneous atmosphere, and their analysis sheds considerable additional light on this problem.

## DIRECT MEASUREMENTS OF RADIO REFRACTION

It is important to emphasize that most of the preceding results represent calculated values of refraction based on ray-tracing using Snell's Law. Consequently, it is fortunate that radio methods and equipment have been developed which are capable of directly measuring this refraction. The best presently available direct measurements of radio refraction have been made by using the Collins radio sextant. Anway [1963] has recently described these results in some detail, and Bean and Thayer [1963] have shown that these direct measurements of the bending are in excellent agreement with their predictions using the CRPL Standard Sample. Figure 6, taken from Bean and Thayer's paper, shows the excellent agreement between the mean and the standard deviation of the values of the bending (a) as measured with the Collins radio sextant, and (b) as predicted using the CRPL Standard Sample. The departures between the observed and predicted standard deviations at the larger elevation angles, above 30 degrees, are attributed to the effects of horizontal inhomogeneities not included in the ray-tracings which were carried out on the assumption that the atmosphere is horizontally homogeneous. Bean and Thayer [1963] also discuss the agreement of their prediction methods with several other sets of direct radio measurements but none of these other data are as suitable for this purpose as the Collins radio sextant data.

## VARIANCE OF PHASE ON A LINE-OF-SIGHT PATH

An extremely useful method for studying the effects of radio refraction on radio paths is the measurement of the variations of the phase  $\phi_r$  of radio waves received over a radio path relative to their phase  $\phi_t$  at the transmitting antenna. This phase difference is related to the electrical length of the path  $R_e$ , the radio frequency  $\nu$  and the free space velocity of light,  $c$ , by the equation:

$$\phi_r - \phi_t = \frac{2\pi\nu R_e}{c} \quad (1-5)$$

# PREDICTED AND OBSERVED MEAN ATMOSPHERIC RADIO REFRACTION AT 1.85 cm

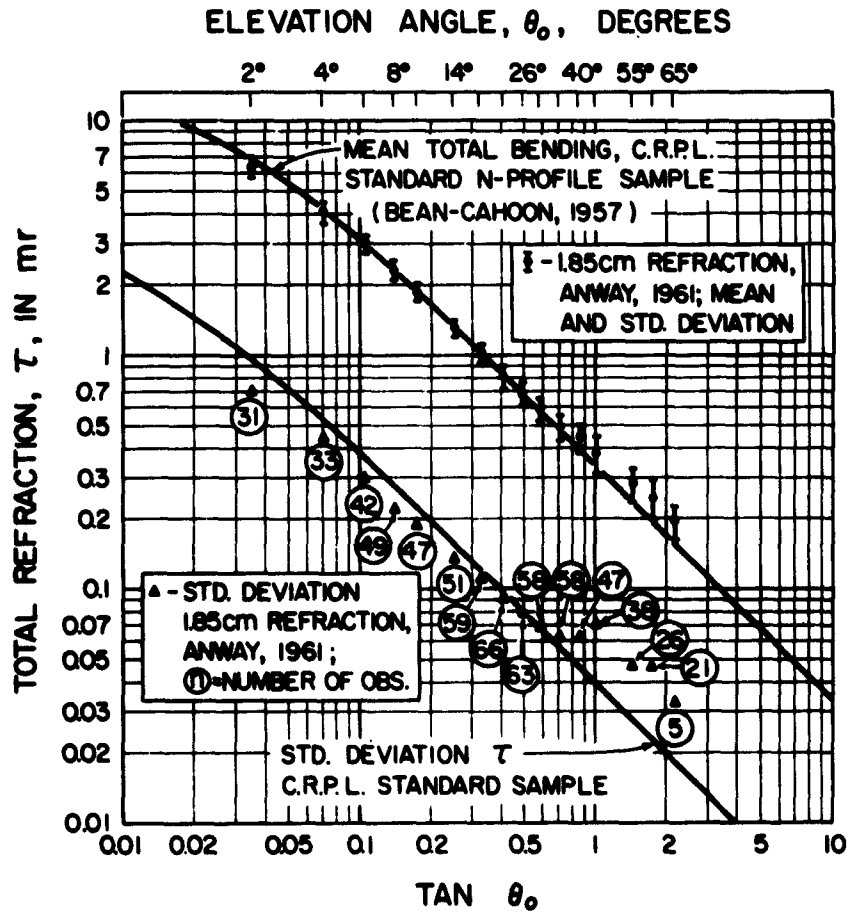


Figure 1-6

Herbstreit and Thompson [1955] developed a method for measuring variations  $\Delta\phi$  in the phase difference  $\phi_r - \phi_t$  by transmitting precisely controlled c.w. frequencies  $\nu$  over line-of-sight paths and in this way obtained accurate measurements of the variations  $\Delta R_e$  in the electrical length of the propagation path:

$$\Delta R_e = \frac{c}{\nu} \left( \frac{\Delta\phi}{2\pi} \right) . \quad (1-6)$$

Continuous observations of  $\Delta R_e$  as determined in this way have been made on a variety of line-of-sight paths over long periods of time [Thompson and Janes, 1959; Thompson, Janes and Kirkpatrick, 1960; Norton, et al, 1961; Norton, Barrows, Thompson and Janes, 1962; Janes, 1963; Janes, Kirkpatrick, Waters and Smith, 1963; and, Janes and Thompson, 1963]. The variations with time of  $\Delta R_e$  as obtained in this way have the appearance of noise, and it has proved to be valuable to study the spectra of these variations.

Figure 7 shows typical values for a 15.5 km path observed at 30-minute intervals of the variations of  $\Delta R_e$ , together with the variations in refractivity  $N$  at each end of the path. Only relative values are shown for each of these three variables and the scale is graduated in parts per million. It is evident that there is some correlation in the variations of all three variables. Since the values shown in Figure 7 were read only at 30-minute intervals, they do not illustrate the very rapid fluctuations which occur with a smaller amplitude at frequencies greater than two per hour, i.e.,  $5.5 \times 10^{-4}$  cycles per second.

Figure 8 shows the correlation between  $\Delta R_e$  and  $N_s$ , the refractivity at the lower end of the path, and illustrates that only the lower-frequency fluctuations of  $\Delta R_e$  are correlated with  $N_s$ . These data were obtained by a digital high-pass filtering process. This consists of replacing the original data with their deviations from running averages of  $m$  data points spaced  $\delta$  seconds apart,

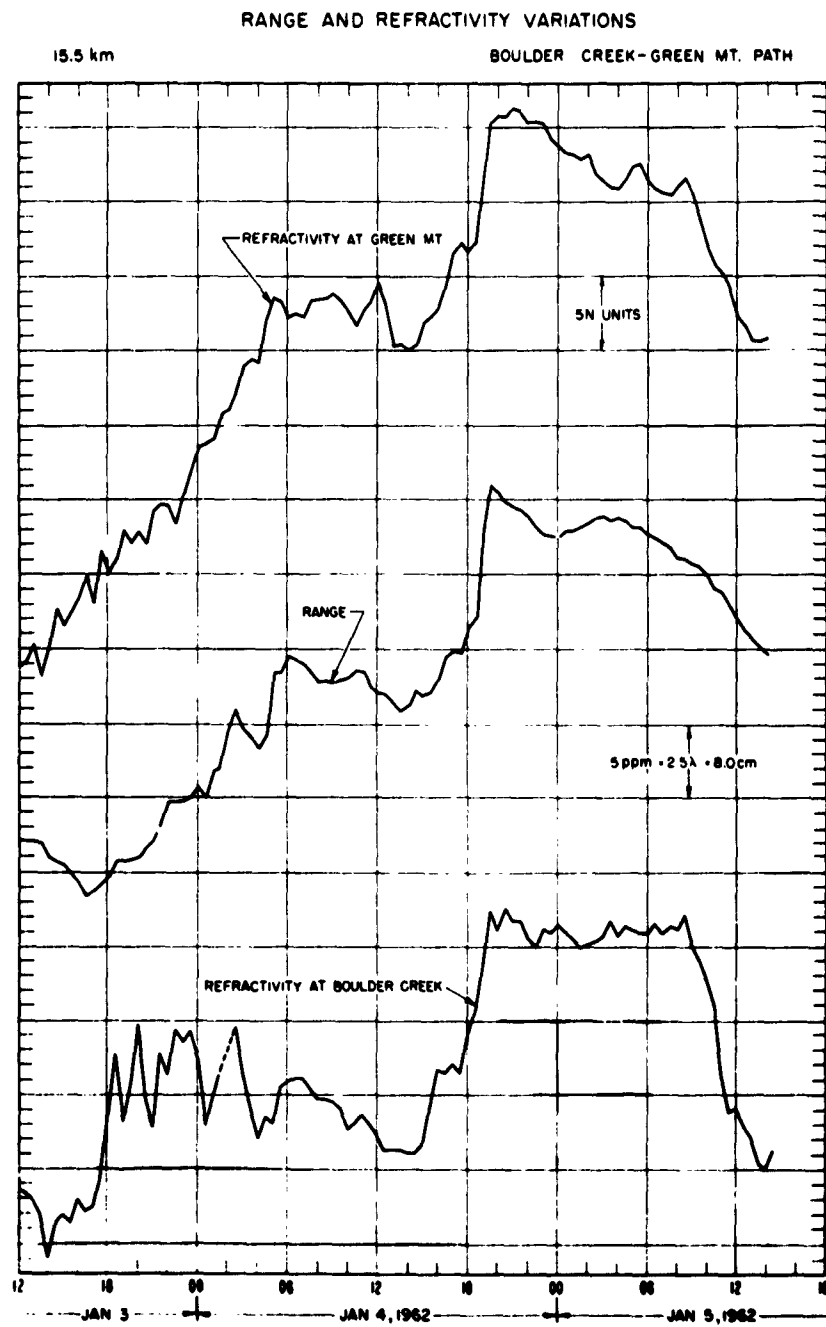


Figure 1-7

CORRELATION OF RANGE AND SURFACE REFRACTIVE INDEX AS A  
 FUNCTION OF HIGH-PASS FILTER CUT-OFF FREQUENCY  
 BOULDER CREEK - GREEN MT. PATH JANUARY 3-5, 1962

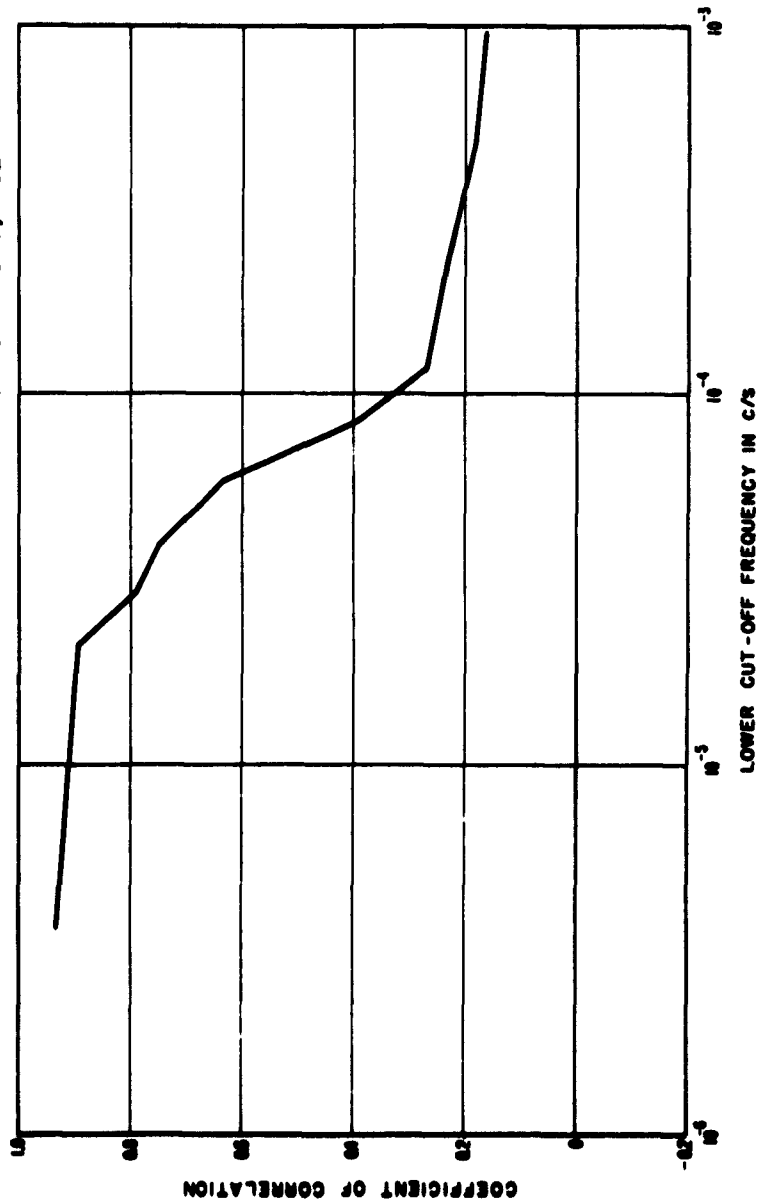


Figure 1-8

and then repeating the operation on the deviation's themselves to further sharpen the response of the "filter." By increasing the sample length  $T \equiv m\delta$  over which the running average is taken, an increasing amount of low-frequency variations are included. In fact, this repeated process acts like a high-pass filter having the characteristics  $\left[1 - \left(\frac{\sin \pi T f}{\pi T f}\right)\right]^4$  with a lower cut-off frequency equal to  $(0.85878/T)$  cycles per second at the half-power point.

Since the lower frequency fluctuations of  $\Delta R_e$  are closely correlated with  $N_s$  and since most of the variance of  $N_s$  is associated with these lower frequency fluctuations, it is convenient, in obtaining an understanding of the long-term variance of  $\Delta R_e$ , to study the variations of  $N_s$  as obtained over long periods of time from U.S. Weather Bureau data using the Smith and Weintraub [1953] formula:

$$N = 77.6 \frac{P}{T} + 3.73 \times 10^5 \frac{e}{T^2}, \quad (1-7)$$

where

$P$  is the pressure expressed in millibars,

$e$  is the partial pressure of water vapor, and

$T$  is the temperature in degrees Kelvin.

Figure 9 shows the power spectra of the variations of  $N_s$  as obtained at three locations: Cape Canaveral (Patrick Air Force Base) in Florida, Denver, Colorado, and at Maui, Hawaii.

The spectra of  $N_s$  shown in Figure 9 illustrate the fact that  $W_{N_s}(f)$  varies approximately as  $f^2$  for fluctuation frequencies less than one cycle per year, as  $(1/f)$  for fluctuation frequencies between one cycle per year and one cycle per day, and as  $(1/f^{5/3})$  for fluctuation frequencies greater than one cycle per day.



POWER SPECTRA OF LONG-TERM REFRACTIVE INDEX VARIATIONS  
EACH SPECTRUM BASED ON APPROXIMATELY 8 YEARS OF  
U.S. WEATHER BUREAU DATA

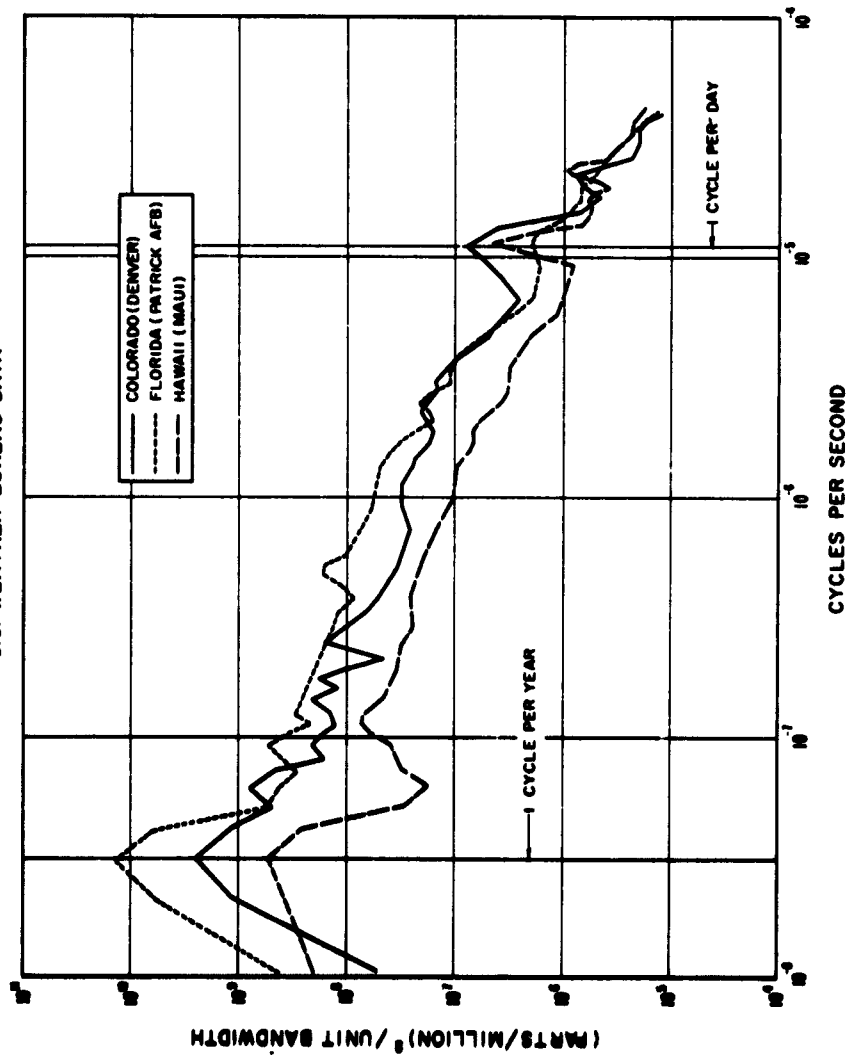


Figure 1-9

In order to illustrate how various portions of the spectrum contribute to the total variance  $\sigma_{Ns}^2$  of  $N_s$ , we may express this variance in the following form:

$$\sigma_{Ns}^2 = \int_0^{\infty} W_{Ns}(f) df = \int_{\ln f = -\infty}^{+\infty} f W_{Ns}(f) d(\ln f) . \quad (1-8)$$

Figure 10 shows  $fW_{Ns}(f)$  plotted on a linear scale versus  $f$  plotted on a logarithmic scale, and it is evident from Equation (1-8) that the total variance  $\sigma_{Ns}^2$  would be proportional to the area under these curves if they were extended from  $-\infty$  to  $+\infty$ . It is interesting that the largest contribution to the variance at Cape Canaveral occurs at one cycle per year, the largest contribution at Denver, Colorado, occurs at one cycle per day, and that Maui has the smallest total variance.

The variance of  $N_s$  depends upon the length of the period of time studied. The data from which the spectra shown on Figures 9 and 10 were obtained represent meteorological measurements made once every two hours. These data have been analyzed to show how the variance increases with the length of the data sample by using the means of the sample variances relative to running averages with sample lengths of 4 hours, 8 hours, etc. Table 1-1 gives the standard deviations  $\sigma_{NsT}$  within sample lengths  $T$  as a function of sample length. A good estimate of the total variance  $\sigma_{Ns}^2$  may be obtained by squaring the standard deviation given for the entire eight-year period. Since the total variance  $\sigma_{Ns}^2$  is equal to the sum of the within-groups variance  $\sigma_{NsT}^2$  and the variance  $\sigma_{Ns}^2$  between the group means, an estimate of the standard deviation  $\sigma_{Ns}$  of the mean surface refractivity for the period of time  $T$  may be obtained from:

$$\sigma_{Ns} = \sqrt{\sigma_{Ns}^2 - \sigma_{NsT}^2} . \quad (1-9)$$

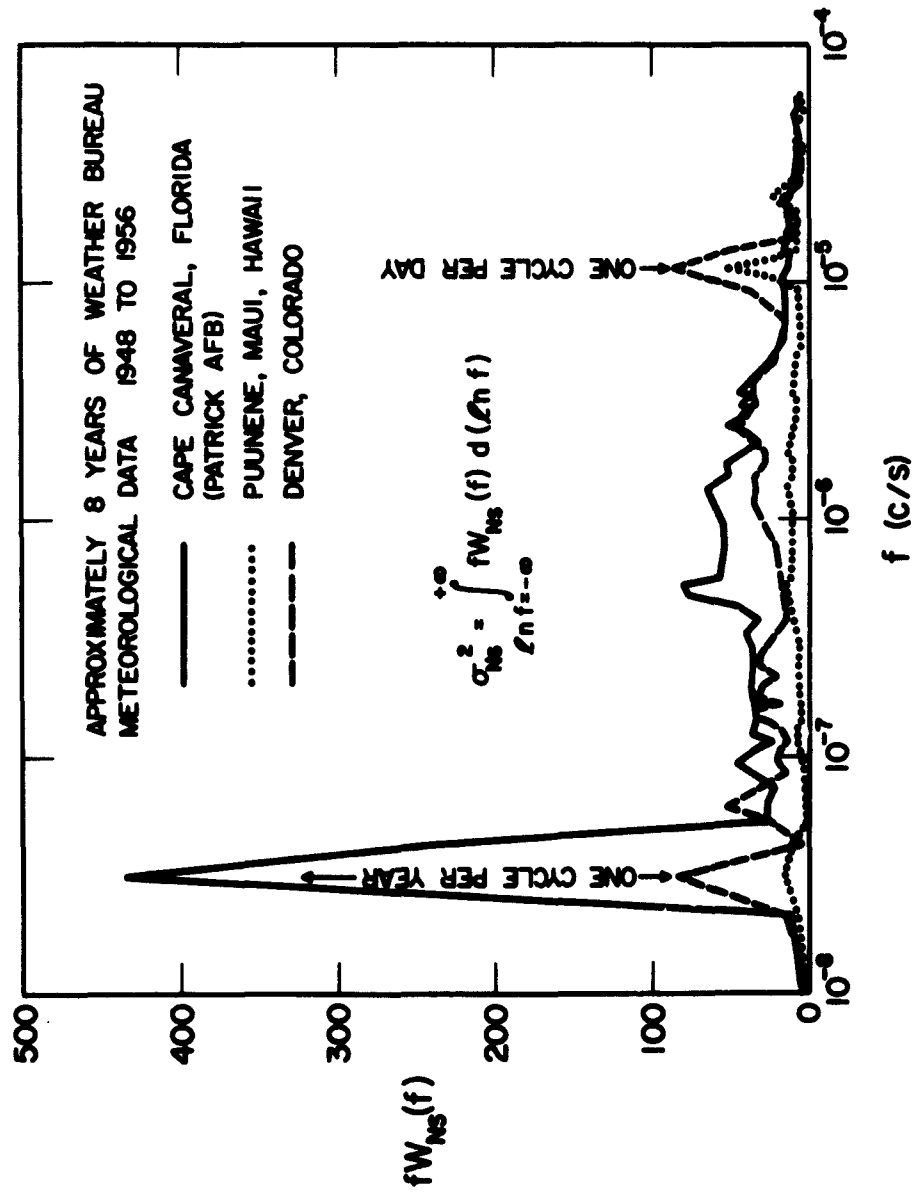


Figure 1-10

Table 1-1

Standard Deviation  $\sigma_{NsT}$  of Surface Refractivity within  
 Samples of Length T and Standard Deviations  $\sigma_{Ns}$  of the  
 Mean Surface Refractivity for Samples of Length T

$$\sigma_{Ns}^2 = \sigma_{Ns}^2 - \sigma_{NsT}^2$$

Sample Length, T			Puene, Maui		Denver, Colorado		Cape Canaveral, Florida	
Hours	Days	Months	$\sigma_{NsT}$	$\sigma_{Ns}$	$\sigma_{NsT}$	$\sigma_{Ns}$	$\sigma_{NsT}$	$\sigma_{Ns}$
4			4.34	8.91	4.16	13.78	4.71	21.59
8			4.92	8.60	5.99	13.09	5.70	21.35
16			5.84	8.11	7.71	12.16	6.66	21.07
32	1.33		6.32	7.63	8.65	11.51	7.98	20.61
64	2.67		6.90	7.11	9.61	10.72	9.64	19.88
128	5.33		7.47	6.51	10.50	9.84	11.15	19.07
256	10.66		7.96	5.90	11.26	8.97	12.80	18.00
512	21.33		8.24	5.50	11.82	8.21	14.01	17.08
1024		1.4	8.58	4.96	12.19	7.65	15.09	16.12
2048		2.8	8.75	4.65	12.78	6.62	16.34	14.86
4096		5.7	9.17	3.75	13.53	4.92	18.37	12.12
8192		11.4	9.44	3.01	14.30	1.65	21.46	5.19
16384		22.8	9.42	3.09	14.32	1.43	21.68	4.23
TOTAL: 8 YEARS $\sigma_{Ns}$			9.91		14.40		22.10	

These standard deviations are also given in Table 1-1 for three geographical locations.

Note that most of the variance of the surface refractivity occurs for periods of time in excess of one day, and as is evident from Figure 8, the variations in  $\Delta R_e$  which occur at these low fluctuation frequencies are closely correlated with the corresponding variations in  $N_s$ . It follows from this that a very large reduction in the variance of  $\Delta R_e$  may be obtained by using the prediction Equation (1-4). However, as we will see, the value of  $N_s$  to use in this equation is the mean value averaged over, say three hours, since the use of values of  $N_s$  averaged over shorter periods of time will actually increase the variance of such an adjusted value of  $\Delta R_e$ .

Figure 11 shows spectra of  $(\Delta R_e 10^6/R_e)$ , of  $N_s$ , and of the difference  $[(\Delta R_e 10^6/R_e) - N_s]$  for the frequency range from one cycle in four hours to one cycle in two minutes. The measurements of  $\Delta R_e$  and of  $N_s$  from which these spectra were obtained were made on a 15.5 kilometer path between Boulder Creek and Green Mountain in Colorado. The Green Mountain terminal was at an angular elevation of 44 milliradians, i.e., about 2.5 degrees, relative to the Boulder Creek terminal where the measurements of surface refractivity were made. A detailed description of these and other related measurements will be available shortly in a paper by Janes and Thompson [1963]. For fluctuation frequencies greater than about one cycle per hour, the spectra of  $N_s$  decrease as  $f^{-5/3}$  as would be expected in accordance with the Obukhov-Kolmogorov theory of atmospheric turbulence. In this same frequency range, the spectra of  $\Delta R_e$  decrease as  $f^{-8/3}$ , i.e., one higher power of  $f$ , by virtue of the fact the variations of  $\Delta R_e$  represent variations in the value of  $N$  averaged along the 15.5-km path.

Figure 12 shows some of the same spectra as in Figure 11, but multiplied by  $f$  and shown on a linear scale since the area under this curve from  $\ln f = -\infty$  to  $\ln f = +\infty$  then represents the total

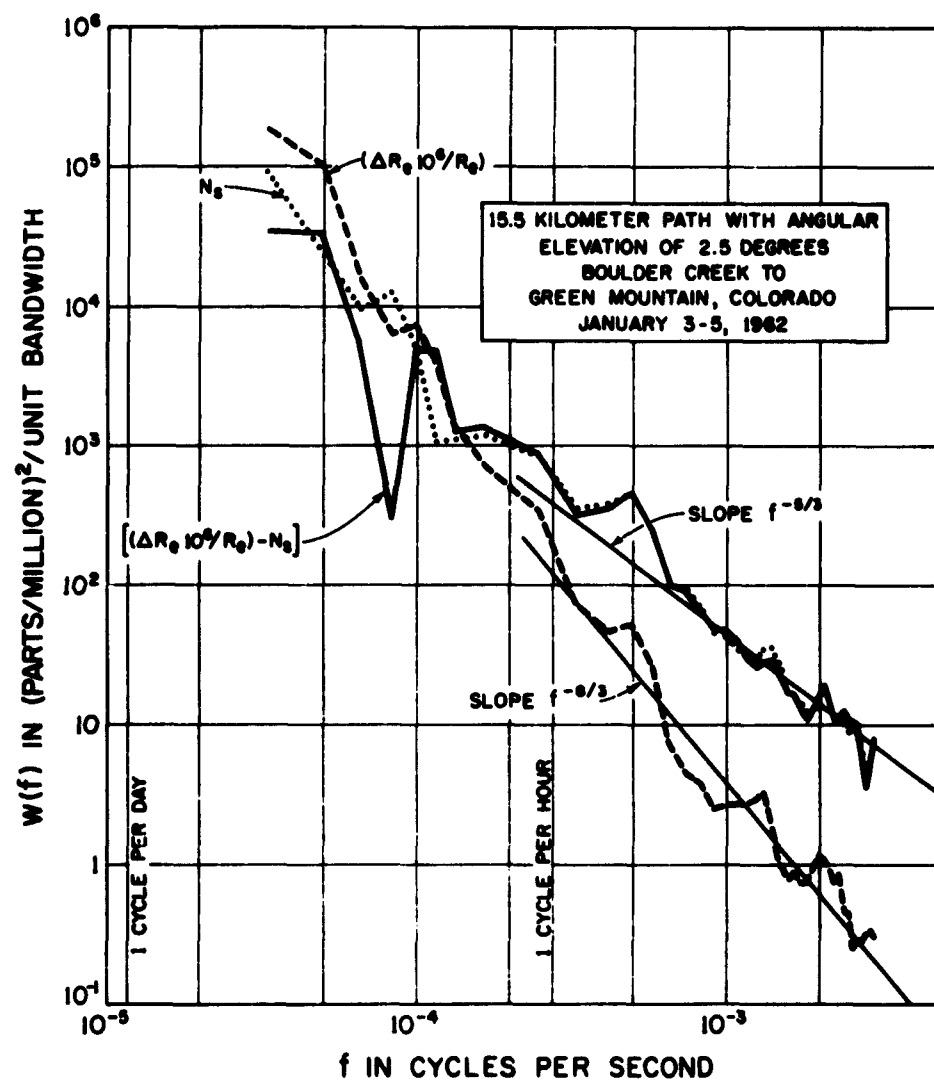


Figure 1-11

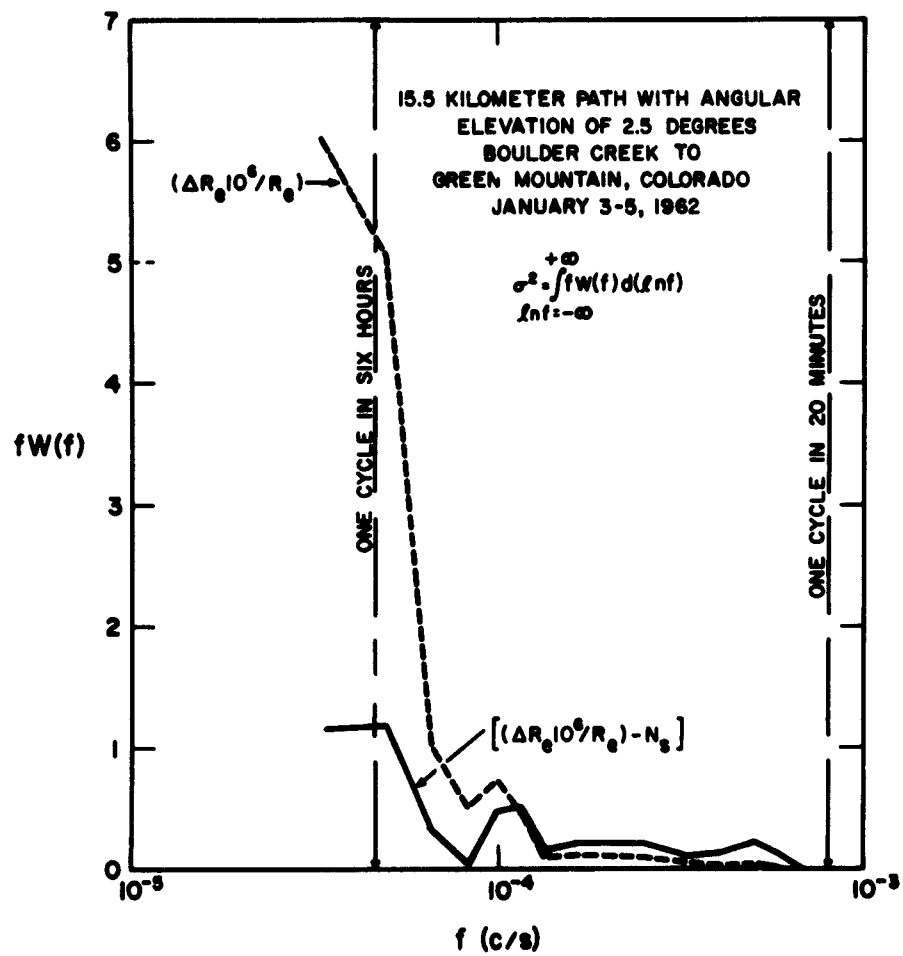


Figure 1-12

variance. The solid curve in Figure 12 represents the spectrum after correcting the observed values of range variations for their dependence on the surface value of the refractivity. Note that the area under this solid curve is very much reduced relative to the area under the dashed curve which represents the spectrum of the range variations before correction for the measured values of the surface refractivity. It is unfortunate that simultaneous measurements were not made of both  $\Delta R_e$  and  $N_s$  over a longer period of time so as to see how the corrected spectrum decreases with decreasing frequency. Such a decrease would be expected at fluctuation frequencies of the order of  $10^{-5}$  and lower by virtue of the high correlation between  $\Delta R_e$  and  $N_s$  illustrated in Figure 8, and by virtue of the finite length of the propagation path. The theory [Barrows, 1963; Norton, Barrows, Thompson and Janes, 1962] indicates that, for a turbulent atmospheric structure moving normal to the propagation path with a mean velocity  $U$  meters per second, the finite length of the propagation path acts as a high pass filter which reduces the variations in  $\Delta R_e$  by a spectral density factor  $f$  for frequencies  $f < f_{Re}$ :

$$f_{Re} = 0.16 \frac{U}{R_e} \quad (1-10)$$

For the data shown on Figures 11 and 12,  $R_e = 15,500$  meters and, assuming that the wind is blowing normal to the path with a mean speed of  $U = 2$  meters per second,  $f_{Re} = 2.1 \times 10^{-5}$  cycles per second. It is significant to note that this finite path-length filter factor  $f$  has just the right magnitude to change the slope  $f^{-8/3}$  of the  $\Delta R_e$  spectrum so that it agrees, at frequencies less than  $f_{Re}$ , with the slope  $f^{-5/3}$  of the  $N_s$  spectrum.

Measurement programs are currently planned which will extend these spectra to lower fluctuation frequencies.



Note also in Figure 12 that the corrected spectrum at fluctuation frequencies in excess of about one cycle in three hours ( $f = 9 \times 10^{-5}$  c/s) is larger than the uncorrected spectrum of  $\Delta R_e$ . This is to be expected by virtue of the lack of correlation between  $\Delta R_e$  and  $N_s$  at these high fluctuation frequencies. Thus, in order to yield the optimum reduction in the variance of the corrected values, it appears that observed values of  $N_s$  should be averaged over a period of, say three hours, before they are used in applying a correction to  $\Delta R_e$ .

In applications to space vehicle guidance systems, it is also necessary to have a knowledge of the first derivative  $\dot{\Delta R}_e$  since this represents the error in the determination of the velocity of the vehicle. The spectrum of  $\dot{\Delta R}_e$  may be obtained from the spectrum of  $\Delta R_e$  simply by multiplying the latter by the factor  $(2\pi f)^2$ . Figure 13 shows the spectra of  $\dot{\Delta R}_e$  before and after correction by  $N_s$ . In this case as before, it is clearly desirable to average  $N_s$  for a period of the order of three hours before applying the correction to  $\Delta R_e$ ; otherwise, the corrected values would have a very much larger total variance. Note that a large contribution to the variance of the uncorrected spectra of  $\dot{\Delta R}_e$  occurs at fluctuation frequencies of the order of one cycle in six hours and this contribution to the variance is substantially reduced by the  $N_s$  correction. Here again, measurements for lower fluctuation frequencies are desirable. Note that the contributions to the variance of  $\dot{\Delta R}_e$  slowly increases with increasing fluctuation frequency at the higher fluctuation frequencies; based on the Obukhov-Kolmogorov theory of atmospheric turbulence, this contribution (as shown on this logarithmic frequency scale) would be expected to increase as  $f^{1/3}$  up to a frequency:

$$f_w = U \sqrt{\frac{v}{cR_e}}, \quad (1-11)$$

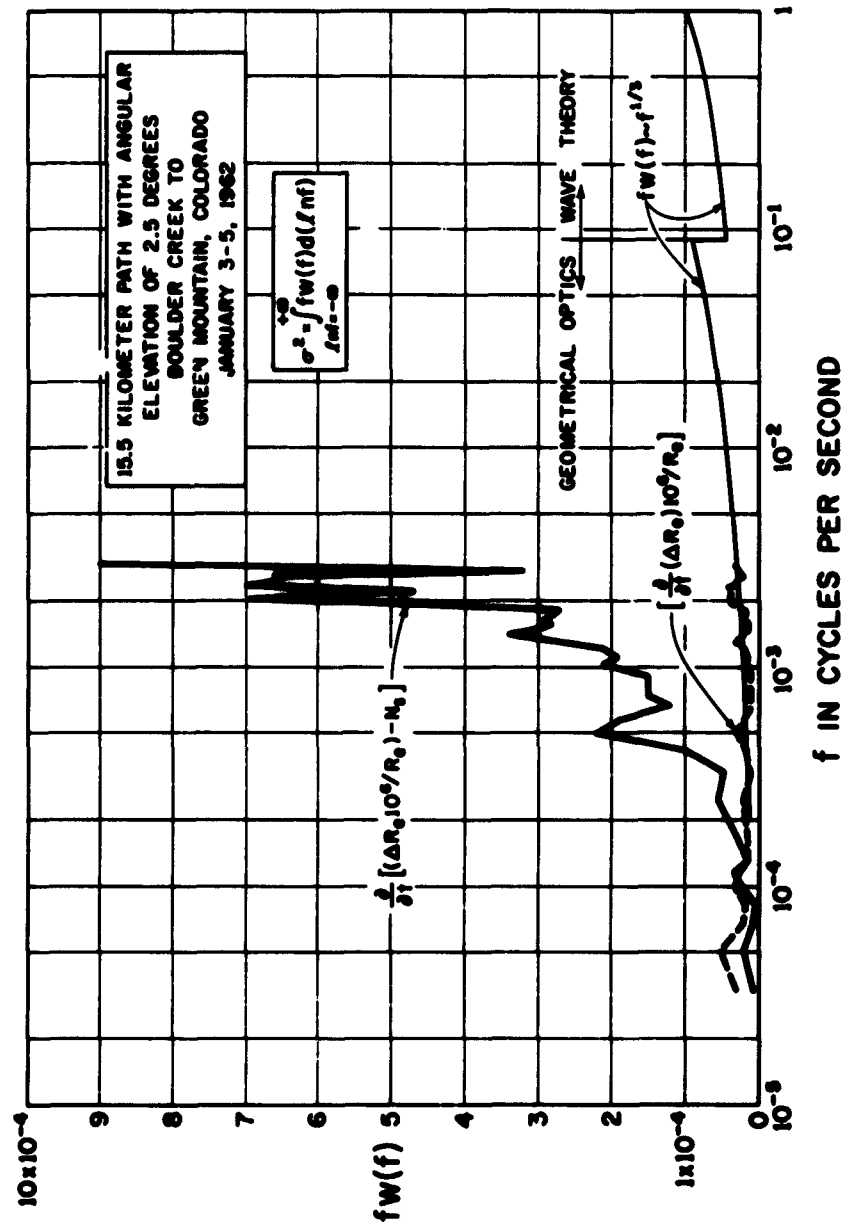


Figure 1-13

where

$U$  is the mean velocity in meters per second with which the turbulent structure moves in a direction normal to the propagation path,

$c$  is the velocity of light in meters per second,

$\nu$  is the radio frequency at which the measurements of  $\Delta R_e$  are made, and

$R_e$  is path length in meters.

For fluctuation frequencies less than  $f_w$ , it is permissible to use a geometrical optics theory and in effect to assume that the radio waves are influenced only by the refractive index precisely on the line joining the centers of the two antennas. For fluctuation frequencies greater than  $f_w$ , it is necessary in obtaining the correct expression for the variance of  $\Delta R_e$  to use a more exact wave theory, and thus to allow for scatter from off the line-of-sight path. The theory [Barrows, 1963] indicates that the spectral density decreases by one half in the neighborhood of  $f_w$  and this is indicated on the theoretical curve shown in Figure 13. The measurements of  $\Delta R_e$  were made at a radio frequency  $\nu = 9.4 \times 10^9$  cycles per second so that, assuming a mean wind speed of 2 meters per second,  $f_w = 0.09$  cycles per second; because the wind speed normal to the path will be variable, the drop shown in Figure 13 at 0.09 cycles per second will, in practice, be spread over a range of fluctuation frequencies. At frequencies higher than  $f_w$  the spectral density is expected to continue to increase as  $f^{1/3}$  up to a frequency  $f_a$  at which averaging over the transmitting and receiving antenna apertures sharply reduces the variations in the measured values of  $\Delta R_e$ . This critical frequency is:

$$f_a \approx 0.26 \frac{U}{d}, \quad (1-12)$$

where

$d$  is the diameter of the parabolic antennas expressed in meters.

For a typical mean wind speed of 2 meters per second and a 10-meter diameter antenna,  $f_a = 0.052$  cycles per second.

Measurements of the spectrum at these higher fluctuation frequencies are available in papers by Thompson and Janes [1959] and by Thompson, Janes and Kirkpatrick [1960]; these measurements were made with antennas having relatively small apertures ( $f_a \approx 1.04$  cycles per second) and established that  $fW(f) \sim f^{1/3}$  for the spectrum of  $\Delta R_e$  up to frequencies of the order of one cycle per second. These facts demonstrate the potential importance of using antennas with very large apertures in order to reduce the variance in the measured values of space vehicle velocities. The desirability of this procedure has not yet been established experimentally but such measurements are planned for the near future.

At the XIIIth General Assembly of U.R.S.I. in London and in a paper published at about that time [Norton, 1960], I emphasized the importance of making measurements of the wave-number spectrum of atmospheric turbulence in an effort to determine whether the spectrum of refractivity decreases more rapidly with increasing wave number in the vertical direction than in the horizontal direction. Thus, the forward scattering of radio waves gives an indirect indication that the spectrum of refractivity may vary in the vertical direction as the wave number to the -3 power rather than as the -5/3 power as would be inferred from the measured spectra shown in Figure 11. It is important to note that the measured frequency spectra shown in Figure 11 may be translated into wave-number spectra by considering that the atmosphere moves in a horizontal direction with some mean wind speed past the point at which  $N_s$  is measured. Thus, all of the

spectra shown in this report refer to horizontal motions of the atmosphere and may be used then only to infer the nature of the wave-number spectrum in the horizontal plane.

In space vehicle guidance applications, the line joining the ground station to the vehicle will move through the atmosphere with a much larger vertical than horizontal component of velocity during the initial and most important phase of the vehicle launching. Thus, in this application as well, the wave-number spectrum in the vertical direction is likely to be of at least comparable importance to the spectrum in the horizontal plane. If the wave number spectrum varies in the vertical direction as the wave number to the -3 power, as inferred from the forward scattering of radio waves, then  $fW(f)$  may be expected to vary as  $f^\alpha$ , where  $\alpha$  lies between -1 and  $1/3$ , rather than as  $f^{1/3}$  for the spectrum of the errors in velocity measurements during the launching of a space vehicle. It is evident from Figure 13 that fluctuation frequency components above about  $10^{-3}$  cycles per second might then no longer be important, there might then be little gain in the use of large aperture receiving antennas and the importance of correcting for  $N_s$  might then be even greater.

The above discussion provides the motivation for making measurements with spaced refractometers of the wave-number spectrum in three dimensions in the manner described in my 1960 paper. Such a program has been started at the Central Radio Propagation Laboratory, but the results of these studies are not yet available for publication.

The velocity spectrum of  $\dot{\Delta R}_e$  is [see Equation (1-6)]\* also the spectrum of the expected variance of a radio frequency after transmission over a line-of-sight path. The application of such spectra

---

\*When multiplied by the dimensionless factor  $(c/2\pi R_e 10^6 \nu)^2 = 1.62 \times 10^{-25}$ , the uncorrected spectrum shown in Figure 13 yields the spectrum of  $(\Delta \nu/\nu)$  of a constant radio frequency  $\nu$  after transmission over this 15.5-km line-of-sight path.

to the problem of determining the degradation in the precision of frequencies and of time intervals after propagation over a line-of-sight path is discussed in a recent paper by Norton, Barrows, Janes and Thompson [1962].

Barrows [1963] will shortly publish a comprehensive theoretical discussion of the phase instability of radio frequencies propagated over line-of-sight paths. This paper will include a treatment of a non-homogeneous atmosphere, a problem of some importance for radio waves traveling through the actual atmosphere in which the contribution to the variance of  $\Delta R_e$  decreases more or less exponentially with height above the surface and for which the wind speed varies along the path.

A conclusion of considerably importance which was revealed by Barrows' analysis is the fact that the variations in  $\Delta R_e$  as measured on two different radio frequencies,  $\nu_2$  and  $\nu_1$  ( $\nu_2 > \nu_1$ ), propagated over exactly the same propagation path, will not be exactly correlated.

The contribution to the covariance spectrum of  $\Delta R_{e1}$  and  $\Delta R_{e2}$  for the frequencies  $\nu_1$  and  $\nu_2$  falls to one-half at the frequency  $f_{w12}$ :

$$f_{w12} = \frac{U}{\sqrt{cR_e}} \sqrt{\frac{2\nu_1\nu_2}{\nu_2 + \nu_1}}, \quad (1-13)$$

and the correlation between the variations of  $\Delta R_e$  on the frequencies  $\nu_1$  and  $\nu_2$  falls rapidly to zero for fluctuation frequencies greater than  $f_{c12}$ :

$$f_{c12} = \frac{U}{\sqrt{cR_e}} \sqrt{\frac{2\nu_1\nu_2}{\nu_2 - \nu_1}}. \quad (1-14)$$

In Equations (1-13) and (1-14),  $c$  is the velocity of light. Note that, as  $v_1$  approaches  $v_2$ ,  $f_{c12}$  increases without limit, the correlation between  $\Delta R_{e1}$  and  $\Delta R_{e2}$  approaches unity for all fluctuation frequencies, as expected, and  $f_{w12}$  as given by Equation (1-13) approaches the value given by Equation (1-11). On the other hand, as  $v_1$  approaches zero both  $f_{w12}$  and  $f_{c12}$  approach zero and the correlation between the variations of  $\Delta R_{e1}$  and  $\Delta R_{e2}$  approaches zero.

Muchmore and Wheelon [1963] discuss the correlation in the frequencies transmitted over line-of-sight paths and, although qualitatively the same as that of Barrows, their results are presented in a form such that direct comparison with his results is somewhat difficult. Note that Barrows' theoretical covariance spectrum of  $\Delta R_{e1}$  and  $\Delta R_{e2}$ , when multiplied by  $(2\pi f)^2$ , is proportional to the covariance spectrum of the frequencies  $v_1$  and  $v_2$ .

In a paper to be published shortly, Janes, Kirkpatrick, Waters and Smith [1963] describe measurements of the cross-correlation between the variations in  $\Delta R_{e1}$  and  $\Delta R_{e2}$  at  $v_1 = 9.2$  gc/s and  $v_2 = 9.4$  gc/s over a 47-km line-of-sight over-water path at Eleuthera Island in the Bahamas. For these measurement conditions and an assumed mean wind speed  $U = 2$  meters/second,  $f_{w12} = 0.0514$  cycles per second and  $f_{c12} = 0.495$  cycles per second; as would be expected from Barrows' theory, the spectrum of  $\Delta R_{e2} - \Delta R_{e1}$  was observed to be less than the spectrum of  $\Delta R_{e2}$  for fluctuation frequencies  $f < 0.5$  cycles per second and increased to about twice that of  $\Delta R_{e2}$  for  $f \gg 0.5$  cycles per second.

It is important to emphasize that all of the  $\Delta R_e$  and  $\dot{\Delta R}_e$  spectra shown in this paper were obtained with stationary paths so that the speed  $U$  with which the turbulent atmospheric structure moves normal to the path is that of the wind and thus is of the order of two meters per second. The line-of-sight to a moving space vehicle

will move through the turbulent atmospheric structure with a velocity  $U$  which varies from zero at the surface end of the path up to values of the order of 200 to 2000 meters per second at the vehicle end of the path. An approximation to the spectra appropriate to the space vehicle application may be obtained by simply increasing the values of the fluctuation frequencies shown in Figures 11, 12, and 13 by the ratio of the velocity near the mid-point to the mean wind velocity, i.e., a factor of the order of 50 to 500. A more precise treatment is given by Barrows [1963] who makes a more appropriate allowance for the variations in the velocity along the path.



## REFERENCES

1. Schulkin, M., "Average Radio-Ray Refraction in the Lower Atmosphere," Proc. IRE, 40 No. 5, 554-561, May 1952.
2. Bean, B.R., and Cahoon, B.A., "The Use of Surface Weather Observations to Predict the Total Atmospheric Bending of Radio Waves at Small Elevation Angles," Proc. IRE, 45, No. 11, 1545-1546, November 1957.
3. Anderson, L.J., "Tropospheric Bending of Radio Waves," Trans. AGU, 39, 208-212, April 1959.
4. Fannin, B.M., and Jehn, K.H., "A Study of Radar Elevation Angle Error due to Atmospheric Refraction," IRE Trans., Antennas and Propagation, AP-5, No. 1, 71-77, January 1957.
5. Bean, B.R., and Thayer, G.D., CRPL Exponential Reference Atmosphere, NBS Monograph No. 4, October 1959b.
6. Bean, B.R., and Cahoon, B.A., "Effect of Atmospheric Horizontal Inhomogeneity Upon Ray Tracing," NBS J. Res., 63D, No. 3, 287-292, November 1959.
7. Bean, B.R., Cahoon, B.A., and Thayer, G.D., Tables for the Statistical Prediction of Radio Ray Bending and Elevation Angle Errors Using Surface Values of the Refractive Index, NBS Tech. Note 44, March 1960.
8. Bean, B.R., "Climatology of Ground-Based Radio Ducts," NBS J. Res., 63D, No. 1, 29, July-August, 1959.
9. Iliff, W.R., and Holt, J.M., "Use of Surface Refractivity in the Empirical Prediction of Total Atmospheric Refraction," NBS J. Res., 67D, No. 1, 31-35, January-February 1963.
10. Anway, A.C., "Empirical Determination of Total Atmospheric Refraction at Centimeter Wavelengths by Radiometric Means," NBS J. Res., 67D, No. 2, 153-160, March 1963.

11. Bean, B.R., and Thayer, G.D., "Comparison of Observed Atmospheric Radio Refraction Effects with Values Predicted Through the Use of Surface Weather Observations," NBS J. Res., 67D, No. 3, 273-285, May-June 1963.
12. Bean, B.R., and Thayer, G.D., "On Models of the Atmospheric Refractive Index," Proc. IRE, 47, No. 5, 740-755, May 1959a.
13. Bean, B.R., Thayer, G.D., and Cahoon, B.A., "Methods of Predicting the Atmospheric Bending of Radio Rays," J. Res. 64D, No. 5, 487-492, September-October 1960.
14. Adamsson, L., "Low Level Coverage of Elevated Radar Stations," Electronics Dept., Res. Instit. of Nat'l. Defense, Stockholm, Sweden, November 1962.
15. Martin, F.L., and Wright, F.E., "Radar-Ray Refraction Associated with Horizontal Variations in the Refractivity," J. Geophys. Res., 68, No. 7, 1861-1869, April 1963.
16. Herbstreit, J.W., and Thompson, M.C. Jr., "Measurements of the Phase of Signals Received over Transmission Paths with Electrical Lengths Varying as a Result of Atmospheric Turbulence," Proc. IRE, 43, No. 10, 1391-1401, October 1955.
17. Thompson, M.C. Jr., and Janes, H.B., "Measurements of Phase Stability over a Low-Level Tropospheric Path," NBS J. Res., 63D, No. 1, 45-51, July-August 1959.
18. Thompson, M.C. Jr., Janes, H.B., and Kirkpatrick, A.W., "An Analysis of Time Variations in Tropospheric Refractive Index and Apparent Radio Path Length," J. Geophys. Res., 65, No. 1, 193-201, January 1960.
19. Norton, K.A., Herbstreit, J.W., Janes, H.B., Hornberg, K.O., Peterson, C.F., Barghausen, A.F., Johnson, W.E., Wells, P.I., Thompson, M.C. Jr., Vetter, J.J., and Kirkpatrick, A.W., "An Experimental Study of Phase Variations in Line-of-Sight Microwave Transmissions, NBS Monograph, No. 33, November 1961.
20. Norton, K.A., Barrows, E.C., Thompson, M.C. Jr., and James, H.B., "Variance of Radio Frequency Caused by Atmospheric Turbulence in Line-of-Sight Transmissions," IRE Trans., Instrumentation, I-11, No. 3 and 4, 153-155, December 1962.

21. Janes, H.B., "Correlation of the Phase of Microwave Signals on the Same Line-of-Sight Path at Different Frequencies," IEEE Trans., Antennas and Propagation, (to be published in 1963).
22. Janes, H.B., Kirkpatrick, A.W., Waters, D.M., and Smith, D., "Phase and Amplitude Diversity in Over-Water Transmissions at Two Microwave Frequencies, (to be published in 1963).
23. Janes, H.B., and Thompson, M.C. Jr., "An Experimental Study of Atmospheric Errors in Microwave Range and Range Difference Measurements, (To be published in 1963).
24. Smith, E.K., and Weintraub, S., "The Constants in the Equation for Atmospheric Refractive Index at Radio Frequencies," Proc. IRE, 41, No. 8, 1035-1037, August 1953.
25. Barrows, E.C., "Phase Instability in a Tropospheric Relay Link, (to be published in 1963).
26. Norton, K.A., "Carrier-Frequency Dependence of the Basic Transmission Loss in Tropospheric Forward Scatter Propagation," NBS Tech. Note 53, May 1960; J. Geophys. Res., 65, No. 7, 2029-2045, July 1960.
27. Muchmore, R.B., and Wheelon, A.D., "Frequency Correlation of Line-of-Sight Signal Scintillations," IEEE Trans., Antennas and Propagation, AP-11, No. 1, 46-51, January 1963.
28. Barton, D.K., "Reasons for the Failure of Radio Interferometers to Achieve Their Expected Accuracy," Proc. IEEE, 51, No. 4, 626-627, April 1963.